THREE DEGREE OF FREEDOM HAPTIC FEEDBACK FOR ASSISTED DRIVING OF HOLONOMIC OMNIDIRECTIONAL WHEELCHAIRS

by

Quinton M. Christensen

A thesis submitted to the faculty of
The University of Utah
in partial fulfillment of the requirements for the degree of

Master of Science

Department of Mechanical Engineering

The University of Utah

August 2011

Copyright © Quinton M. Christensen

All Rights Reserved

The University of Utah Graduate School

STATEMENT OF THESIS APPROVAL

The thesis of **Quinton M. Christensen**

has been approved by the following supervisory committee members:

Stephen Mascaro	, Chair	**06/09/2011** Date Approved
Mark Minor	, Member	**06/13/2011** Date Approved
David E. Johnson	, Member	**06/09/2011** Date Approved

and by **Tim Ameel**, Chair of the Department of **Mechanical Engineering**

and by Charles A. Wight, Dean of The Graduate School.

ABSTRACT

Increased demand for powered wheelchairs and their inherent mobility limitations have prompted the development of omnidirectional wheelchairs. These wheelchairs provide improved mobility in confined spaces, but can be more difficult to control and impact the ability of the user to embody the wheelchair. We hypothesize that control and embodiment of omnidirectional wheelchairs can be improved by providing intuitive control with three degree of freedom (3-DOF) haptic feedback that directly corresponds to the degrees of freedom of an omnidirectional wheelchair. This thesis introduces a novel 3-DOF Haptic Joystick designed for the purpose of controlling omnidirectional wheelchairs. When coupled with range finders, it is able to provide the user with feedback that improves the operator's awareness of the area surrounding the vehicle and assists the driver in obstacle avoidance. The haptic controller design and a stability analysis of the coupled wheelchair joystick systems are presented. Experimental results from the coupled systems validate the ability of the controller to influence the trajectory of the wheelchair and assist in obstacle avoidance.

TABLE OF CONTENTS

LIST OF FIGURES

ACKNOWLEDGEMENTS

I would like to thank my wife, Wendy, and my children, Emma, Caleb, Andrew, Sam, and Simon. I am grateful for their support as I have completed this degree. I love all of you.

I would like to thank my parents, Carl and Launa Christensen. They set my feet on this path by encouraging me to pursue my interests. Special thanks to my "other mothers": Elaine Petersen, my mother-in-law, and her sister, Eileen Rich. Without their assistance my family would have never made it through.

I would also like to extend special thanks my brother, Tony, for loaning me his laptop when mine died mid-thesis.

I would especially like to thank my advisor, Stephen Mascaro, for taking a chance on me. His patience, encouragement, support, guidance and friendship have meant more that I am able to express. Thanks to my colleagues and lab mates who have put up with me for all this time.

Most of all, I would like to thank my Father in Heaven who has blessed me with everything I have, everything I am, and everything which I hope to become.

2 Peter 1:5-8

"And beside this, giving all diligence, add to your faith virtue; and to virtue knowledge; and to knowledge temperance; and to temperance patience; and to patience godliness; and to godliness brotherly kindness; and to brotherly kindness charity. For if these things be in you, and abound, they make you that ye shall neither be barren nor unfruitful in the knowledge of our Lord Jesus Christ."

CHAPTER 1

INTRODUCTION

1.1 Motivation

The objective of this research is to improve the ability of a human operator to drive an omnidirectional wheelchair using haptic feedback. Omnidirectional wheelchairs have the potential to significantly improve the ability of disabled persons to navigate in confined areas, but require more coordination in order to control the additional degrees of freedom. We hypothesize that by providing force feedback to the driver through an omnidirectional joystick, we can assist the driver to navigate the wheelchair in a natural and coordinated manner.

This thesis introduces a novel 3-DOF Haptic Joystick designed to improve control of omnidirectional wheelchairs by providing the operator velocity control and haptic feedback which intuitively corresponds to the degrees of freedom of the omnidirectional wheelchair. This joystick will assist the user to avoid collision by providing force and torque cues that encourage them to navigate the wheelchair away from obstacles. It is the expectation that this will help the wheelchair user to be more aware of the location of their chair in relation to obstacles in their surroundings and enable users to more readily embody their wheelchair.

1.1.1 Increasing demand

For the elderly and persons with disabilities, increasing personal mobility is a key factor in improving and maintaining quality of life, increasing independence, and reducing the financial resources needed for care. As the population ages, demand for assistive technology is increasing. The Administration on Aging estimates that there will be about 71.5 million Americans over the age of 65 by the year 2030 [1]. This will account for approximately 19.3% of the population, which represents a significant increase from 12.6% in 2000. According to the Cornell University 2007 Disability Status Report, 52.9% of the population 75 and older were classified as disabled [2]. Given current aging projections and disability statistics, it is estimated that 8.9% of the population will be classified as disabled due to effects of aging by the year 2050.

The primary method for improving personal mobility in the disabled population is through the use of wheelchairs, both manual and powered. One study has shown that the number of wheelchair users doubled from 1980 to 1996. Increased wheelchair use remains a continuing trend, with 1.3% of the entire population dependant on wheelchairs for mobility in 2005 [3, 4]. Because manual wheelchairs require upper body strength and flexibility, power wheelchairs are typically employed for the elderly, those with degenerative muscle conditions or neurological disorders, and those who otherwise lack the ability to operate a manual wheelchair.

1.1.2 Challenges with wheelchairs

Two significant problems with powered wheelchairs are embodiment and difficulty of control. Embodiment can be thought of as the operator's sense of the location

of the wheelchair with respect to the environment [5]. Most people have a fairly good understanding of how their body interacts with their immediate surroundings. For example, in a crowded elevator, most people know how far back to step to allow another person on without looking back or running into anyone else. Opinions vary among disciplines as to how people are able to do this, but, many researchers believe the process involves a learned sense of their body from tactile feedback and proprioception, or the person's ability to sense the position of their body [6, 7]. When a person is placed in a wheelchair, their instinctive interaction with their surroundings is changed. The footprint of the chair alters their personal space and they are less aware of their position with respect to obstacles in their surroundings. This problem also occurs with users in cars and explains the difficulty many people have in backing up or parallel parking.

Conventionally, powered wheelchairs are controlled using a two-dimensional, position-sensing joystick with forward and reverse velocity commands mapped proportionally to the position of one axis and steering angle or rotational velocity mapped to the position of the other. A recent review of assistive robotics technology in the United States found that 40% of new powered wheelchair users find steering nearly impossible with conventional interfaces [8]. The same review found that the need for cooperative control systems is increasing, citing distinct benefits from sensory or haptic feedback in robotic assistive devices. Much of the difficulty in embodying and learning to control a conventional wheelchair is due to a lack of feedback to the user. Research has shown that embodiment and control of a wheelchair can be greatly enhanced by the application of haptic or force feedback [9, 10].

Additionally, many in the disabled population have extreme difficulty or are

entirely unable to operate a conventionally controlled power wheelchair. These may include those with neurological disorders such as Parkinson's disease and cerebral palsy, or degenerative conditions like muscular dystrophy, where coordination is impeded by tremors or muscle weakness. Very young children who lack the ability to walk also need mobility solutions for proper brain development but are typically unable to operate a wheelchair without assistance [10]. These groups would benefit from the development of smart wheelchairs which can provide the required assistance in place of a caregiver, increasing their independence.

1.2 **Haptic Devices**

Many research institutions are implementing haptic control systems on powered wheelchairs to address the needs of disabled users [11, 12]. Haptic devices present a user with physical sensations or tactile feedback intended to mimic real world forces. They are being implemented in an ever increasing range of applications from simple vibrotactile displays on cell phones to complex kinesthetic devices used to control surgical robots [13]. Haptic devices are often combined with visual displays to enhance the user's awareness of a virtually created world but have also proven particularly useful in situations requiring improved human control. Research shows that haptic guidance enhances motor learning especially with young children in steering oriented tasks [14, 15].

These devices are typically designed to impart linear forces, but may be extended to provide moments and tactile feedback in addition to forces [16]. Kinesthetic haptic devices can be divided into two primary categories, impedance and admittance devices

[17]. Admittance devices are force sensing rigid robots and constrain the user's position to match a desired deflection. Impedance devices, by contrast, are back-drivable systems that sense the user's position and apply appropriate forces to provide the desired haptic rendering. For the purposes of this thesis, discussion of haptic devices is limited to impedance based kinesthetic devices designed to impart forces on a user's hand.

1.2.1 Commercially produced haptic devices

Most commercially produced haptic devices are intended to render forces in three dimensions. The SensAble Technology PHANToM Premium and the PHANToM Omni are serial linkage robots which function as haptic devices. They vary in work space, force capabilities, and price, but both are intended to provide haptic rendering in three dimensions [18]. By adding an active spherical wrist as a stylus interface, the PHANToM Premium can be extended to provide six degrees of feedback, three linear and three rotational [19]. Parallel linkage mechanisms have also been implemented as haptic devices. Examples of these are the 5-DOF, pantograph based, Haptic Wand by Quanser, the Force Dimension Omega, and the low-cost Novint Falcon [20-22].

While these devices are useful for a variety of applications, their size and configuration make them inappropriate for use as a mobile wheelchair controller. The force capability of these devices ranges from just 3 N for the PHANToM Omni, to 22 N for the PHANToM Premium. The stylus on the PHANToM Premium is capable of producing a maximum of 515 mNm of torque in the yaw and pitch directions, but only 170 mNm in the roll. The Haptic Wand, Falcon, and Omega have maximum force capabilities of 7.5 N, 8.9 N and 12 N, respectively, and are not natively equipped to

produce rotational feedback.

1.2.2 Educational haptic devices

The prohibitive cost of most commercially produced haptic devices has prompted many universities to develop simple, single degree of freedom Haptic Paddles [23, 24]. These simple devices are typically low-cost and able to produce high fidelity haptic rendering. This is of interest because the final joystick design used in this research is a derivative of these devices.

Figure 1.1 shows the Haptic Paddle developed by Provancher and Doxon at the University of Utah. It functions as an impedance device and is capable of producing a maximum of 47 N of force at the handle. Its design is derived from the Haptic Paddles

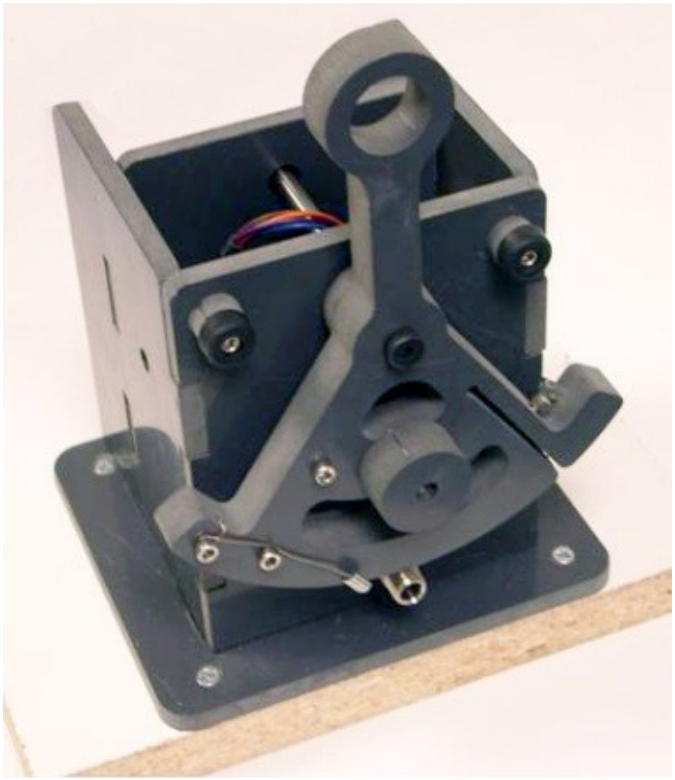

Figure 1.1: The University of Utah Haptic Paddle developed by Provancer and Doxon.

introduced at Stanford University and is similar to those produced by Rice University [25, 26]. Both the Rice and Stanford designs use a capstan drive mechanism similar to the University of Utah Haptic Paddle, but use Hall Effect sensors for position measurement rather than incremental encoders.

These devices were designed to provide a cost effective way to teach students the basics of control system design and to give them a tangible understanding of how changes in a control law can change the response of a system [27]. In order to extend the functionality of these devices, some institutions have enhanced the basic Haptic Paddle. For example, Johns Hopkins University has coupled two haptic paddles to form the Snaptic Paddle, a modular haptic device which can render forces in two degrees of freedom [28].

1.2.3 Force feedback joysticks

The joystick is the most common control input to a powered wheelchair and force feedback joysticks are frequently used for research in haptically controlled wheelchairs. The Logitech Force Pro and Microsoft Sidewinder Force Feedback 2 are two low-cost, commercially available gaming joysticks that provide two degrees force feedback. The primary advantage to using a gaming joystick in research is that they are supported in many software packages. Some institutions are using these types of joysticks for wheelchair research with varying degrees of success [29-31].

Most researchers studying haptically controlled wheelchairs, however, either use high-end, commercially produced joysticks or design and build their own [32, 33]. A commonly used high-end, haptic joystick is the Immersion Technologies Impulse Stick.

This joystick uses a USB interface and is Direct X compatible. It is capable of producing a maximum force of 14.5 N in two dimensions [34]. It provides for 40 degrees of travel in each axis and has a positional resolution of .01º.

Another joystick produced by the same company, the Impulse Engine 2000, is a capstan driven 2-DOF joystick that has been used in rehabilitation experiments [35]. Although it provides similar positional range and resolution, it is only capable of producing a maximum of 8.9 N of force. Neither of these joysticks is currently in production, but the Impulse Stick is still available through several companies selling refurbished units. Even refurbished, however, the Impulse Stick is prohibitively expensive, costing about $4000.00 each.

1.3 **Omnidirectional Wheelchairs**

Due to their mobility limitations, the adoption of a wheelchair may require modification of existing housing to accommodate the wheelchair or relocation to a home that is already configured for wheelchair use. Even though many conventional powered wheelchairs have a zero turning radius, they still require large spaces to align with and pass through doors. Additionally, conventional wheelchairs are unable to navigate well in confined spaces. The Americans with Disabilities Act and international building codes describe the space requirements for various types of wheelchairs [36]. These building codes are based on the kinematic limitations of conventional wheelchairs. These limitations have prompted many independent groups to pursue development of viable omnidirectional wheelchairs [37-48].

1.3.1 Holonomic omnidirectional wheelchairs

In robotics, the term holonomic refers to the ability to simultaneously control all degrees of freedom of the robot (or vehicle) [49]. A classic example of a non-holonomic vehicle is a car. The two controls available on a car, velocity and steering angle, do not directly correspond to the planar space in which the car operates. With a car, no immediate lateral translation is possible. In order for it to move laterally, such as when parallel parking, it is necessary to use a sweeping sinusoidal-like path [50].

A holonomic omnidirectional vehicle, by contrast, is able to move in any arbitrary direction on the plane in which it operates. The omnidirectional wheelchair is able to simultaneously translate in the X and Y directions as well as rotate about its center as seen in Figure 1.2. Humans are intrinsically capable of this type of motion. We are able to side step around obstacles, turn in place, and rotate while walking or running. While omnidirectional wheelchairs are capable of this type of motion they do not provide the

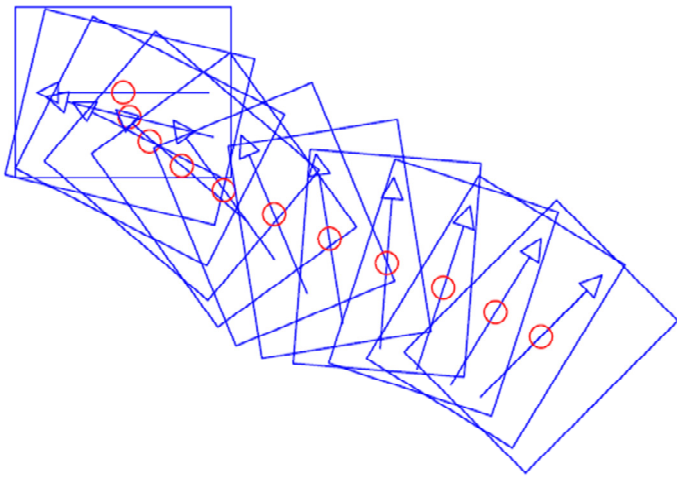

Figure 1.2: Example of holonomic omnidirectional motion recorded on the wheelchair base used in this research. Humans are able to move in this type of omnidirectional motion.

user proprioceptive feedback, making embodiment of the wheelchair more difficult.

Figure 1.3 shows a comparison of conventional vs. omnidirectional wheelchair trajectories in a confined space. The omnidirectional wheelchair is able to sidestep obstacles and easily aligns to pass through the door. The conventional wheelchair, however, must rotate in close proximity to obstacles and walls increasing the likelihood of collision. While an omnidirectional wheelchair is better able to navigate in confined spaces, the extra degrees of freedom can be more difficult to control.

Omnidirectional motion can be achieved in a number of ways. The omnidirectional wheelchair used for this research was developed by Asada and Mascaro at MIT [51]. On this vehicle, each wheel is composed of a spherical ball held in a rotary assembly and supported by bearings as seen in Figure 1.4. This configuration allows motion in one active and one passive degree of freedom for each wheel. The velocity of

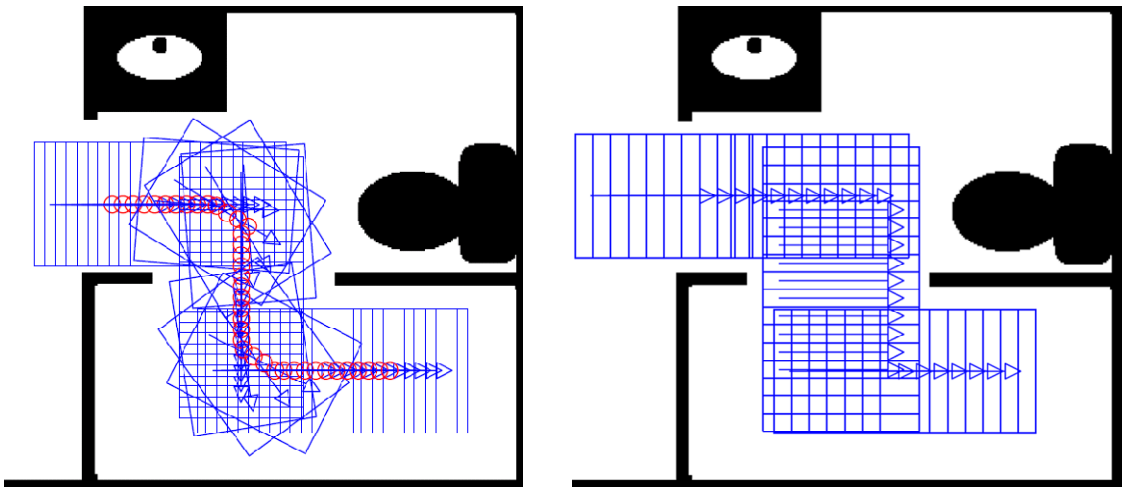

(a) (b)

Figure 1.3: Comparison of example trajectories for a conventional wheelchair, (a), and holonomic omnidirectional wheelchair, (b), in a confined space. The conventional wheelchair requires more attention to environmental obstacles to reach the same position.

Figure 1.4: Omnidirectional Ball Wheel mechanism on the wheelchair used for this research.

the vehicle is determined by the sum of all of the active degrees of freedom as seen in Figure 1.5 (a).

Most current omnidirectional wheelchair research is performed using either Mecanum wheels [29, 41, 52-55] or omni-wheels [9, 56-60]. This popularity is due to the commercial availability of Mecanum wheels and platforms [61, 62]. Mecanum wheels are comprised of a disk with rolling elements around the circumference, set at an angle to the wheel's axis of rotation, as seen in Figure 1.5 (b). Likewise, omni-wheels have rolling elements around the circumference; however, they are perpendicular to the axis of rotation. In both types, the configuration of the rolling elements gives each wheel one active and one passive degree of freedom.

Both the Ball-Wheeled and Mecanum based platforms are driven by one motor per wheel. By varying the speed of the motors, motion in any planar direction or orientation can be achieved. In both cases, the motor velocities required for a desired

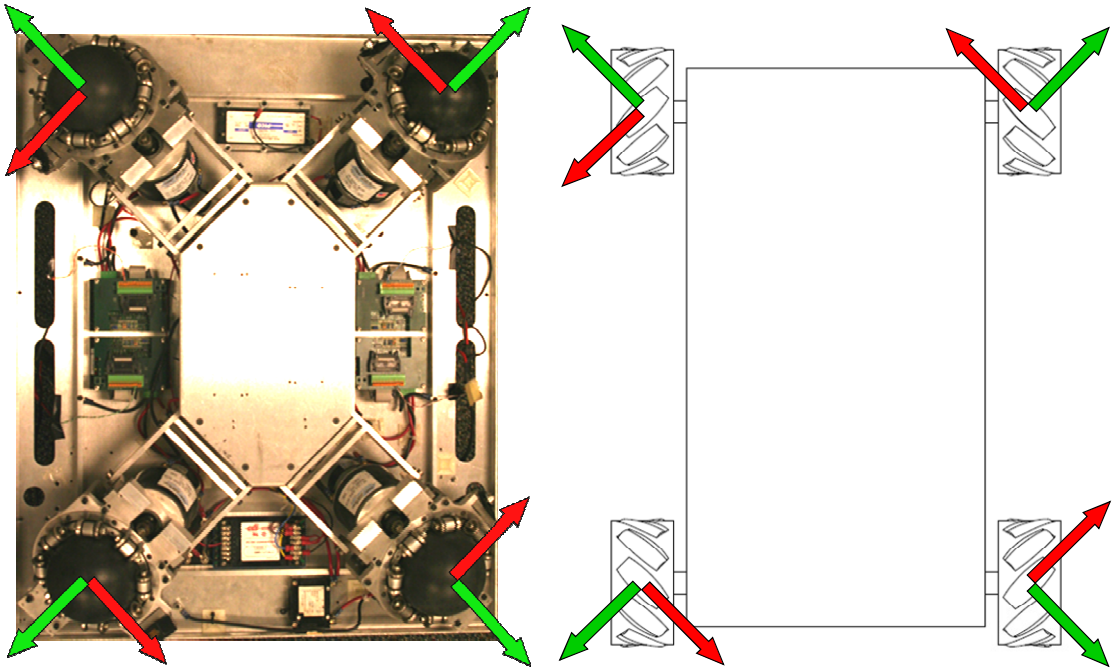

Figure 1.5: Bottom view of the omnidirectional wheelchair and a schematic of a Mecanum wheel design with active degrees of freedom indicated in red and passive in green.

omnidirectional trajectory can be determined by a simple inverse kinematics algorithm.

The extra maneuverability of omnidirectional wheelchairs does not come without a cost. The complexity of creating omnidirectional motion requires some form of intelligent control to calculate the required motor velocities, whereas, conventional powered wheelchairs are can be operated with simpler control systems. Further, the problems of embodiment and difficulty of control associated with conventional powered wheelchairs still exist for omnidirectional wheelchairs. These problems can, in fact, be even more pronounced because operators must coordinate forward, lateral, and rotational motions simultaneously. Additionally, the unusual combinations of velocities and accelerations associated with omnidirectional motion, without proprioceptive feedback,

may lead to motion sickness and feelings of disorientation, compounding the difficulty of driving.

1.4 **Literature Review**

The application of haptic feedback in wheelchair control is a very active field of research [63-69] with large portions of work specifically dedicated to omnidirectional wheelchairs [42, 59, 70]. However, some research is more relevant to this work and merits special consideration. These works use similar techniques in feedback, have a similar goal to the work presented in this thesis, or represent the state of the art in haptically controlled wheelchair systems.

1.4.1 Haptic feedback applied to wheelchair training

The work of Chen, Ragonesi, Galloway, and Agrawal at the University of Delaware titled, “Training Toddlers Seated on Mobile Robots to Drive Indoors Amidst Obstacles” represents the state of the art in terms of motor training as applied to wheelchairs [14]. The goal of this research is to train toddlers to drive a mobile robotics platform using haptic feedback. The subjects in this study are children under three years of age, some of whom have mobility impairments. A small, commercially available mobile robotics platform, fitted with ultrasonic and laser range finders is used as a wheelchair and feedback is provided by an Immersion Technologies Impulse Stick. The children are encouraged to drive the wheelchair through a pre-defined workspace with regularly spaced obstacles to retrieve a toy at the far end.

Control inputs from the joystick are mapped as a conventional wheelchair control

system with the velocity, v, mapped proportionally to the Y axis of the joystick and the rotational velocity, ω, mapped to the X axis. The feedback law is implemented as a two-dimensional force field. The workspace of the joystick is divided into three general areas, a virtual cone (Region 1) oriented to the nominal steering command, two regions on either side of the cone where virtual wall effects are enabled (Region 2), and the remainder is where forces drive the joystick back to the center position (Region 3). Feedback is applied when the joystick is outside the preferred steering direction indicated by the cone. The wall effect in the side regions is based on a typical potential field method, applying attractive forces for the goal and repulsive forces for all obstacles. When the joystick is in the cone region, the only forces acting on the joystick are damping forces to stabilize control. In the other regions, the virtual wall forces and centering forces are added to the damping forces as shown in (1.1).

$$F = \begin{cases} F_d\,, & \text{Region 1} \\ F_d + F_w, & \text{Region 2} \\ F_d + F_c, & \text{Region 3} \end{cases} \tag{1.1}$$

In this equation F_d F_w and F_c are given by (1.2),(1.3), and (1.4) respectively.

$$F_d = -k_d\left[\dot{xl}, \dot{yl}\right]^T \tag{1.2}$$

$$F_\omega = k_C\left[([xl, yl]^T)\dot{xl}, \dot{yl}\right]^T \dot{xl} \tag{1.3}$$

$$F_C = -k_C[xl, yl]^T \tag{1.4}$$

The terms k_c and k_d are tunable parameters used to alter the wall stiffness and damping and the joystick position is given by xl and yl.

The intent of the feedback law is not to directly steer the subjects, but encourage them to steer the robot in the nominal direction while they select how fast the vehicle

should move. The nominal path is selected by an error correcting control law using a pre-determined nominal trajectory through the operating environment. The path planning algorithm uses way points through the potential field to eliminate local minima in the defined space.

With haptic feedback the subjects were able to improve their obstacle avoidance abilities over the course of several days to a level, which in previous research without haptic feedback, required several months of training. Additionally, once trained, the subjects retained the driving skills by demonstrating their ability on a different course. These results support the evidence that haptic feedback enhances motor learning in toddlers.

Similar work performed at the University of California, Irvine by Marchal-Crespo, Furumasu, and Reinkensmeyer is intended to train young wheelchair users to operate their wheelchairs by improving their sense of the wheelchair's motion and steering capabilities. Published in 2010, this work is titled, "A robotic wheelchair trainer: design overview and a feasibility study" [15]. This is the continuation of many years of work training young wheelchair users with haptic feedback [10, 71, 72].

The wheelchair used for this study is a conventional powered wheelchair. An Immersion Technologies Impulse Stick is used for controller input with the same velocity control mapping previously discussed. To reduce costs and improve accessibility to training, the system uses a USB camera and a laser pointer to measure the distance between the target trajectory, indicated by a black line on the floor, and the wheelchair's actual position.

The study subjects are children from four to nine years of age, some of whom

have motor disabilities. The research task involves having the children follow a black line on the floor, keeping the laser pointer dot as close to the line as possible. To keep the children engaged, they get to play a game of "tag" with an autonomous line following robot. The subjects attempt to follow the line as fast as possible to catch the robot. If the subjects try to cheat the game by cutting corners, a buzzer sounds and they are penalized by a reduction in the wheelchair's maximum speed.

The only force feedback presented to the subjects is in the X or steering direction, permitting the children to choose the appropriate velocity. The calculation of the force feedback is dependent on a "look-ahead" error calculation shown in (1.5).

$$F_{assist} = Kj \cdot (Jx - Jx_{des}) + Bj \cdot \frac{d(Jx)}{dt} \quad \textbf{(1.5)}$$

where *Kj* and *Bj* are the joystick stiffness and damping coefficients, *Jx* is the current joystick position, and Jx_{des} is given by (1.6)

$$Jx_{des} = Kd \cdot e_{dis} + Ka \cdot e_{ang} + Ba \cdot \frac{d(e_{ang})}{dt} \quad \textbf{(1.6)}$$

This equation provides the look-ahead function of the controller by incorporating the distance and directional error into the calculation given by e_{dis} and e_{ang} respectively. The values for the error measurements are recorded at a known distance in front of the wheelchair to ensure that they accurately reflect the ability of the driver. The algorithm is described as a faded control algorithm because "firmness" of the joystick stiffness and damping are modulated as the training continues, giving less assistance as performance improves.

The results of this work show that steering ability improves linearly with age. All subjects in the training group showed improvement in their ability to control the

wheelchair while the control group showed little improvement from the first to the last trial. Their findings support the hypothesis that haptic feedback significantly improves the user's understanding of how their chair operates. This group plans to add obstacle avoidance in future revisions of their work by adding doorways and other obstacles to their training circuit.

1.4.2 Strategies for obstacle avoidance

Two primary techniques from mobile robotics motion planning research are frequently used in intelligent wheelchairs for obstacle avoidance. These are the Artificial Potential Field method introduced around 1985 and the Vector Field Histogram (VFH) method proposed by Borensein in 1991 [73, 74]. The VFH method is a real time motion planning technique designed to overcome some of the problems of the Potential Field technique. It uses a statistical model of the robot's surroundings based on range finder measurements to determine a collision free path. Because it is statistically based, it is very tolerant of sensor misreading, but requires a fairly large sensor array to provide reliable results.

Despite some of the claimed shortcomings of the Potential Field method, it is still implemented by many research groups for obstacle avoidance [75, 76]. This is because the method is computationally simple, can be easily tuned to meet research needs, and can be extended to improve functionality. Potential field planning is capable of directly modifying vehicle trajectory or can be routed through a haptic feedback system to indirectly alter vehicle trajectory. Both of the previously discussed methods of using haptic feedback to training young wheelchair users implement modified potential field

laws [14, 15].

"The NavChair Assistive Wheelchair Navigation System" introduced by Levine, Bell, Jaros, Simpson, Koren, and Borenstein in the Department of Biomedical Engineering at the University of Michigan in 1999 uses the VFH path planning technique [63]. This project was started in 1993 and provided semiautonomous obstacle avoidance in a conventional wheelchair outfitted with a full array of ultrasonic range finders. Early work on the NavChair proved that the VFH algorithm which was developed for mobile robotics was too "jerky" for use as a control algorithm for smart wheelchairs. This prompted the modification of the algorithm to develop the Minimal Vector Field Histogram (MVFH) algorithm specifically for use in proximity obstacle avoidance.

In this work, control inputs to the wheelchair are given using a conventional joystick with the standard velocity mapping previously discussed. The work states that the NavChair restricts itself to minor navigational responsibilities and collision avoidance. Obstacle avoidance is accomplished by intercepting the joystick commands and altering them to avoid obstacles while continuing to move in the general direction indicated by the user. Optimum paths were selected using either VFH or MVFH techniques as determined by a weighting factor.

Alterations to the wheelchair trajectory were performed without providing haptic feedback to the user. This is a primary short coming of this work. It can be disturbing for users, because the chair alters course without being explicitly steered. Another problem with this method is the necessity to switch modes to pass through doors and permit operation close to environmental obstacles.

More recent work has taken the basic concepts of the VFH and MVFH algorithms

and adapted them to apply force feedback to the user rather than directly altering the trajectory of the wheelchair. Bourhis, and Sahnoun from the Laboratoire d'Automatique des Systemes Cooperatifs, at the University of Metz published their work, “Assisted Control Mode for a Smart Wheelchair” in 2007 [31]. Their work was the resumption of work started in 1989 under the name of VAHTM the French acronym for "Autonomous Vehicle for People with Motor Disabilities". The primary goal of this research is to alter the earlier work from the University of Michigan, adapting it to make a collaborative control system and to modify the law to work with the research group’s two smart wheelchairs.

As an initial step, this research was conducted using a two-dimensional virtual environment created in Matlab and Simulink with the VR toolbox. Both control input and feedback are provided by a Microsoft Sidewinder Force Feedback 2 joystick. The research task is for users to navigate a representation of the research team’s two wheelchairs through a virtual scale model of a building. Performance is measured by the speed at which the task is accomplished and the number of collisions encountered.

Their first attempt to provide force feedback was using the potential field method with a repulsive field inversely proportional to the distance to all obstacles detected by the virtual range finders. In this algorithm, the feedback presented to the user was the vector sum of all forces resulting from detected obstacles. This method proved problematic in confined or crowded spaces. The potential field algorithm was replaced with a modified version of the hybrid VFH and MVFH method.

With the VFH/MVFH method, several collision-free paths were calculated as the user navigated through the course. Force feedback was applied in the calculated collision-

free direction that most closely matched the user's steering command, encouraging them to alter course toward the collision-free region.

Their results show that applied feedback improved the performance of subjects as they navigated along the designated path. In confined spaces, feedback based on the MVFH algorithm provided the most significant improvement in completion time and reduction of collisions. The researchers also noted that in open spaces, no significant improvement of performance was noted between the trials with or without feedback.

Because this research was based on a virtual driving simulation, the researchers were able to investigate the effects of the control law without having to deal with noise in the range finders. Had this research been performed with the physical wheelchairs, instead virtually, they would have had to overcome problems, such as sensor noise, and the outcome may have been different. This work included no discussion of the range of forces applied by the feedback law. This is probably because they had little control over magnitude or resolution of available forces with the joystick they used.

1.4.3 Obstacle avoidance in omnidirectional wheelchairs

Of all the literature on haptic guidance for omnidirectional wheelchairs, perhaps the most relevant to the work presented in this thesis comes from the Department of Production Systems Engineering at Toyohashi University of Technology. The work of Kondo, Miyoshi, Terashima, and Kitagawa published in 2008 and titled, "Navigation guidance control using haptic feedback for obstacle avoidance of omni-directional wheelchair" is particularly relevant to this thesis [56]. This work uses a similar omnidirectional wheelchair and is providing haptic guidance for obstacle avoidance. This

is the continuation of ten years research beginning in 1998 [9, 57-60, 77].

The omnidirectional wheelchair used in this research was constructed with omni-wheels and is outfitted with two Hokuyo URG-04LX laser range finders. Earlier investigations of this research team focused on implementing a haptic joystick and providing assistive control of the wheelchair to a caregiver through a 6-DOF force sensor attached to handles on the back of the wheelchair. The researchers constructed their own haptic joystick using gear head motors coupled to the handle by timing belts and using potentiometers for position measurement.

In their control system, the linear velocity of the wheelchair is mapped proportionally to the angular position of the joystick in the X and Y directions. Rotational control is accomplished by a two part mechanism with a toggle switch on the top of the joystick handle and a potentiometer on the control console. The switch controls the rotational direction, while rotational velocity is controlled by the potentiometer.

The research team has implemented several feedback laws; however, most are based on a potential field used to alter the impedance of the joystick. Their work in obstacle avoidance utilizes the two laser range finders to identify the position of obstacles with respect to the wheelchair and applies a torque in the opposite direction of the closest obstacle. The wheelchair's feedback algorithm does not alter the wheelchair's trajectory directly, but indirectly, by altering the impedance of the joystick through an applied torque. The applied torque is calculated using variable impedance based on the distance to obstacles and velocity of the wheelchair as shown in (1.7) and (1.8)

$$\tau = D\dot{q} + Kq \tag{1.7}$$

where D is the viscous damping coefficient, q is the angular displacement from the center

point of the joystick, and *K* is given by (1.8)

$$K = k_0 \left\{ \frac{v/v_{max} + \alpha}{(r/r_{max})^2} + 1 \right\} \quad \textbf{(1.8)}$$

where k_0 is the standard stiffness, *v* is the input velocity, *r* is distance to the obstacle, and α is a tunable parameter based on the user's typical characteristic driving ability.

The work includes no information on human trials, but does show the result of the feedback on several sample obstacle avoidance trajectories. No rotational avoidance is implemented due to the lack of feedback in the rotational control. All obstacle avoidance is accomplished by translating out of the obstacles path maintaining the wheelchair's orientation.

CHAPTER 2

HAPTIC JOYSTICK

2.1 **Design Constraints and Requirements**

In order to implement the wheelchair control system, a device with control inputs that intuitively correspond to all of the degrees of freedom of the wheelchair is needed. It is desired that all inputs be integrated into a single device controlling all degrees simultaneously, as shown in Figure 2.1. This will be done with a conventional joystick configuration where the linear velocities of the vehicle, $\dot{X}$ and $\dot{Y}$, are mapped respectively

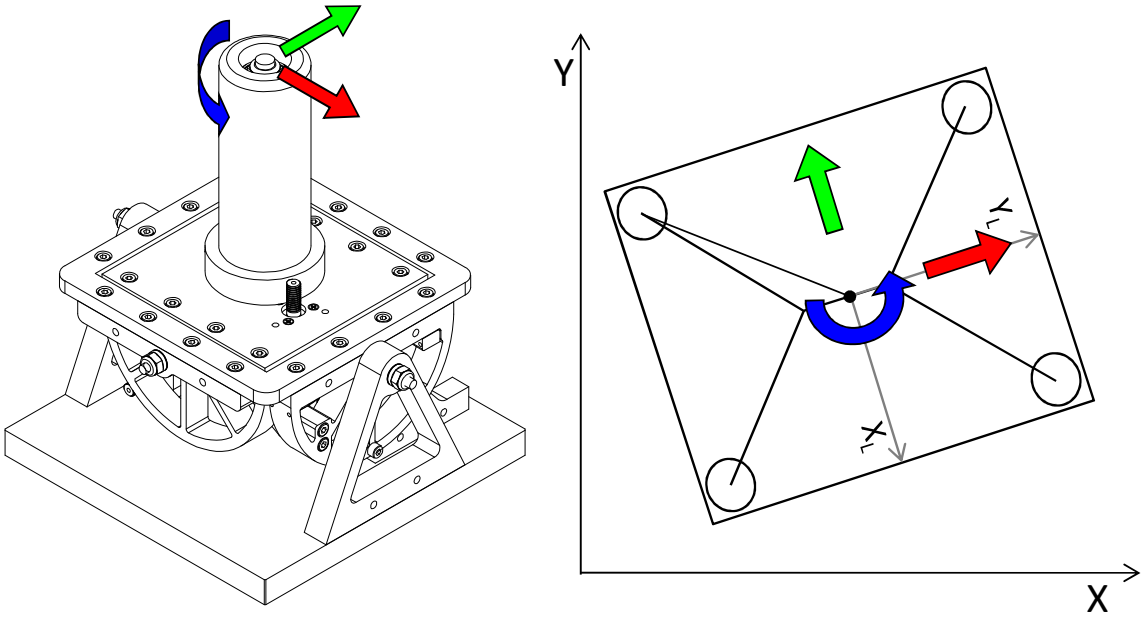

Figure 2.1: Joystick design and a schematic of the omnidirectional wheelchair marked with corisponding degrees of freedom.

to the angular position of the joystick's X and Y axes and with rotational velocity about the wheelchair's center of rotation, $\dot{\theta}$, mapped to the angular displacement of the twist grip handle. This configuration has been implemented on other omnidirectional vehicles and we believe that it will provide an efficient and intuitive control system for the omnidirectional wheelchair [29, 78].

Given this control scheme, it is just as likely that a collision with an obstacle will result from a rotation command as from a linear or translational command. Therefore, we hypothesize that providing feedback corresponding to all three degrees of control will most effectively inform the operator of obstacles in the environment. Based on the literature presented, we anticipate that this configuration of feedback will significantly improve the operator's ability to embody and control the wheelchair.

The use of a joystick for both control of the omnidirectional wheelchair and haptic feedback imposes several design constraints. The first is that the joystick must operate as smoothly, backlash, and vibration-free as possible. Backlash in the system can decrease the accuracy of navigation. Because the device must be able to provide feedback in all degrees of freedom, each axis must be actuated, provide sufficient force for effective haptic rendering, and be back drivable to ensure a smooth feel for the control system. Additionally, the system must be vibration-free because the user may misinterpret vibration in the handle as feedback from the system.

Another design constraint comes from the use of the joystick on the armrest of the wheelchair. It must occupy a minimal volume. Ideally, the entire drive assembly should fit within a four inch cube with the control handle protruding above. Damage to motors or sensors due to impact with obstacles while driving could cause the wheelchair to become

unstable and could have disastrous consequences. It must, therefore, enclose motors, sensors, and associated connectors within the body of the joystick to prevent damage by collision.

2.1.1 Required force capabilites

The required forces for effective force feedback and haptic rendering have been the subject of many papers [79-82]. However, the majority of publications limit their investigation to a single degree of freedom in the hand or feedback to a single finger. The work of Dicianno, Cooper et al. is particularly interesting as they investigate force strategies for joystick control of wheelchairs [68, 83, 84]. The force feedback sensitivity of the position sensing joystick used in their work was in the range of 3 N to 5N. Their work, however, is primarily devoted to the application of linear isometric joysticks, rather than the position-sensing joystick proposed for this research. With the joysticks included in their work, no rotational control input would be possible.

Little information was available about specific force sensitivity of the human hand and wrist in the configuration proposed for this work. Therefore, the desired force capabilities for the joystick were determined by a survey of commercially available haptic devices. The surveyed devices include the SensAble Technologies, PHANToM Omni and PHANToM Premium, the Force Dimension Omega, and the Novint Falcon [18, 21, 22]. Forces provided by these devices range from 3N to 22N with the roll degree of rotational feedback from the spherical wrist on the PHANToM Premium providing 170 mNm of torque.

Matching the force capabilities of the surveyed devices, the target range of force

capabilities selected for the joystick design is from 4 N to 12 N with a nominal torque feedback available from the handle of 170 mNm. This target range is validated by comparison against two devices that could be considered the gold standard in terms of force feedback joysticks, the Immersion Technogies Impulse Engine 2000 and the Impulse Stick which produce a maximum of 8.9N and 14.5N respectively.

2.2 **Joystick Design Iterations**

As a conventional joystick with a twist grip handle was selected to control the wheel chair, it was anticipated that a commercially available joystick would provide the desired functionality. However, after an extensive search for force feedback joysticks; it became evident that no joystick capable of producing twist grip feedback is currently in production. The lack of a readily available option prompted the effort to modify an existing force feedback joystick, adding the third degree of actuation.

2.2.1 Modified Logitech Force Pro force feedback joystick

A Logitech Force Pro joystick was modified by replacing the stock handle with a motorized handle as shown in Figure 2.2. While this configuration was sufficient to control the wheelchair, we found that the X and Y axes lacked sufficient power or resolution to effectively provide haptic rendering. To remedy this problem, the motor drivers were replaced with a more powerful variety. However, the lash in the drive gears and the under-powered motors rendered the joystick unusable for the desired purpose. When a modified commercially available joystick failed to meet the research need, it was decided to design and build a custom 3-DOF Haptic Joystick.

Figure 2.2: Modified Logitech Force Pro gaming joystick. Rotational feedback is provided by a Maxon gear head motor enclosed in the handle. Handle provides about 180º of rotation.

It is interesting to note that the research group at UC, Irvine initially attempted to use a force feedback gaming joystick in their research but, because they were underpowered and lacked the desired resolution, opted to use feedback steering wheels and later switched to an Impulse Stick. Whereas for cost and performance considerations, the Toyohashi University researchers skipped gaming joysticks all together and opted to build their own force feedback joystick.

2.2.2 Haptic paddle based joystick design

Several relevant designs for force feedback joysticks and haptic devices were investigated to assist in the design of the 3-DOF Haptic Joystick. The simplicity of the

Haptic Paddle, its ease of manufacture, and its low-cost were significant factors which influenced the design. Related work on the "Snaptic Paddle" at Johns Hopkins University, the Immersion Corp. Impulse Engine 2000, and other capstan drive based devices were considered in the design process [28, 85].

Implementing a capstan drive mechanism similar to these devices should result in a smooth operating, stiff or low slip, and lash-free drive system [86]. The final design shown in Figure 2.3 is an adaptation and extension of the Haptic Paddle, each axis functioning as an independent Haptic Paddle set perpendicular to the other two axes. Because the parallel linkages employed on the Snaptic Paddle and the Impulse Engine 2000 would have made the incorporation of the third axis more difficult, the design was implemented as a serial manipulator.

2.2.3 First prototype

Two iterations of the Haptic Paddle based design were constructed. Borrowing from the manufacturing technique for the University of Utah Haptic Paddles, the first prototype was produced primarily on a water jet cutter. The rough cut pieces were then mounted to a tooling plate and bearing pockets were machined. Finally, the pieces were cross drilled and tapped for the final assembly.

When this prototype was assembled, it became apparent that the manufacturing method was insufficient. The tapered cut produced by the water jet prevents the capstan sector pulley from being properly aligned with its respective axis. Additionally, the taper produced a side load on the capstan cables and caused them to drift out of position. The resulting angular misalignment between the axes also prevented smooth operation over

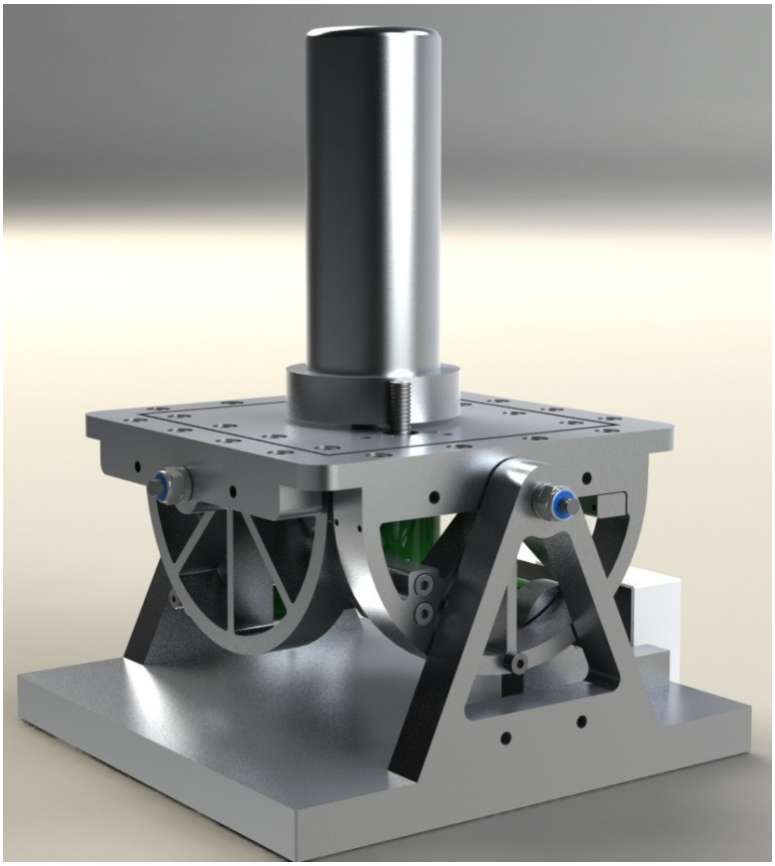

Figure 2.3: A rendered image of the solid model for the final design of 3-DOF Haptic Joystick.

the full range of motion in the Y axis. The initial prototype demonstrated a need for more clearance between axes and more precision in the manufacturing process.

2.3 **Final Design and Functional Prototype**

The flaws in the design and the problems with manufacturing of the first prototype prompted modification of the design and a complete rework of the manufacturing technique. The chassis was enlarged from the first prototype to increase the gear ratio, to allow for more clearance between axes, and to give more interior room for encoders, motors and connecting wires. Each axis is driven by a single motor with a to 15:1 gear ratio capstan drive for torque transmission and an incremental encoder for

position measurement. The X and Y axes permit ± 25 degrees of displacement and the θ axis, with a capstan gear ratio of 7.8:1, allows approximately ± 90 degrees of twist in the handle.

The capstan drive cable is tensioned to maintain sufficient traction between the cable and capstan pulley to provide rapid response to input torque. The .024 in., 7x7 strand, uncoated stainless steel cable from the first prototype was replaced with .028 inch nylon-coated stainless steel cable to reduce wear on the both the cable and capstan components. The gap between the capstan pulley and the capstan sector pulley was reduced to the cable diameter + .005 in., or .033 in. This reduced excessive deflection in the motor shaft. Additionally, the capstan pulleys were machined with a .25 inch .042 pitch spiral groove to improve the tracking of the cable on the capstan sector pulley.

The most challenging design aspect of the final prototype was the configuration of the bearings shown in APPENDIX D. The configuration of the bearings on the first two axes permits adjustment of the axis position parallel with the axis of rotation. It also permits all four bearings in the axis to be properly preloaded for smooth operation. It was necessary to recess the inner bearings to allow clearance for the Y axis inside the X axis frame. All bearing counter bores were sized to provide a transition fit, which accurately locates the bearings without needing to press them into or out of place.

2.3.1 Manufacturing process

All frame elements for the second prototype were rough cut on the water jet and brought to final dimensions on a CNC mill. Alignment holes for positioning the components on the tooling plate were located in the work piece by piercing a narrow hole

with the water jet as they were rough cut. The hole was brought to the correct diameter on a drill press. The rough cut components were then attached to the tooling plate with shoulder bolts. Bearing pockets and motor mounts were machined and the parts were brought to final outer dimensions. This process removed the taper produced by the water jet on the finished capstan mating surfaces, which eliminated the cable drift found on the first prototype. It also resulted in more accurate placement when machining operations were required on both sides of the work piece.

2.3.2 Joystick control hardware

The completed functional prototype shown in Figure 2.4 utilizes one US Digital E4P 360 counts per revolution encoder to record angular position. One AMC 30A8 servo amplifier in current mode is used to drive each Maxon 2322 permanent magnet motor. Encoder counts are read and analog outputs to the amplifiers are produced by a single Sensoray 626 card.

2.4 **Joystick Control System**

With the large mass of the handle positioned above the axes, the joystick system creates a 2-DOF inverted pendulum. The lack of return springs or counterweights make it necessary to continually control the joystick to maintain the zero position. This is accomplished using a simple PD controller. P gains were selected to return the joystick to the home position after a disturbance. The derivative gains were selected to reduce the sensitivity of the joystick to disturbances. Final values were selected through an iterative tuning process.

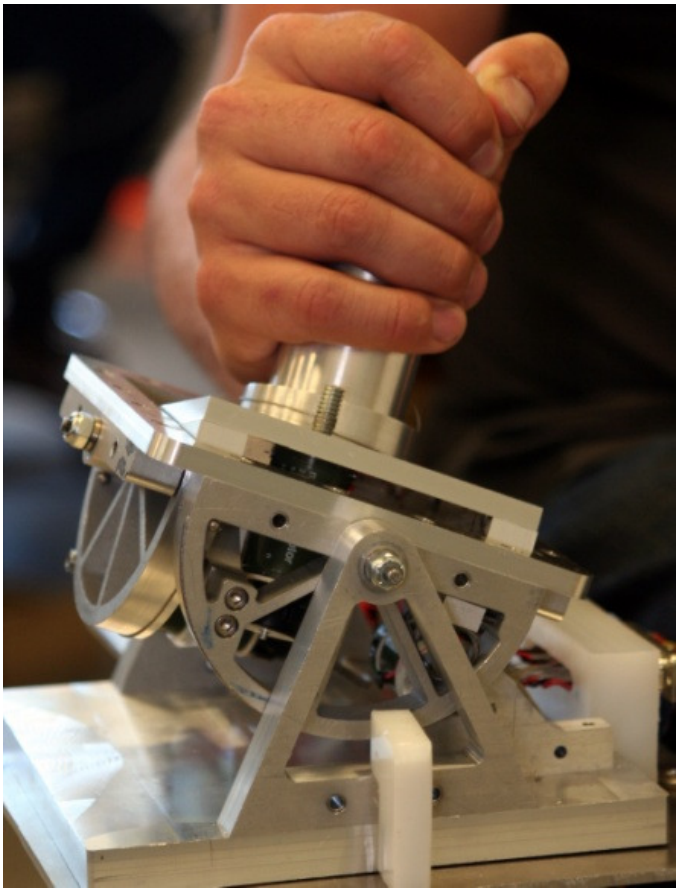

Figure 2.4: Completed functional joysticks prototype. The prototype uses one Maxon 2322 DC motor with a USDigital E4P encoder per axis. Torque transmission provided by capstan cables.

2.4.1 Additional compensation needed

Without additional compensation, the P-gains required to maintain the zero position rendered the joystick too stiff for effective use as a feedback device. They could have been reduced by adding an integral control action to eliminate the steady state error. This option was not chosen because the joystick is used as a wheelchair controller. Implementing an integrator in the controller would result in accumulated error and increasing return forces when a velocity command is maintained for an extended period

of time. This integrator wind up could be misinterpreted by the user as a feedback force from obstacles in the environment.

2.4.2 Gravity compensation

Another option for returning the joystick to the zero position with minimal P gains is to implement a gravity compensation algorithm. This counteracts torques due to gravity, reducing the required torque from the PD controller to return the joystick to the zero position. Treating the eccentrically positioned components, including capstan sector pulleys, motors, motor mounts and the handle, as point masses, the compensation algorithm calculates their effective torque due to gravity. An opposite torque of equal magnitude is applied to compensate for these moments.

The equations for the compensation algorithm are given by (2.1)-(2.3). The compensation for the X axis in (2.1) is based on the position of both the X and Y axes, as predicted in the dynamic modeling. The required compensation torque for the Y axis, however, is independent of the other axes as seen in (2.2). Because gravity has no asymmetrical effects on the rotational handle, it requires no gravity compensation. Because the gravity compensation law is simply the sum of moments for all of the elements, a derivation is not very enlightening; however, a complete list of the numerical parameters used for the gravity compensation algorithm are given in APPENDIX A.

$$\tau_{gx} = -m_h g L_h \left|c\theta_y\right| s\theta_x - m_{m3} g L_{m3x} \left|s\theta_y\right| c\theta_x - m_{m2} g L_{Ymot} c\theta_x - m_{Ycap} g L_{Ycap} c\theta_x - m_{Ymnt} g L_{Ymnt} c\theta_x \quad \textbf{(2.1)}$$

$$\tau_{gy} = -m_h g L_h s\theta_y - m_{m3} g L_{m3Y} c\theta_y \quad \textbf{(2.2)}$$

$$\tau_{g\theta} = 0 \quad \textbf{(2.3)}$$

In these equations, cθ is the cos(θ) and sθ, equals sin(θ). The respective subscripts indicate the axis with which the angle is associated. The acceleration due to gravity is given by g and m_h is the mass of the handle. The masses of motors, capstan sector pulleys, and motor mounts are given by m_{mx}, m_{Ycap}, and m_{Ymnt} respectively. Moment arms are indicated by *L*, with the subscript indicating to which mass they are associated. Additionally, the subscript indicates which axis of rotation from which the moment arm is measured.

Gravity compensation eliminates the nonlinear response of the joystick due to gravity so that it can be treated as a linear system. This improves the function of the PD controller, permitting the use of much lower PD gains to return the joystick to the zero position. The gravity compensation algorithm also improves joystick operation as a wheelchair control input, improving overall stability. Figure 2.5 shows the complete, gravity compensated control algorithm for the joystick.

2.5 **Limitations of the Current Prototype**

Experimentation has revealed several design limitations in the current prototype. The most significant is under powered motors. The desired maximum force capabilities of the initial design were to be from 4N to 12N. Because of cost considerations, surplus Maxon 2322 motors with back-shafts and 102:1 gear heads were purchased. According to

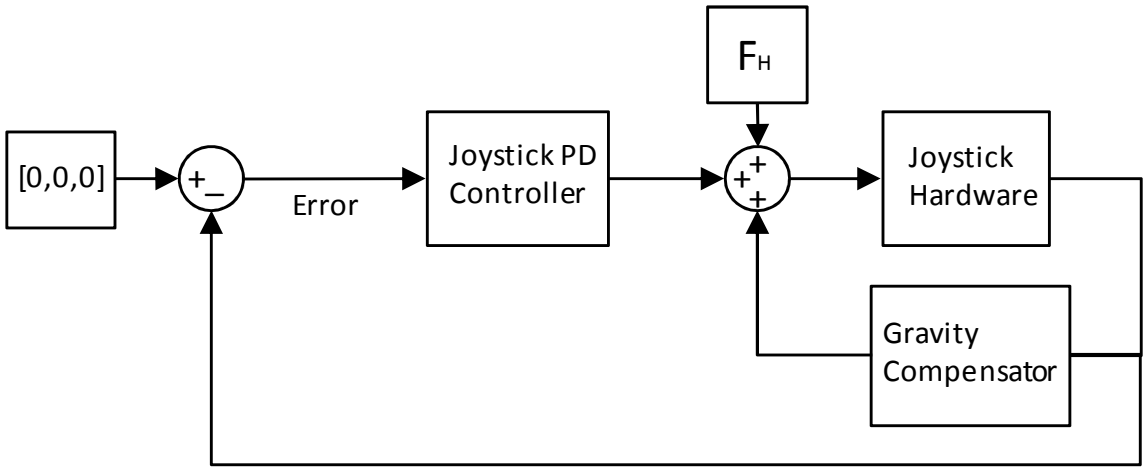

Figure 2.5: Gravity compensated joystick PD controller.

the datasheet for these motors, they have a K_t value of $24.6\ mNm/A$ and a maximum continuous current rating of $0.53\ A$. Given the gear-head ratio and the joystick handle length, these should provide for approximately 10.46 N of force, as shown in (2.4), without exceeding the maximum continuous current limits of the motors.

$$F_{max} = .5\ A \cdot 24.6 \frac{mNm}{A} \cdot \frac{1\ Nm}{1000\ mNm} \cdot \frac{102}{1} \cdot \frac{1}{.12m} = 10.46N \qquad \textbf{(2.4)}$$

Unfortunately, after the motors were purchased, it was discovered that the gear heads were not back drivable. As a result, they needed be removed. This reduced the available torque and the maximum force capability to about 1.5 N without over driving the motors. With the gear heads removed, experimental measurements show that the motors are only capable of producing about 3.5N of force at the handle with the motors overdriven to 1.8 amps. Because the motors are being overdriven, force feedback can only be enabled for short periods of operation, without overheating the motors.

Another design limitation is the lack of absolute position sensing. The measured

position is relative to the starting position of the joystick. The lack of absolute position measurement causes the design to be subject to slip in the capstan drive. This has also caused problems with gravity compensation. In situations where the control system is started with the joystick away from true center, the gravity compensation algorithm is unable to perform correctly and causes instability in control. Additionally, if the wheelchair were operated on a hill, the orientation of the gravity compensation would be off by the pitch of the hill. This problem could be remedied by the incorporation of an accelerometer to the joystick base so that a gravity reference is always available.

One physical limitation of the prototype can be attributed to the bearings used on the X and Y axes. A small bearing with a .25 inch ID and a .375 inch OD was selected to minimize size of the bearing brackets and to keep the center deck as close to the axis of rotation as possible. While similar bearings perform well on haptic paddles, they are undersized for this application because of the configuration of the bearing pairs on the two primary axes. The preload required to keep the Y axis aligned when a torque is applied causes the bearings to intermittently bind. To remedy this problem, the preload on the bearings was reduced until smooth operation was achieved. However, this resulted in .01 in. to .02 in. of deflection and slight angular misalignment at the corner when the maximum torque is applied by the motors.

CHAPTER 3

WHEELCHAIR

3.1 **Wheelchair Hardware**

The wheelchair base consists of four ball wheels enclosed in a rotary ring of bearings. This constrains the motion of the ball about its circumference but permits free motion in all directions perpendicular to the axis of rotation. The rotary rings are angled at 30º to the floor. This moves the point of contact away from the axis of rotation, providing a moment arm producing a linear motion perpendicular to the axis of rotation. Contact between each ball and the floor is maintained by a four bar linkage suspension system with gas shocks as seen in Figure 1.4. The rotary ring of each of the four wheels is coupled to a ring gear and is driven by a Cleveland Motion Controls MH350 permanent magnet DC servo motor. The motors are driven by an SSA PWM amplifier operating in current mode. The angular position of the motor is measured with a US Digital E3 encoder that gives 2500 counts per revolution.

3.1.1 Wheelchair system hardware

Power for the wheelchair is provided by two 12v, 54 amp-hour, sealed, lead-acid batteries in series, which provide 24v DC to the motor amplifiers. Hardware control for both the wheelchair and joystick systems is implemented on a 2.8 GHz Pentium 4 PC

with a DC to ATX power supply that enables it to run from the batteries. Hardware IO is provided by two Sensoray 626 DAQ cards. The Sensoray cards provide four, 14-bit analog outputs, sixteen, 16-bit analog inputs, 48 general purpose digital IO ports and up to six encoder counters per card. These two cards provide sufficient IO to control the seven degrees of freedom of the coupled system, the eight IR range finders for obstacle detection, and several other auxiliary functions which simplify data acquisition. A complete schematic of controller hardware connections is included in APPENDIX E. Software control algorithms are implemented in Simulink with Windows Real-Time Target, providing the interface to the Sensoray cards. The system proved to be most stable with the control loop operating at 1 kHz and with data logging decimated to 1/100 of the sample frequency.

3.2 **Wheelchair Control System**

3.2.1 Inverse kinematics

The wheelchair velocity is controlled with a simple PD controller. The desired velocity, as measured by the joystick position, is fed to the controller as a 3x1 vector consisting of the desired velocities in Cartesian space, $\dot{X}$, $\dot{Y}$ and $\dot{\theta}$. This vector is converted to the desired velocities for each wheel in joint-space by the inverse kinematics given in (3.1),

$$\begin{bmatrix} \omega_1 \\ \omega_2 \\ \omega_3 \\ \omega_4 \end{bmatrix} = J^{-1} R_z^T(\Theta) \begin{bmatrix} \dot{X} \\ \dot{Y} \\ \dot{\Theta} \end{bmatrix} \tag{3.1}$$

where $R_z^T(\Theta)$ is the rotational transform about the Z axis in the global reference frame and J^1 is the inverse Jacobian matrix given by (3.2).

$$J^{-1} = \begin{bmatrix} -\frac{\sqrt{2}}{2} & \frac{\sqrt{2}}{2} & \alpha L_3 \\ -\frac{\sqrt{2}}{2} & -\frac{\sqrt{2}}{2} & \alpha L_3 \\ \frac{\sqrt{2}}{2} & -\frac{\sqrt{2}}{2} & \alpha L_3 \\ \frac{\sqrt{2}}{2} & \frac{\sqrt{2}}{2} & \alpha L_3 \end{bmatrix} \tag{3.2}$$

The term α in (3.2) is found using (3.3) and is derived from the physical dimensions and constraints of the wheelchair indicated in Figure 3.1.

$$\alpha = \frac{L_2^2 + L_3^2 - \frac{1}{4}L_1^2}{2L_2L_3} \tag{3.3}$$

These equations were derived by Mascaro for the original control system of this mobile robotics platform [51].

The velocity commands produced by the inverse kinematics are integrated to provide a desired position for each wheel in joint space, which is maintained by the PD controller. The control system is kept in the local frame of the wheelchair, defined in Figure 3.1, by maintaining a fixed angle, Θ, in the inverse kinematics. This keeps velocity commands from the joystick in the orientation of the rider. A block diagram of the complete wheelchair control algorithm is shown in Figure 3.2.

3.2.2 Forward kinematics

It is necessary to use the forward kinematics given in (3.4) to determine the velocity of the wheelchair in the local frame. Because the wheelchair system is over-

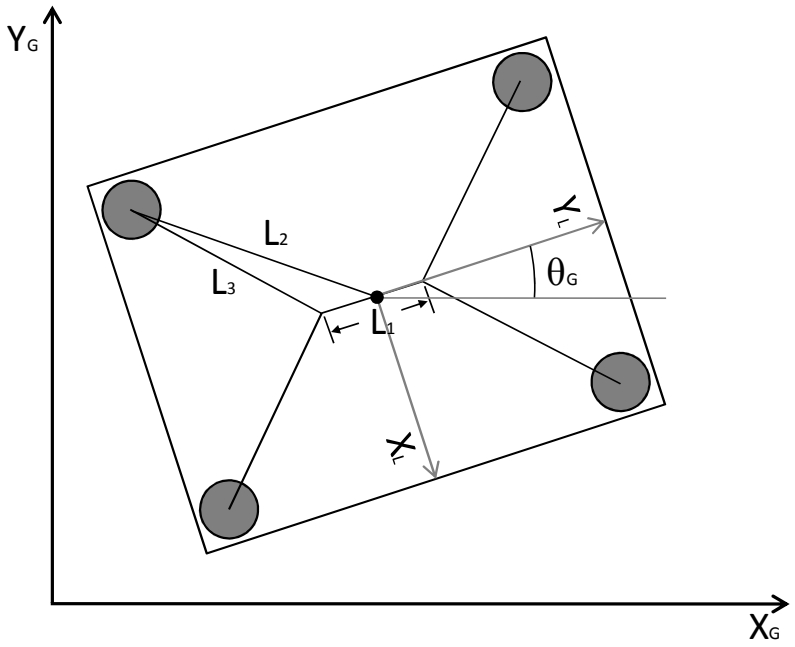

Figure 3.1: Schematic of wheelchair base showing global and local reference frames and dimensions used to calculate $J^{-1}$and J^{LM}.

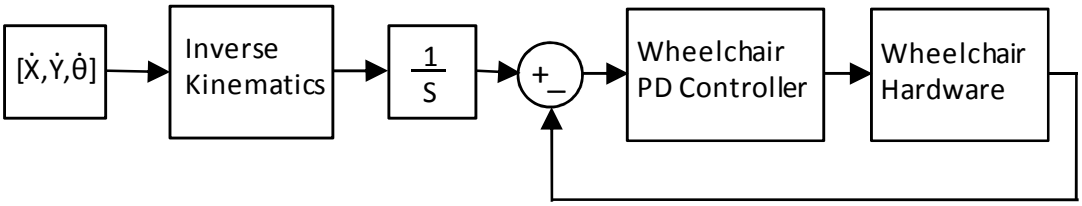

Figure 3.2: PD based velocity controller for the wheelchair base.

constrained, the inverse Jacobian is a 4x3 matrix and cannot directly be inverted. Therefore, the Jacobian matrix is obtained by using the left pseudo-inverse given in (3.5) and is indicated by J^{LM}. The numerical value for J^{LM} used in the algorithm for the forward kinematics is given in (3.6) where α is the same as for J^{-1}. As with the inverse kinematics used earlier these equations were derived for the original control algorithm for this wheelchair [51].

$$\begin{bmatrix} \dot{X} \\ \dot{Y} \\ \dot{\Theta} \end{bmatrix} = R_Z^T(\Theta) J^{\mathrm{LM}} \begin{bmatrix} \omega_1 \\ \omega_2 \\ \omega_3 \\ \omega_4 \end{bmatrix} \tag{3.4}$$

$$J^{LM} = (J^{-T}J^{-1})^{-1}J^{-T} \tag{3.5}$$

$$J^{LM} = \begin{bmatrix} -\frac{\sqrt{2}}{4} & -\frac{\sqrt{2}}{4} & \frac{\sqrt{2}}{4} & \frac{\sqrt{2}}{4} \\ \frac{\sqrt{2}}{4} & -\frac{\sqrt{2}}{4} & -\frac{\sqrt{2}}{4} & \frac{\sqrt{2}}{4} \\ \frac{1}{4\alpha L_3} & \frac{1}{4\alpha L_3} & \frac{1}{4\alpha L_3} & \frac{1}{4\alpha L_3} \end{bmatrix} \tag{3.6}$$

3.2.3 Dead reckoning algorithm

Analysis of the system performance and the feedback algorithm are dependent on being able to record the position and orientation of the wheelchair in the global frame, as shown in Figure 3.1. This is accomplished through the use of a dead reckoning algorithm which integrates the rotational velocity of the wheelchair to find the orientation in the global frame. The linear X and Y velocities in the local frame are transformed to the global frame and integrated to determine the global position. The position and orientation are recorded for later analysis. The orientation of the global frame as recorded by this algorithm is always in the orientation of the wheelchair at the beginning of the

simulation.

3.3 **Control of the Wheelchair with the Haptic Joystick**

The complete wheelchair and joystick system is shown in Figure 3.3. The control algorithms for the two systems are coupled together as shown in the block diagram in Figure 3.4. The angular position output of the joystick controller in Figure 2.5 is converted to the desired velocity vector in Figure 3.2 by the gain Kv. Velocity commands from the user's hand are modeled as a disturbance torque on the joystick. Included in the

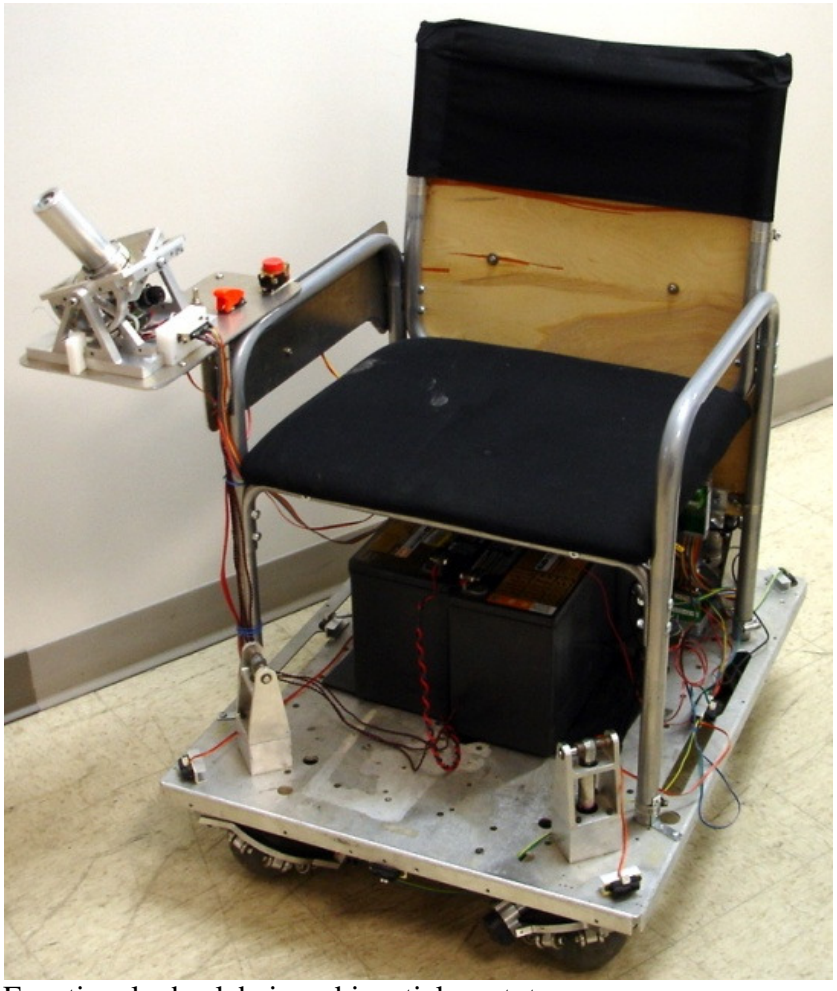

Figure 3.3: Functional wheelchair and joystick prototype.

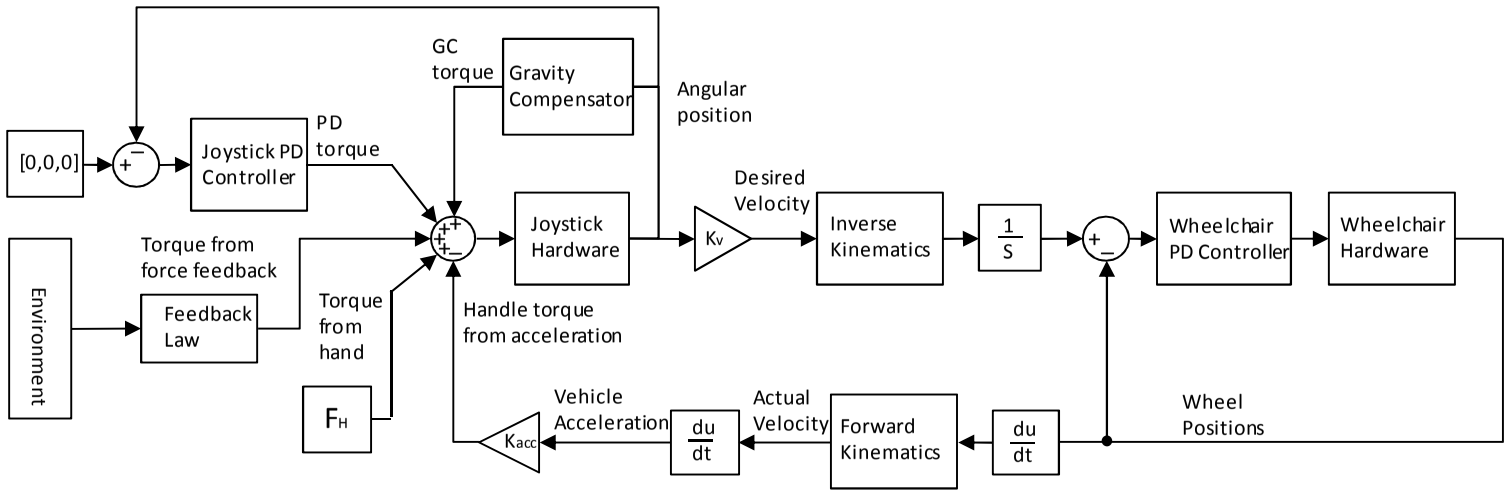

Figure 3.4: Complete wheelchair control algorithm with the joystick control on the left and the wheelchair control system on the right. Desired trajectory is provided as a function of joystick angle. The velocity gain, K_V, translates the angular position of the joystick in radians to the desired velocity in m/s. User input, inertial coupling and feedback are modeled as disturbance torques to the joystick.

feedback path on the control diagram is the inertial coupling between the wheelchair and joystick. This feedback gain K_{acc} relates linear acceleration of the wheelchair base to the resulting torque on the handle. In the model, this term is treated as a disturbance input to the joystick handle.

CHAPTER 4

STABILITY ANALYSIS OF COUPLED SYSTEM

4.1 **Unstable System**

The coupled system reproduces the classic control problem of an inverted pendulum on a cart, with the added complication that the angular position of the pendulum produces a velocity command to the cart. Given this configuration, the joystick system is potentially unstable. However, this system is comprised of two independent, stable, closed-loop-controlled subsystems. Therefore, with the selected sign convention and the gravity compensated joystick control system, it is anticipated that with moderate gain values for K_v, the coupled system should also be stable. This is because the joystick controller produces a negative velocity command in response to a positive acceleration of the wheelchair. It is anticipated, however, that excessive velocity gains may still cause instability.

4.2 **Root Locus Analysis**

In order to analyze the stability of the control system given in Figure 3.4 with a root locus method, it is necessary that it be reduced to a single-input, single-output system. This requires several simplifying assumptions and a dynamic model of multiple system elements. For this analysis, the simplified elements include a second order

approximation for the joystick, G_{JS}, and wheelchair, G_{WC}, and a reasonable approximation of the dynamic coupling between the linear acceleration and the resulting torque disturbance on the joystick, K_{acc}. These system elements were obtained through rudimentary system identification techniques, free-body diagrams, and block diagram reduction.

4.3 **Development of the System Model**

Several assumptions are necessary to model the wheelchair system. It is assumed that with gravity compensation, the response of the joystick handle can be modeled as a linear second order system. Also, it is assumed that the response in the X and Y axes will be symmetrical and identical and that linear acceleration in the wheelchair base will not result in a significant torque disturbance about the Z axis. Therefore, modeling was limited to linear motion in one axis. Other nonlinearities must be neglected in order to produce an approximate linear model. These include gear lash in the chair wheels, coulomb friction, and a command velocity dead zone near the zero point of the joystick.

4.3.1 Second order approximation of the joystick

The system response to a step input shown in Figure 4.1 was used to find an ideal second order characteristic equation that approximates the joystick response (4.1). The characteristic equation is put into the generic closed loop transfer function using the known PD gains from the actual controller. This results in the closed loop transfer function in (4.2).

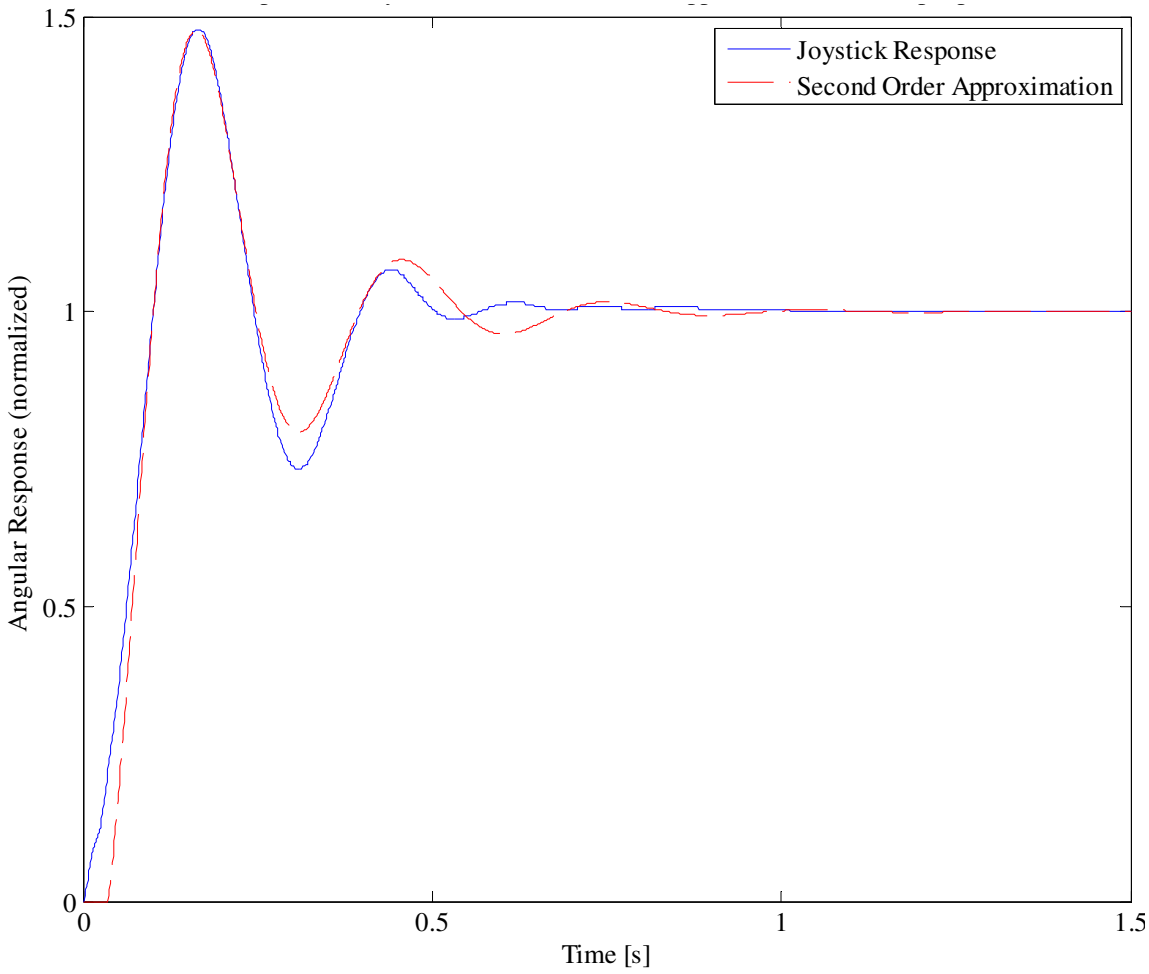

Figure 4.1: Comparison of the second order approximation to the step response of the physical joystick system.

$$G = \frac{{\omega_n}^2}{S^2 + 2\xi\omega_n S + {\omega_n}^2} \quad \textbf{(4.1)}$$

$$CLTF = \frac{\frac{K_P}{J} + \frac{K_D}{J}S}{S^2 + \frac{(b + K_D)}{J}S + \frac{K_P}{J}} \quad \textbf{(4.2)}$$

Substituting the real values of K_D=.0005 and K_P=.025 and calculating $\xi$and ω_n from the second order response of the physical system from Figure 4.1, the numerical transfer function G_{JS} given in (4.3) is obtained.

$$G_{JS} = \frac{9.768\,S\ +\ 488.4}{S^2 + 11.47S + 488.4} \quad \textbf{(4.3)}$$

In order to validate the model, the response of the transfer function to a unity step input is plotted against the response of the physical system, as shown in Figure 4.1. It is apparent from the plot that the physical system is not a perfect second order system. The approximate transfer function is not a perfect match to the physical system but is sufficient for the stability analysis.

4.3.2 Second order approximation of wheelchair system

Whereas the joystick is a serial linkage system and can be modeled using a single-input single-output system, the wheelchair employs a parallel drive system and cannot be modeled so easily. Instead, it is necessary to consider the forward and inverse kinematics outlined in Section 3.2 to obtain a model of the system in Cartesian space. The block diagram reduction outlined inAPPENDIX B shows the elements incorporated for this

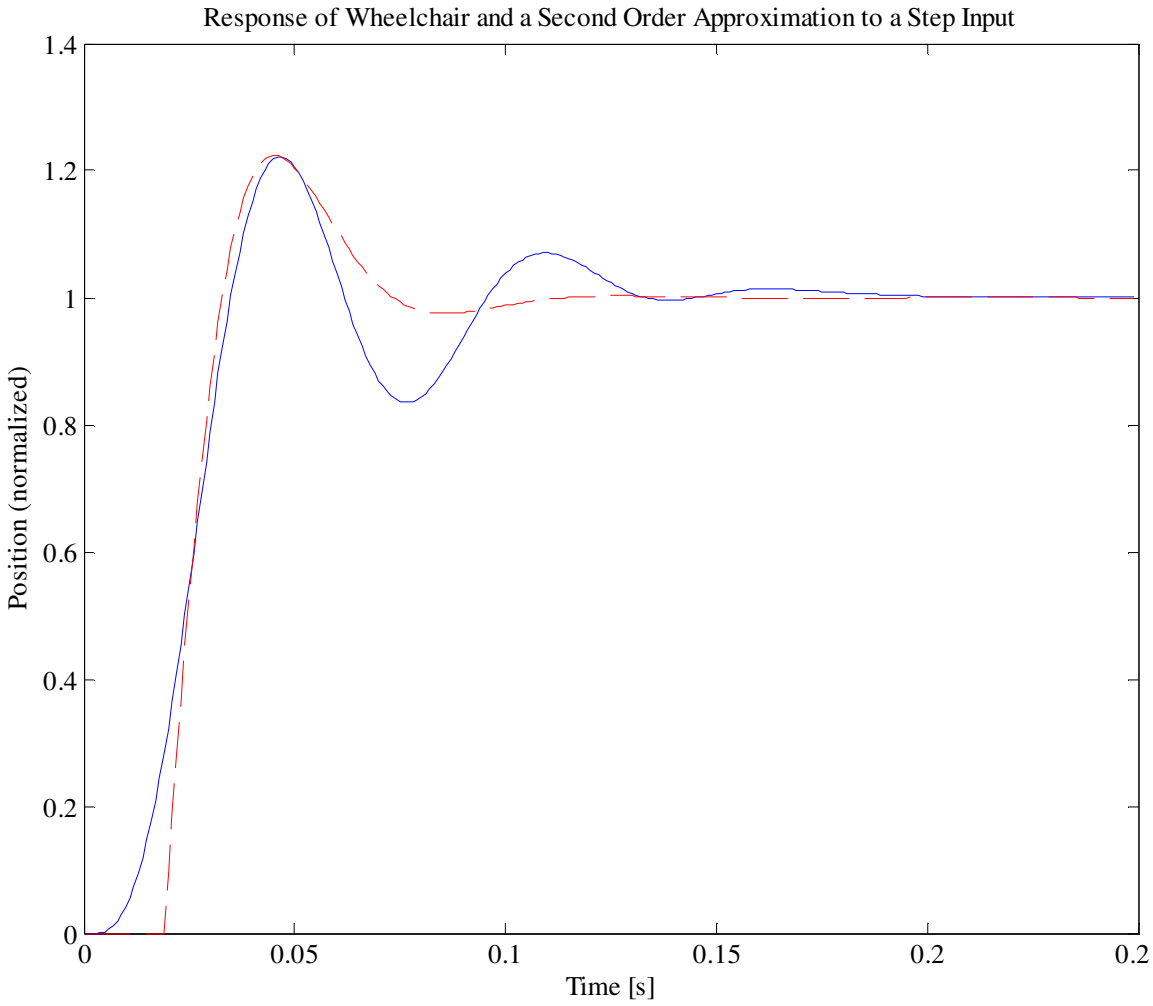

Figure 4.2: Comparison of the step response of both the physical wheelchair and the second order approximation of the system.

second order approximation. Treating the wheelchair as a lumped-parameter, second order system and using the generic second order equation given by (4.1), a reasonable second order model is obtained. Again, the values for ξ and ω_n are taken from the step response of the physical system shown in Figure 4.2. The PD gains of the wheelchair controller are K_P= 65 and K_D= .7. The resulting numerical transfer function G_{WC} used for the system model is given in (4.4).

$$G_{wc} = \frac{96.38S + 8949}{S^2 + 108.8S + 8949} \quad \textbf{(4.4)}$$

As with the joystick model, the step response of G_{WC} is plotted against the step response of the physical system. This second order approximation is not as accurate as the model of the joystick. This can be explained because either the system is not a second order system, or the amplifier saturation apparent in the first .02 seconds of the data masks the second order response. A higher order approximation would be required to produce a more accurate model. A complete derivation of the equations used for the second order approximations is given in appendix A.2.

4.3.3 Derivation of K_{acc} for system model

Beginning with a simple inverted pendulum model shown in Figure 4.3, the relationship between linear acceleration of the wheelchair and the resulting torque on the joystick handle was determined. This relationship, given in (4.5), was found using the free body diagrams for the wheelchair and the joystick handle. A complete derivation of this equation is given in appendix A.3.

$$\left(J + M_h l^2\right)\ddot{\theta} = -m_h l\ddot{X} \quad \textbf{(4.5)}$$

The model of the pendulum dynamics was linearized using the small angle approximation and the nonlinear effects of gravity were ignored because of the gravity compensation algorithm. The feedback gain K_{acc} was found by using the right side of (4.5) as the terms on the left side are lumped into the second order approximation of the joystick. The final gain for the feedback loop is given in (4.6).

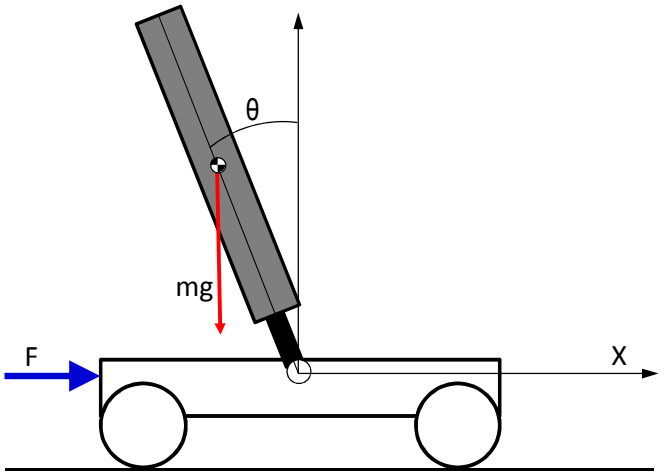

Figure 4.3: Basic inverted pendulum on a cart model used for stability analysis of the system.

$$K_{acc} = -m_h l \tag{4.6}$$

Where m_h is the mass of the joystick handle and l is the length from the axis of rotation to the center of mass. This gain could be further refined by incorporating the other eccentric loads used in the gravity compensation algorithm, but the result is sufficient for the stability analysis.

In order to validate K_{acc}, the physical response of both the joystick and the wheelchair to a step input to the wheelchair control algorithm were recorded. The response is shown in Figure 4.4. The coupling between the two systems is apparent, as a positive acceleration of the wheelchair produces a negative torque on the joystick handle. The position data from the wheelchair was used as the input to the feedback system model by taking the second derivative and multiplying it by the calculated gain K_{acc}. The resulting torque was then input as a disturbance to the second order approximation of the

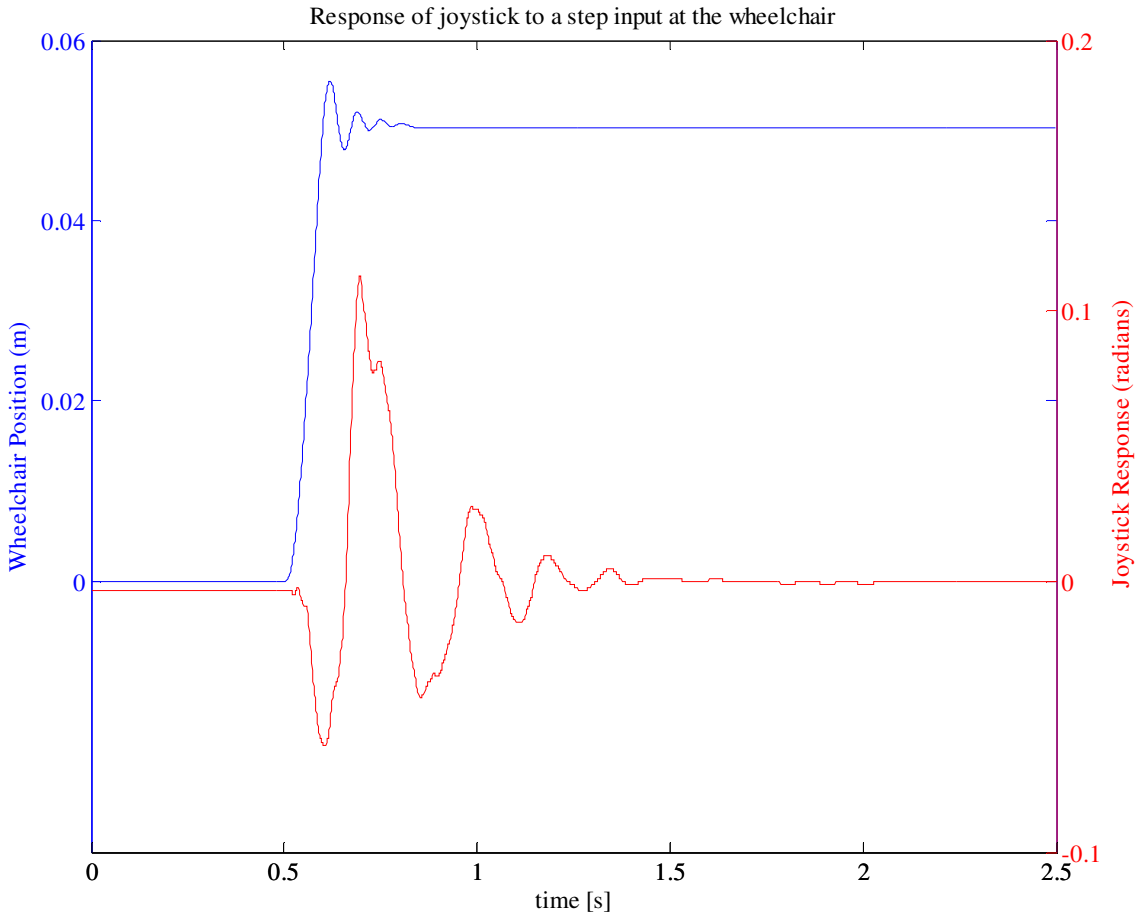

Figure 4.4: Angular response of the joystick to a step input to the wheelchair base with $K_v = 0$.

joystick controller. The result is plotted in Figure 4.5 against the response of the physical joystick to the same input. The close match between the two responses is sufficient to verify that the presented models will provide an acceptable representation of the physical system elements.

4.3.4 Assembling the model

The control system is reduced to the feedback system shown in Figure 4.6 by substituting the second order approximations into the control diagram in Figure 3.4 and performing block diagram reduction. The complete sequence of the block diagram

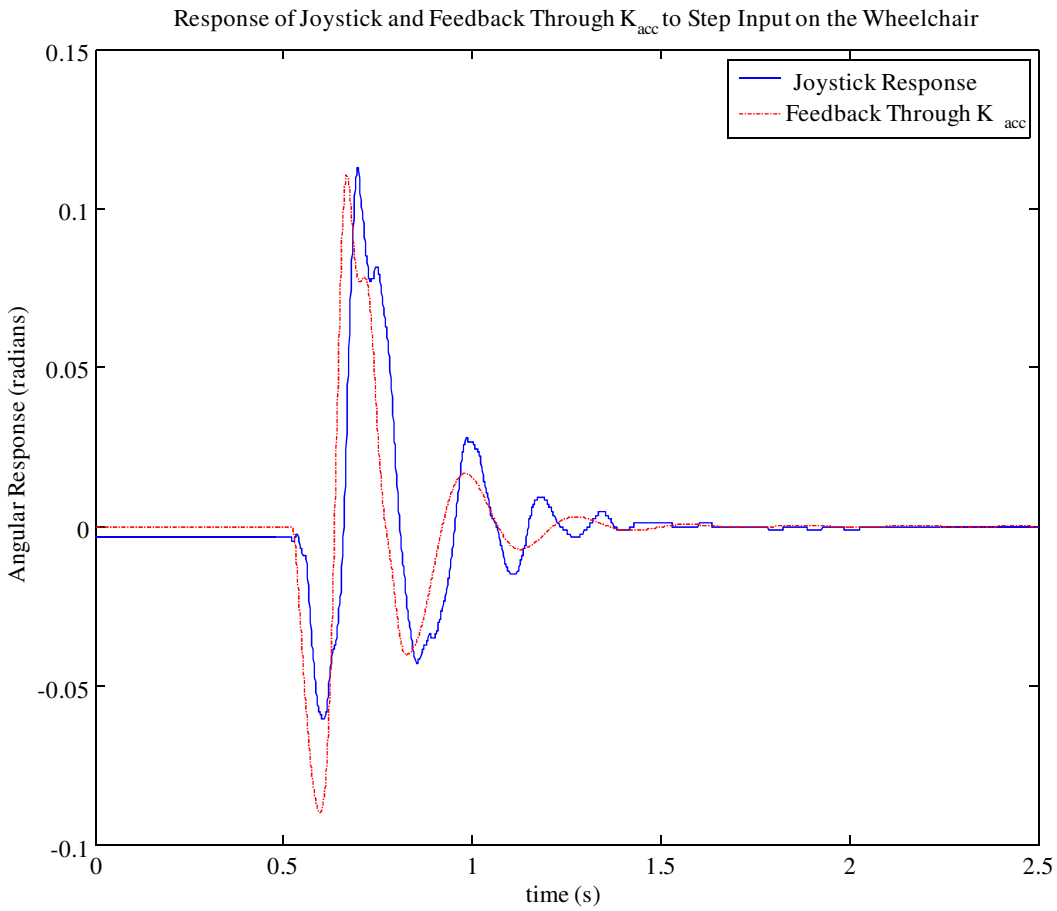

Figure 4.5: Response of joystick and second order approximation through K_{acc} to a step input on the wheelchair.

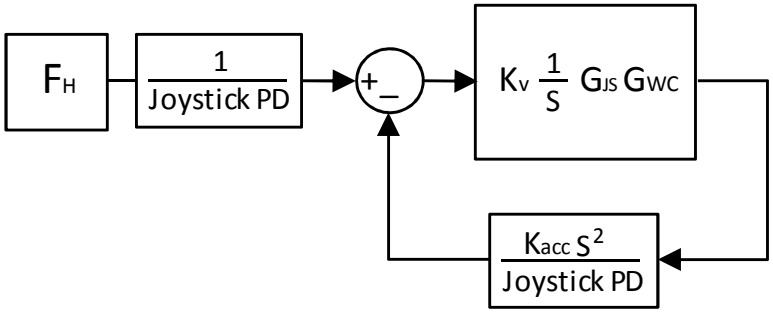

Figure 4.6: The reduced block diagram used for the stability analysis of the combined control system. K_{acc} in the feedback path represents the dynamic coupling between the wheelchair acceleration and torque on the joystick handle. Nonlinearities have been compensated for or neglected.

reduction is included in APPENDIX B. The numeric open loop transfer function for the reduced system was obtained through Matlab and is given in (4.7).

$$OLTF = \frac{19.16\,s^4 + 2737\,s^3 + 88950\,s^2}{0.0005\,s^6 + 0.08512\,s^5 + 8.349\,s^4 + 345\,s^3 + 6080\,s^2 + 10930\,s} \quad \textbf{(4.7)}$$

4.3.5 Evaluation of root locus plot and system stability

The root locus plot of the open loop transfer function is given in Figure 4.7. The wheelchair and joystick systems each contribute one zero and two poles to this plot. The complex pole pair at -5.7 ±21.3i and the zero at -50 are contributed by the slower response of the joystick. The poles at -54.4±77.4i and the zero at -92.8 are from the faster response of the wheelchair. The pole at -50 and double zero at the origin are from the joystick K_D gain and double derivative in the feedback path respectively. From the root locus plot, we estimate that the vehicle is stable through all values of K_v, however, the system becomes much more oscillatory with higher K_v gains.

The aforementioned prediction is consistent with the observed behavior of the real wheelchair system. While the system remains stable, users have reported that the wheelchair is much harder to control with higher gains of K_v. The system is operated at a safe K_V gain of .25(m/s)/radian. This value was determined experimentally based on the desired responsiveness of the wheelchair.

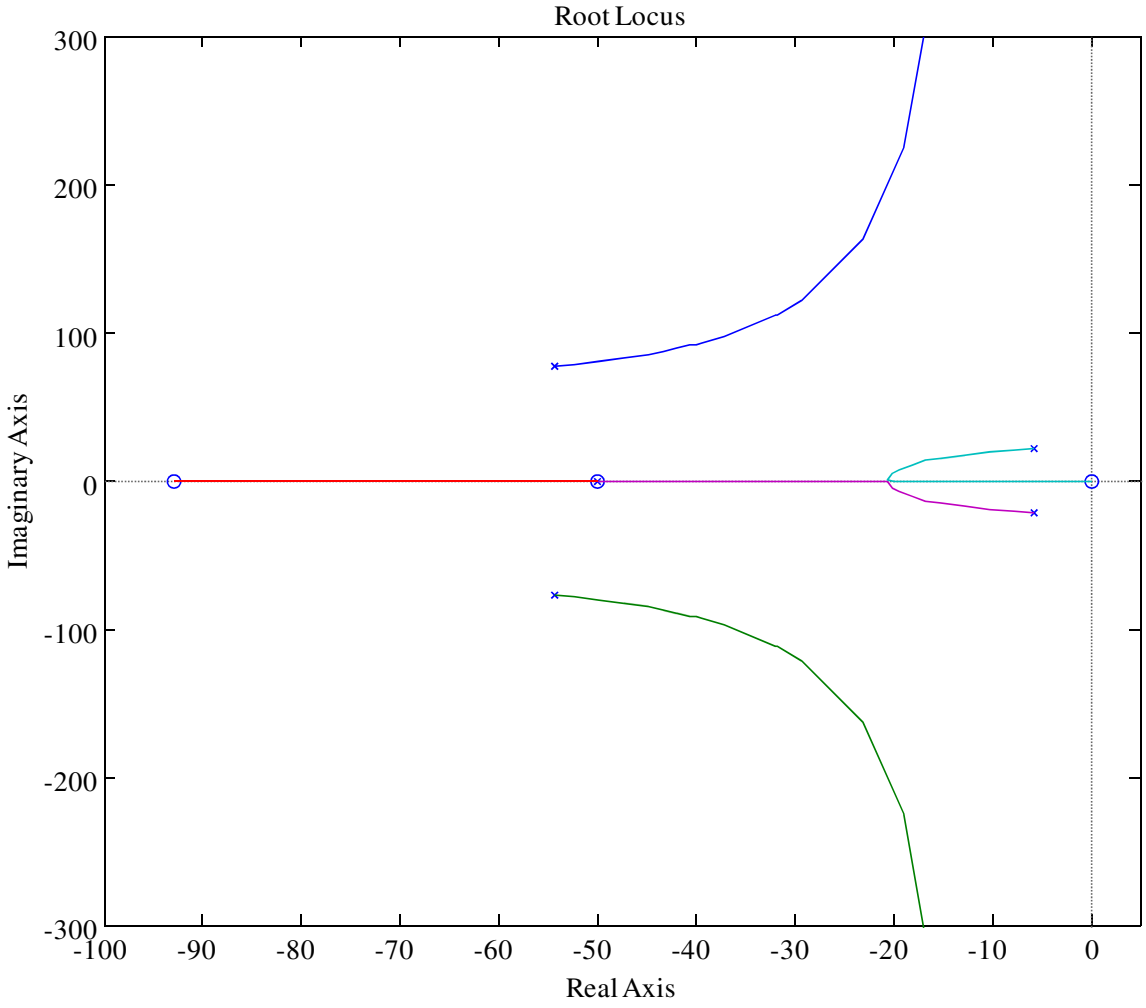

Figure 4.7: Root locus plot of reduced system including second order approximations.

4.4 **System Stability with Human Hand Interaction**

Interaction with the user can significantly alter the dynamics of the coupled system. Therefore, we must also investigate how the interaction with the hand and additional mass of the rider will affect system stability. In the literature, many simple models of the hand or arm are based on either a three or five element configuration [87].

The three element model is based on a fixed mass of the hand or arm combined with the joystick handle mass. Stiffness and damping associated with the muscle conditions in the arm, wrist or fingers is modeled by a virtual damper and spring system as seen in Figure 4.8. The five element model maintains the same mass, stiffness, and damping as the three element model but includes a virtual spring and damper between the mass of the hand and the joystick.

The five element model is typically used in grasping studies and may provide a more accurate representation of the hand dynamics, but it is less relevant for this

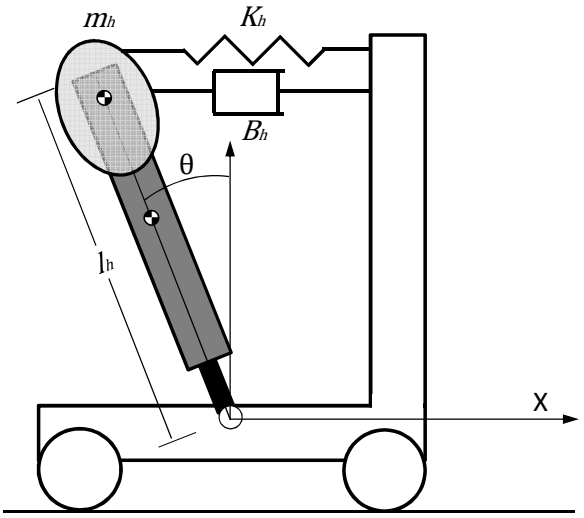

Figure 4.8: Inverted pendulum on a cart with the mass, damping, and stiffness of the human hand included. This model was used to perform stability analysis with human hand incorporated.

investigation and study of the impact of the hand on system stability. The hand interaction will be modeled as a three element system, with the mass of the hand firmly connected to the mass of the handle

In this configuration, the mass, stiffness, and damping of the hand can simply be added to the existing dynamic elements in the joystick model. The mass of the hand can be added to the mass of the handle, effectively increasing its rotational inertia. The spring stiffness of the hand combines directly with the proportional gain K_P from the PD controller and the damping, B, is combined with the K_D gain and the damping b of the physical joystick system as shown in (4.8).

$$CLTF = \frac{\frac{(K_D + B_h)}{\left(J + m_h {l_{js}}^2\right)} S + \frac{(K_P + K_h)}{\left(J + m_h {l_{js}}^2\right)}}{S^2 + 2\frac{(b + K_D + B_h)}{\left(J + m_h {l_{js}}^2\right)} S + \frac{(K_P + K_h)}{\left(J + m_h {l_{js}}^2\right)}} \quad \textbf{(4.8)}$$

Whereas the typical mass of the human hand is well known from the literature, hand stiffness and damping are partially dependent on how the user grasps the handle [88]. This makes modeling the hand interaction more difficult because a user may hold the joystick in a very light grip, offering little resistance, or attempt to overpower the feedback forces. An additional problem in incorporating the hand in the dynamic model is that the existing transfer function was not determined from individual elements but from the step response of the system.

The impact of the mass of the rider and hand interaction to the joystick is found by using the numeric transfer functions from (4.3) and (4.4) and the known values of K_p and K_D for both subsystems. The effective values for M_{wc}, J_{js}, m_h and b are solved, and along with K_P, are increased proportionally and used to recalculate a new numeric

transfer function for each subsystem and a new forward gain K_{acc}. These are then used to produce a new open loop transfer function for the altered system.

The increases to the values of K_P and b were selected arbitrarily, whereas, the other increases were intended to reproduce potential real world circumstances. Figure 4.9 shows the root locus plot of the system with M_{wc}, increased by 400%, J_{js}, and m_h increased by 250%, b increased by 500%, and the stiffness, K_P, increased by 300%. This figure also shows the general trend that each increase has on the position of the respective poles and zeros in the open loop transfer function.

Generally, adding mass has the effect of slowing the system response, moving the open loop poles to the right. The closed loop poles from the joystick transitioned into the right half plane when the added mass reached 180% of the wheelchair mass. Adding the mass of the hand only moved the close loop poles further into the right half plane. Interestingly, the increased damping pulls the open loop zero from the joystick to the right, slowing it down, but also pulled the closed loop poles from the joystick back to the left half plane restoring stability to the system. The damping had to be increased to 280% of the internal damping of the joystick to stabilize these two poles. Increasing the stiffness forces the poles to move away from the real axis and causes an increase in oscillation but had little effect on the closed loop poles of the system.

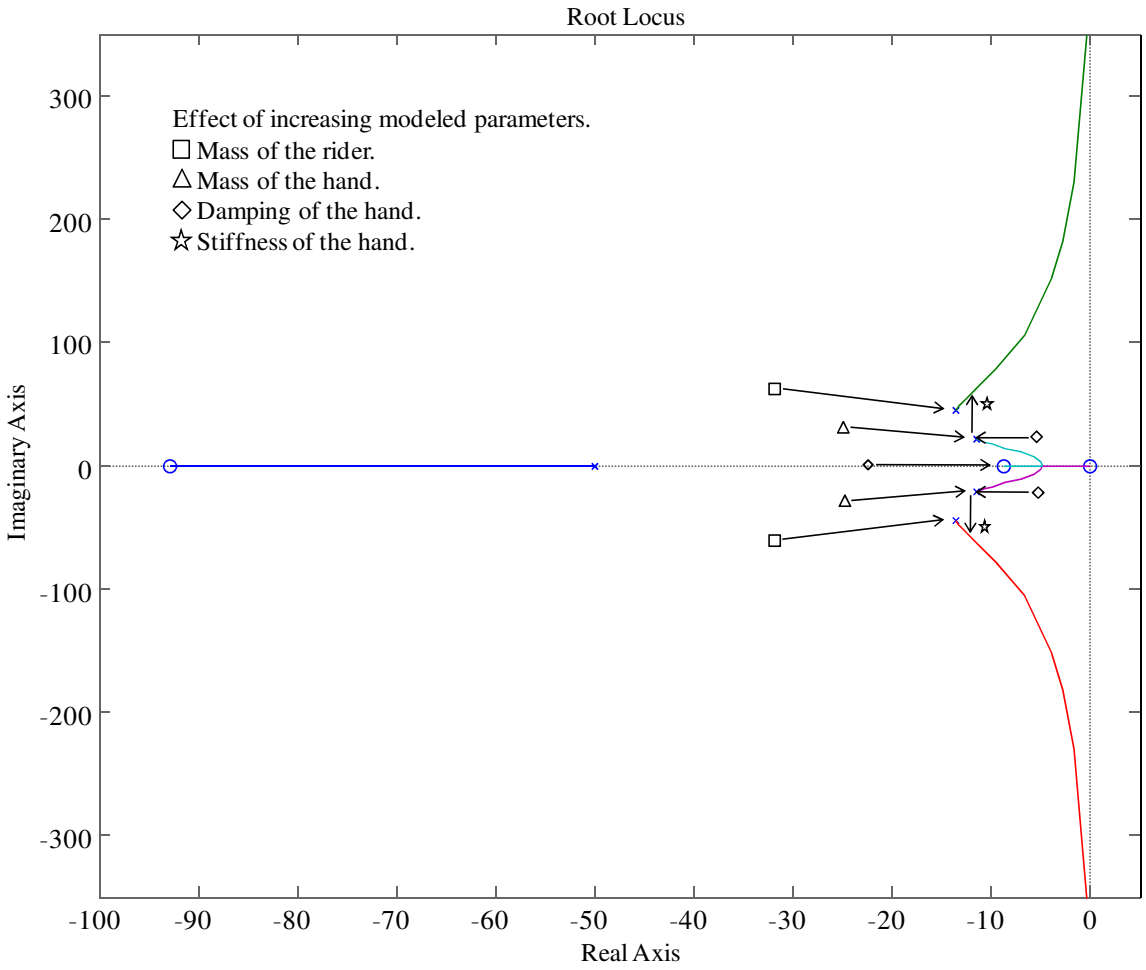

Figure 4.9: Root locus plot of coupled system with rider mass, mass, damping, and stiffness of the human hand included. Trend lines indicate the impact increasing each parameter has on the associated pole or zero.

CHAPTER 5

HAPTIC FEEDBACK FOR OBSTACLE AVOIDANCE

5.1 **Feedback Law**

5.1.1 Feedback objective

In order to inform the user of obstacles immediately surrounding the wheelchair, we want the joystick to apply a force to the hand that will prompt the user to steer away from the obstacle. This cue will be applied linearly in the direction opposite to the obstacle. Additionally, to ensure that a user does not collide with obstacles as a result of rotating the wheelchair, rotational feedback will also be applied. Both types of feedback will be especially important when the user does not have a clear line of sight to the obstacle or must navigate around multiple obstacles simultaneously, such as when backing up or rounding a corner.

To improve operation of the wheelchair in close proximity to obstacles, the feedback law will be implemented as a modified potential field which provides feedback primarily as a virtual damper and secondarily as a virtual spring. Feedback will be proportional to the relative velocity of the vehicle, as measured by the range finders. This method will provide stronger feedback when rapidly approaching an obstacle than when moving slowly toward an obstacle or immediately adjacent to an obstacle. The virtual damping feedback is expected to encourage slower speeds when approaching an obstacle,

whereas, the virtual spring will prompt the driver to maintain a minimum distance between an obstacle and the chair.

The potential field method is the most commonly implemented feedback law for this type of research, but it must be modified from the conventional configuration to provide feedback for obstacle avoidance. Originally designed for path planning, potential fields are implemented using attractive and repulsive forces, pushing and pulling the wheelchair toward the goal. Customarily, these forces are calculated as virtual springs with the force applied proportionally to the distance between the obstacle and the robot. But, because we desire the vehicle to be operated in close proximity to objects, a virtual damper is preferred. In this application, the goal is provided by the user, therefore, only half of the classical path planning technique, the repulsive forces from obstacles, is used. Other path planning methods, like the VFH methods or modulated impedance models described in the literature review, could have been used. However, the available hardware did not lend confidence that they would be successfully implemented.

5.1.2 Sensor placement and the feedback law

Implementing the potential field requires some form of proximity or range finding sensors to determine the distance between the chair and obstacles in order to provide the desired feedback. The feedback law is based on placing one sensor at each corner and one on each side, as shown in Figure 5.1. Both rotational and linear feedbacks have been incorporated into the feedback law. It is implemented using (5.1),

$$F_{fb} = [Q][\dot{X_s}] + [R][X_s] \quad \textbf{(5.1)}$$

where X_s is the 8x1 array of measurements from the sensors, and $\dot{X}_s$ is the relative

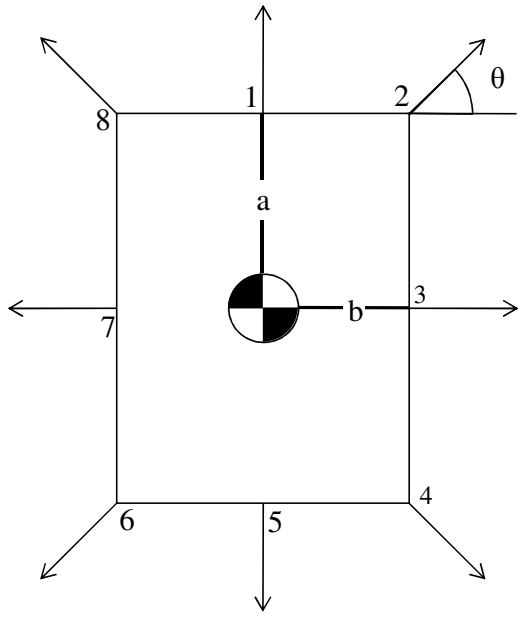

Figure 5.1: Configuration of IR Range finders used in the calculation of the force feedback.

velocity between an obstacle and the wheelchair found by taking the derivative of the using (5.2) and (5.3) respectively. *B* is the virtual damping coefficient and is set much higher than, *K,* the virtual spring coefficient, to ensure that damping is the primary feedback mode. In this equation, $c\theta$ is the cos(θ), $s\theta$ is the sin(θ), and a and b are the respective distances from the center of rotation to the edges of the wheelchair. A complete derivation of the feedback law is given in appendix A.4.

$$[Q] = \begin{bmatrix} 0 & -Bc\theta & -B & -Bc\theta & 0 & Bc\theta & B & Bc\theta \\ -B & -Bs\theta & 0 & Bs\theta & B & Bs\theta & 0 & -Bs\theta \\ 0 & aBc\theta - bBs\theta & 0 & -aBc\theta + bBs\theta & 0 & aBc\theta - bBs\theta & 0 & -aBc\theta + bBs\theta \end{bmatrix} \quad \textbf{(5.2)}$$

$$[R] = \begin{bmatrix} 0 & -Kc\theta & -K & -Kc\theta & 0 & Kc\theta & K & Kc\theta \\ -K & -Ks\theta & 0 & Ks\theta & K & Ks\theta & 0 & -Ks\theta \\ 0 & aKc\theta - bKs\theta & 0 & -aKc\theta + bKs\theta & 0 & aKc\theta - bKs\theta & 0 & -aKc\theta + bKs\theta \end{bmatrix} \quad \textbf{(5.3)}$$

The result is a three-dimensional feedback vector that corresponds to feedback in X, Y, and θ. The calculated forces are passed as a disturbance to the joystick control system in the same way as the user input and inertial coupling described in CHAPTER 3.

5.1.3 IR range finders

Two possible low-cost options for providing the measurements are infrared or ultrasonic range finders. Because they were more readily available, the array was constructed with Sharp IR range finders like the one shown in Figure 5.2. To provide the required distance measurements, these sensors were placed around the wheelchair in the configuration shown in Figure 5.1. The data sheet for the range finders specifies that they have an effective range of approximately 45 cm and a signal update frequency of about 25Hz.

The IR range finders return a voltage that has an inverse relationship to the measured distance. The signal is not linear, but rather parabolic in form with the peak at approximately 7cm in front of the sensor. To accommodate this nonlinear response, the sensors were placed several centimeters back from the outside edge of the wheelchair. With the inverse relationship between the voltage and distance, a positive velocity is defined as being toward the center of the wheelchair.

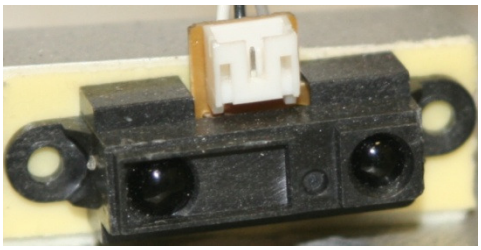

Figure 5.2: Sharp IR range finder used to measure distance to obstacles in the environment.

The primary problem with these sensors is not the parabolic nature, but the noise level of the signal. When out of range of an obstacle, the signal from the sensors is excessively noisy, as shown by the upper trace of Figure 5.3. This is a significant problem, because the force feedback law is based primarily on virtual damping. This requires taking the derivative of the sensor signal in order to find the relative velocity between the wheelchair and the obstacle.

In order to reduce the noise from the sensors, two layers of filtering were used. The first is a hardware RC low-pass filter with a cut off frequency of 20Hz. The second layer of filtration was implemented with a first order, low-pass filter with a frequency cutoff of approximately 15Hz and a voltage saturation which shifted the voltage by approximately one volt. This eliminated the free floating noise when the sensor was out of range of an obstacle. The voltage shift and first order, low-pass filter were both implemented in Simulink as part of the control block diagram. The filtration reduced the sensors' effective range to approximately 30 cm, but returned a signal which was clean enough to use for the feedback law, as seen in the lower trace of Figure 5.3.

Because each sensor has a unique response curve, some of the sensors still produce occasional ripples that make it through the filter. These ripples are interpreted as an obstacle by the feedback law and result in an impulse in the joystick handle. This could be eliminated by implementing a unique calibration constant, first order filter, and voltage shift for each sensor.

5.2 **Stability Analysis of System with Feedback**

Because feedback is added to the joystick as a disturbance, it is sensible to

evaluate the impact of the feedback on system stability. As with the previous stability

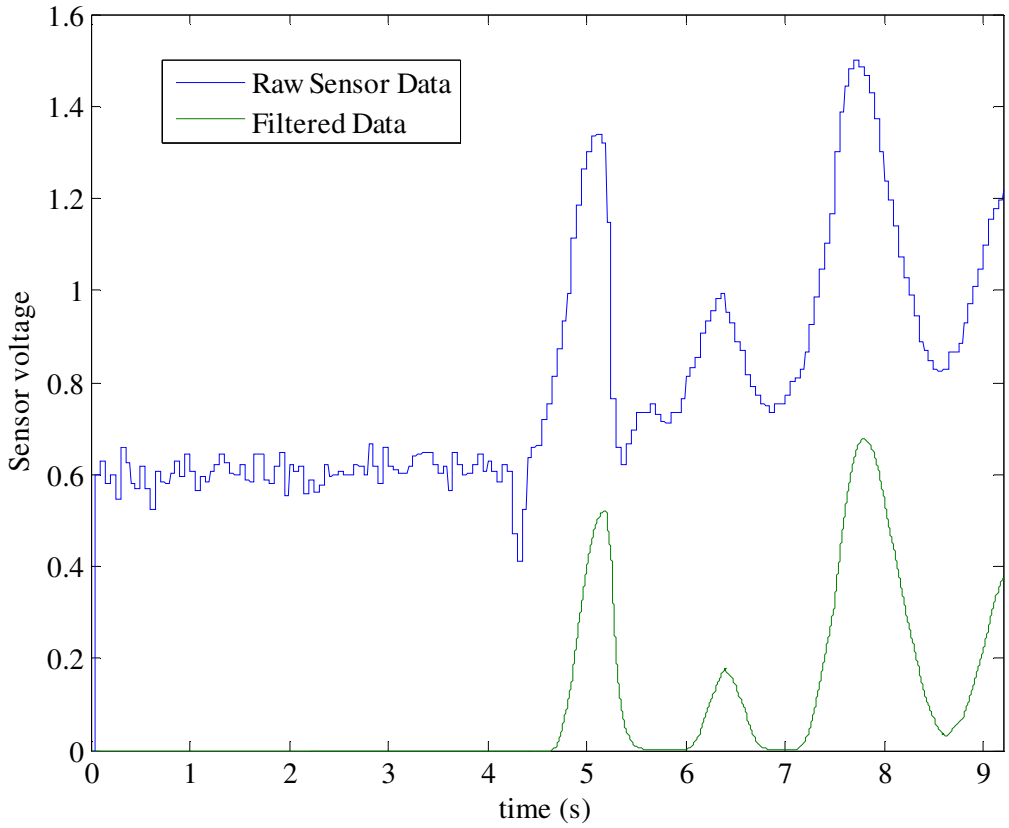

Figure 5.3: A sample of both filtered and unfiltered data from sensor 7 in the proximity of an obstacle.

analysis, the feedback law needs to be simplified in order to incorporate it into the root locus plot. The previous analysis was based on a single-input, single-output system. Consequently, incorporating feedback into the model requires it to be reduced to a single sensor system, as shown in Figure 5.4. For the entire system, the relative velocity for each sensor is positive toward the center of the wheelchair. Therefore, in the simplified model, the velocity relationship between the sensor velocity and the wheelchair velocity is given by (5.4).

$$\dot{X}_s = -\dot{X}_{wc} \tag{5.4}$$

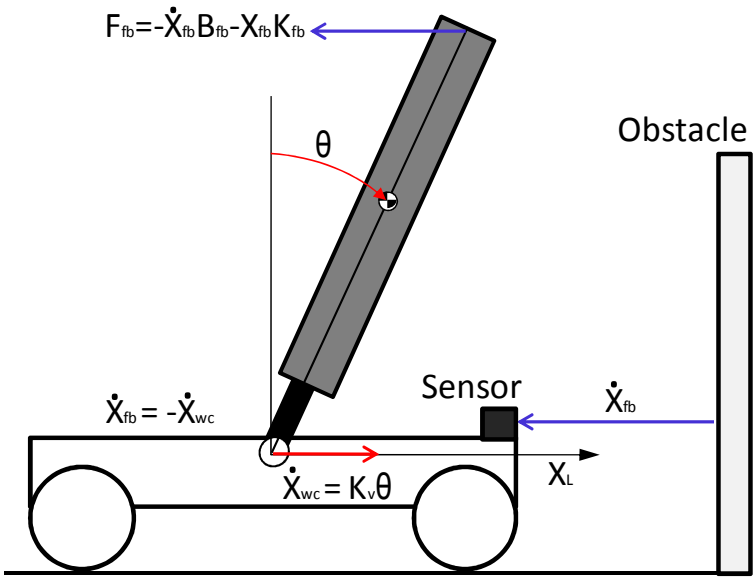

Figure 5.4: Simplified inverted pendulum with force feedback.

Considering only a single sensor reduces the feedback law to (5.5).

$$F_{fb} = -B\dot{X}_s - KX_s \tag{5.5}$$

Equation (5.4) is substituted into (5.5) and incorporated into the feedback path, resulting in the feedback law given in (5.6).

$$F_{fb} = B\dot{X}_{wc} + KX_{wc} \tag{5.6}$$

This law is incorporated into the feedback path of the block diagram shown in Figure 5.5.

The root locus plot of the resulting open loop transfer function is given in Figure 5.6. Incorporating the feedback algorithm in the analysis added one zero to the plot and forced the closed loop poles into the right half plane with high values of K_V. Otherwise, the addition had little effect. This analysis confirms that with reasonable gains of K_V, the system remains stable.

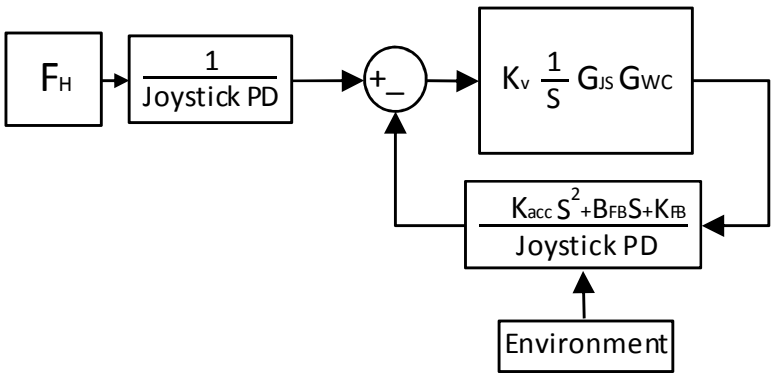

Figure 5.5: Modified block diagram with feedback included.

5.3 **Alterations of the Feedback Law from Experimental Observations**

Experimentation revealed the necessity to alter the feedback configuration. Whereas the virtual damping was effective while approaching obstacles, it was equally applied as the vehicle retreated. This gave the wheelchair system a "sticky" feeling in the proximity of obstacles. The feedback law was modified so that feedback would only be provided if the wheelchair was approaching an obstacle. The feedback law also caused the stationary wheelchair to react as people approached it. Therefore, the control law was further altered so that no feedback would be produced in the absence of an active steering command. The modified feedback law is given by the nonlinear system in (5.7), where the relative velocity for each sensor $\dot{X}_{s_i}$is altered individually based on its sign.

$$F_{fb} = \begin{cases} 1, |\theta| > C \\ 0, |\theta| > C \end{cases} * \begin{cases} B\dot{X}_s & for\ each\ \dot{X}_{s_i} > 0 \\ 0 & for\ each\ \dot{X}_{s_i} < 0 \end{cases} + KX_s \qquad \textbf{(5.7)}$$

Feedback is disabled unless the angular position of any of the joystick axes is greater than the cutoff angle specified by c. The feedback from virtual stiffness is left unaltered from the previous equation.

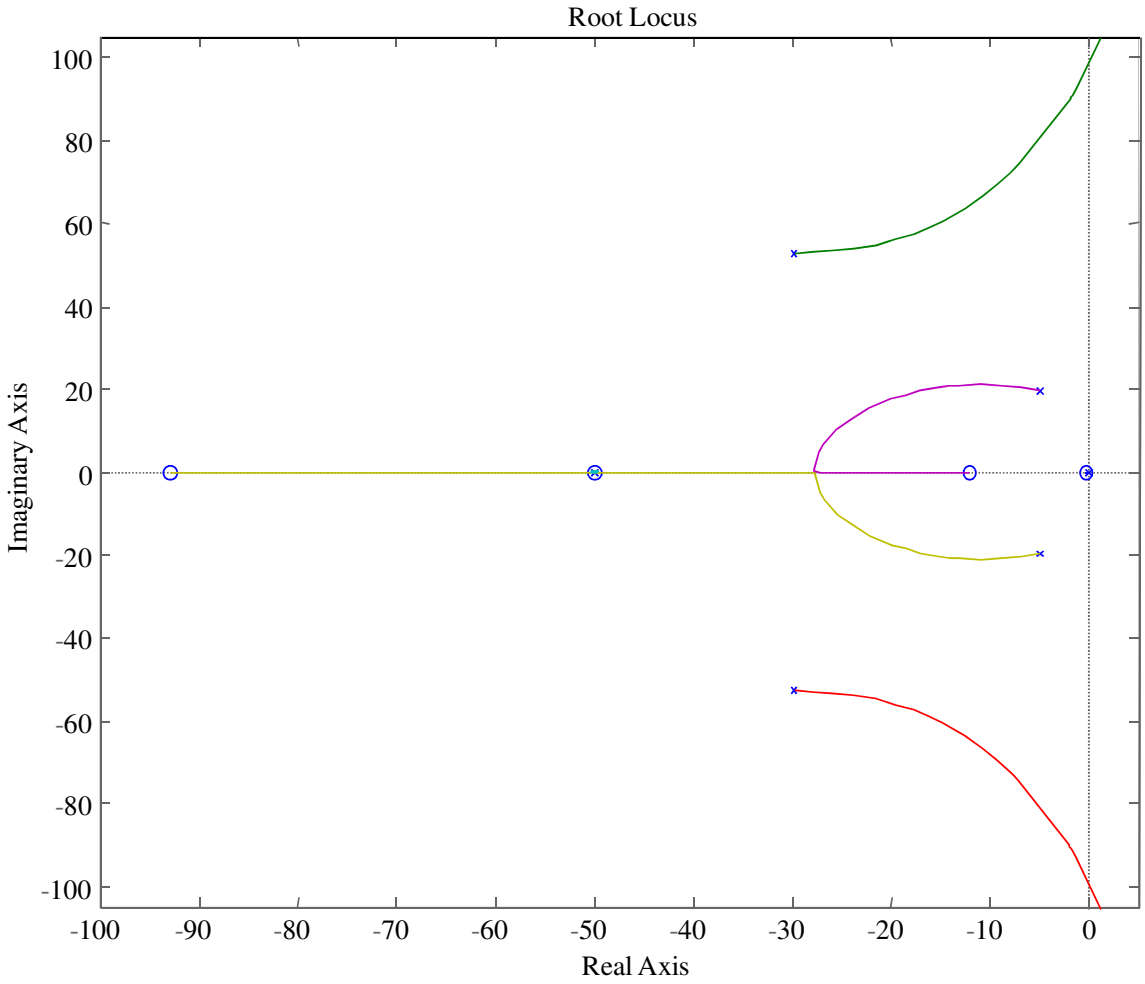

Figure 5.6: Root locus plot of system model including feedback algorithm.

Given these alterations, it is possible to find situations in which the nonlinearities in the system could cause excessively oscillatory or unstable behavior, such as when two obstacles on opposite sides of the wheelchair are detected simultaneously. In such a case oscillation may be caused due to limit cycling from the unidirectional feedback law.

5.4 **Experimental Validation of the Haptic Feedback Law**

5.4.1 Experimental procedure

The functionality of the feedback law given in (5.7) was tested by operating the wheelchair in close proximity to various obstacles. Force feedback commands and the trajectory of the wheelchair, as calculated by the dead reckoning algorithm, were recorded at a rate of 10Hz. Where possible, a similar trajectory, with and without feedback, was recorded to allow for qualitative evaluation of the feedback algorithm's performance.

The results are presented as two graphs. The first graph shows the path of the wheelchair's center of rotation in Cartesian space along with a geometric representation of the operating environment. The wheelchair's orientation at discrete time intervals is also plotted on the graph. The second graph is a series of small graphs showing the feedback corresponding to these time intervals. The feedback forces and torques are plotted as a vector and an arc segment on a representation of the joystick, as seen from above. The X and Y components of the feedback are represented as a single vector with the tail at the center of the joystick. Rotational feedback is presented as an arc segment. The force or torque presented to the user is proportional to the length of these arc and vector segments.

5.4.2 Results

Figure 5.7 shows the recorded path of the wheelchair as it approached an outside corner on the left hand side of the driver with feedback enabled. The objective of this scenario was to approach the corner and follow the wall as closely as possible without

collision. The effect of the feedback is evident. The feedback forces cause both translation and rotation away from the obstacle. These data show that the feedback leads the change in trajectory by approximately 100ms. The effect of the individual range finders on the feedback can also be seen. For example, beginning at approximately 8.5 seconds there is a drop in the feedback, despite the fact that the wheelchair is still in close proximity to the corner. The feedback drops as the corner moves away from sensor 8 on the front left corner of the wheelchair and resumes at approximately 9 seconds as the corner is detected by sensor 7 on the left side of the wheelchair.

This scenario's feedback-free counterpart is shown in Figure 5.8. In this case, the objective was the same as that recorded in Figure 5.7. Although the user slowed to avoid a collision as he approached, he accidentally clipped the corner. In this case, the operator was an experienced rider but was still not fully "embodied" in the wheelchair. The collision occurred at approximately 9 seconds. The ensuing misalignment and shifting of the chair's position is due to a combination of attempting to free the chair from the wall and accumulated error due to slip in the wheels.

The task objective in Figure 5.9 and Figure 5.10 is to approach the wall at an angle and turn, closely following the wall without collision. As with the previous scenario, the feedback was able to alter the behavior of the wheelchair.

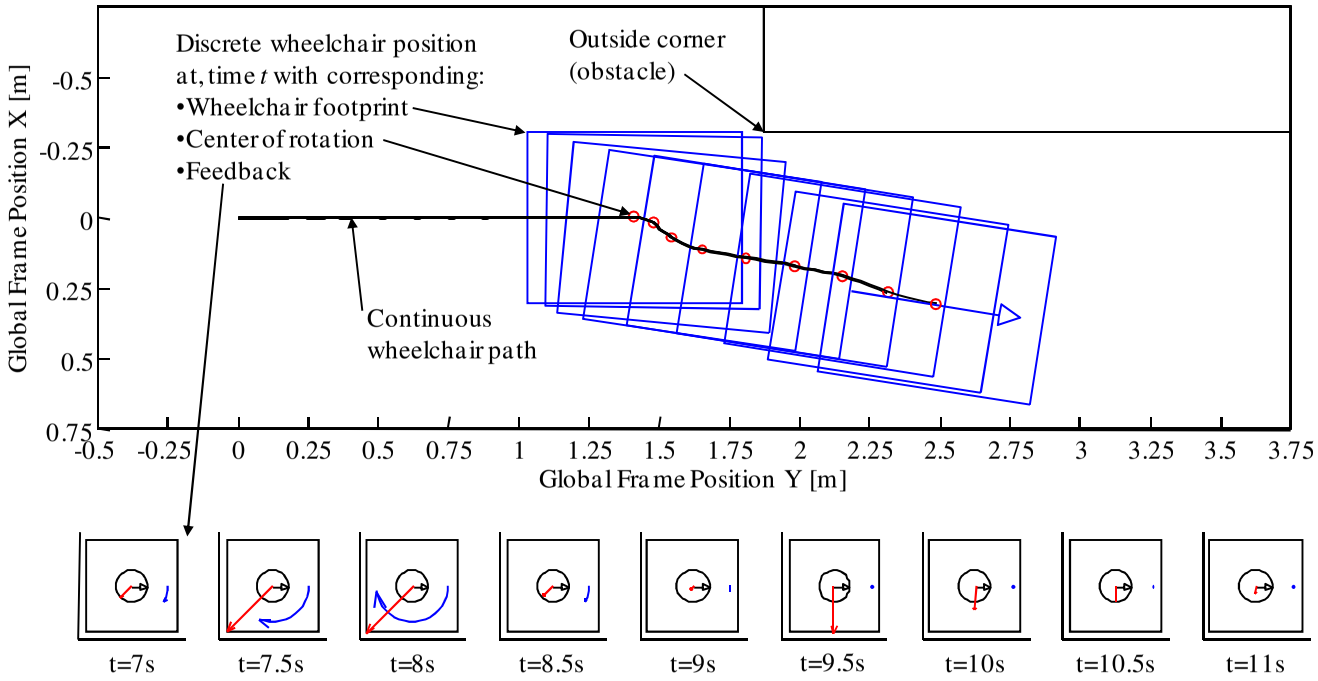

Figure 5.7: Position and orientation of the wheelchair in the global frame while approaching an outside corner. Feedback to the user is shown superimposed on a representation of the joystick as seen from above.

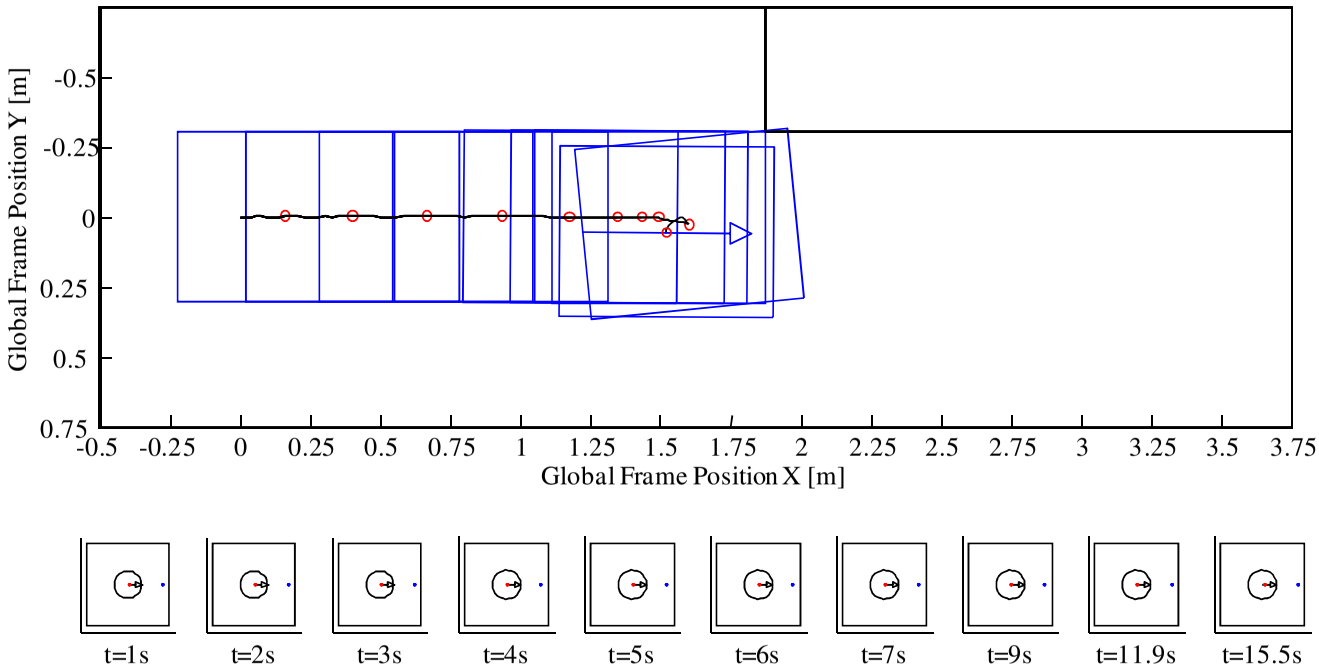

Figure 5.8: Path of wheelchair repeating the trajectory of Figure 5.7 without feedback, despite the user slowing to avoid the corner, an accidental collision was recorded.

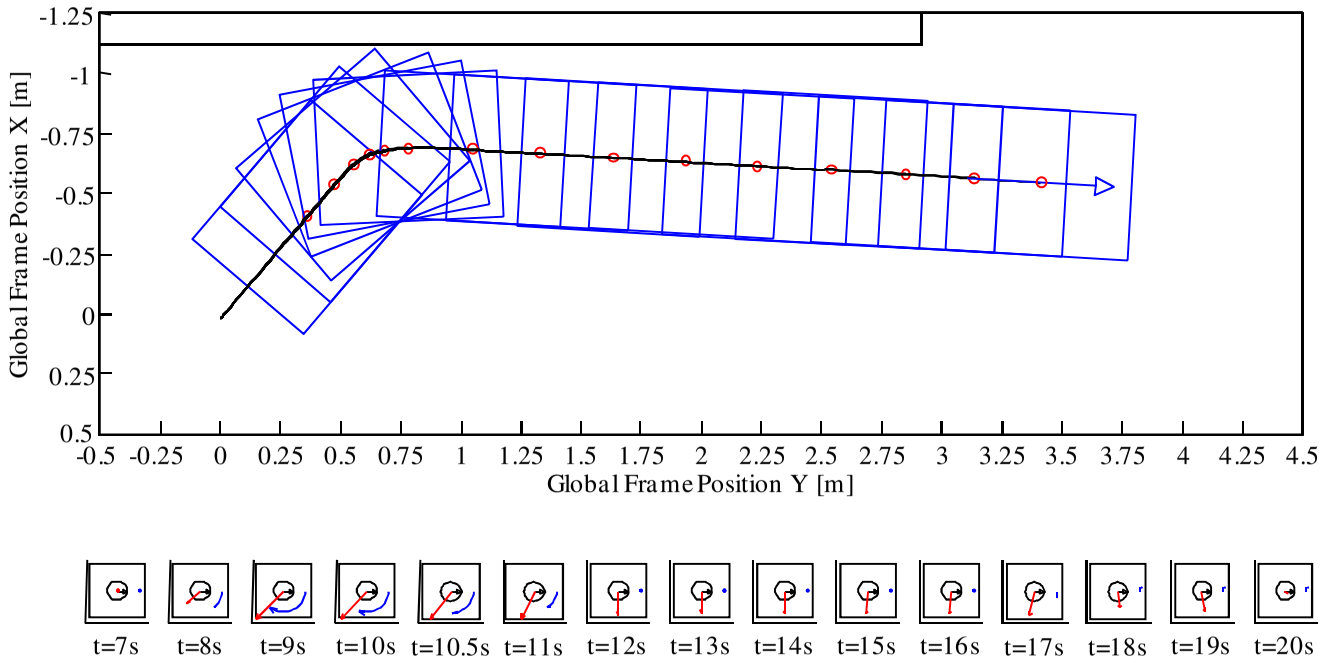

Figure 5.9: Path of wheelchair approaching and turning to follow wall. The feedback helps maintain a smooth trajectory after the turn.

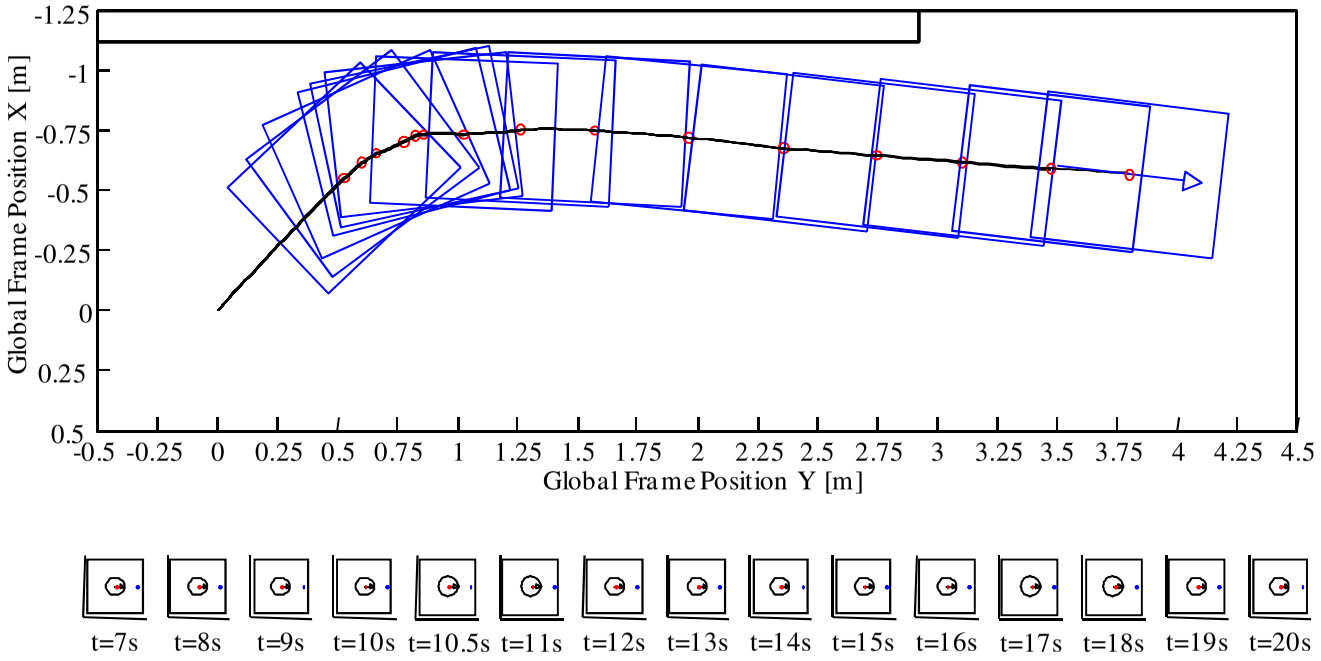

Figure 5.10: Repeating the trajectory of **Figure 5.9** without feedback. The trajectory is not as smooth after the turn to the wall.

The operator reported that the feedback not only assisted in avoiding the wall while turning, but that it also assisted as he paralleled the wall. After the turn, the feedback is a nearly constant force to the right as shown in Figure 5.9. The unassisted path in Figure 5.10 shows greater variation in the velocity and less consistency in the trajectory as the user was required to continually adjust the velocity to avoid collision.

In these two scenarios, variation in the path is more relevant for evaluation of performance than the overall position. Both Figure 5.9 and Figure 5.10 show the wheelchair following a path that separates from the wall. This is contrary to the observations of the rider. The path data is generated by the dead reckoning algorithm. The frame of reference for the global frame is established from the initial position and orientation of the wheelchair. Not shown on these two plots is that the wheelchair starts in the orientation of the global reference frame and then rotates to the angle at which it approaches the wall. The deviation in the orientation is due to error accumulated in the integrator during these rotations and slip in the wheels. This indicates that without an additional external reference, the present implementation of the dead reckoning algorithm will only be viable for short periods with limited angular displacements.

The final scenario used to test the feedback algorithm was to approach and enter a narrow, 32 inch wide hallway. No feedback-free counterpart for this scenario was recorded. This scenario is interesting because both walls were within the range of sensors on either side of the wheelchair at the same time. As mentioned in the stability analysis in section 0, simultaneous inputs from sensors on opposite sides of the vehicle may excite oscillations in the feedback due to limit cycling caused by the unidirectional damping in the force feedback law. This effect was not modeled or evaluated in the stability analysis

and could potentially cause instability. In this scenario, the feedback initially served to align the wheelchair with the hallway but ended with inducing oscillation as seen in Figure 5.11. If the system had been left to settle, the oscillation would have eventually damped out, moving the wheelchair to an equilibrium point near the center of the hallway.

As implemented, the feedback system is capable of influencing the trajectory of the wheelchair and informing the user of obstacles in the environment. However, the system has significant limitations in both the sensor array and the currently implemented feedback law. Although the system is far from optimized, it does provide a foundation from which further research can be performed.

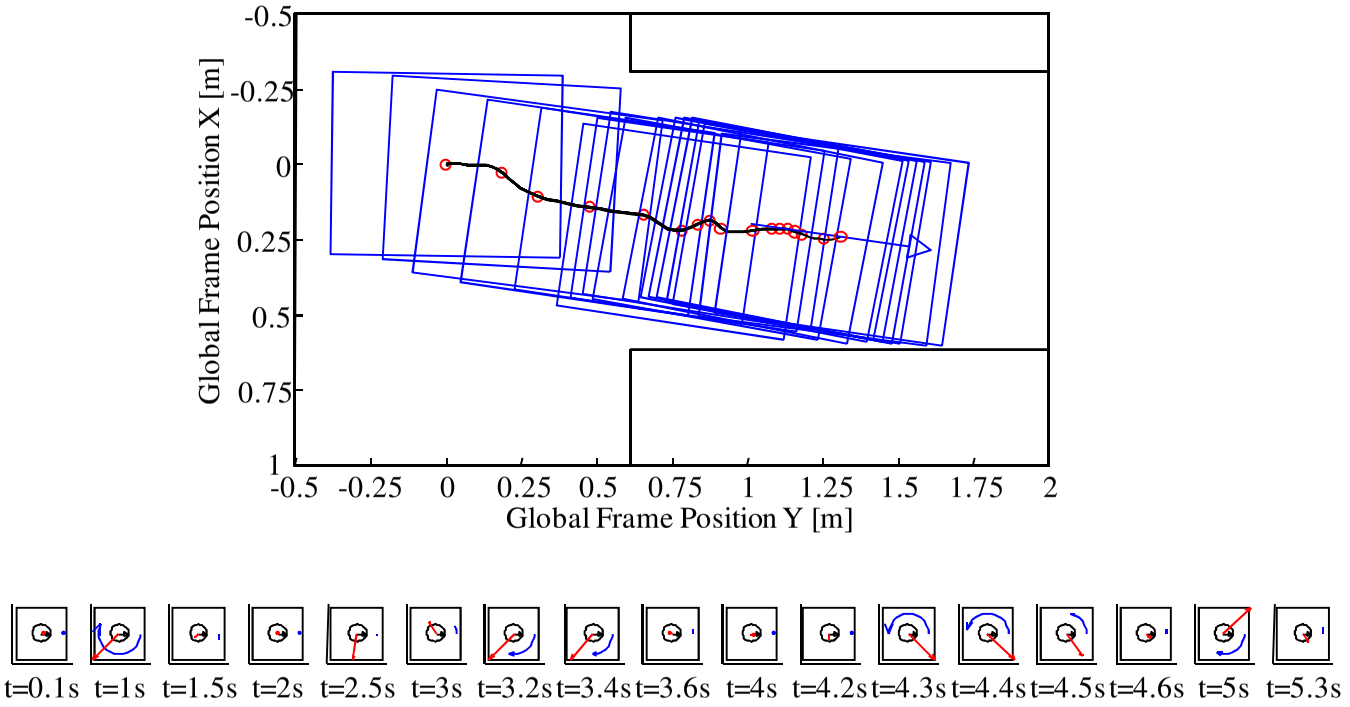

Figure 5.11: Path and feedback of the wheelchair entering a 32 inch wide hallway. Oscillation seen as the system begins to align with the entry.

CHAPTER 6

CONCLUSION

6.1 Summary of Performance and Functionality

Omnidirectional wheelchairs can improve mobility for the growing disabled population. We hypothesize that problems of embodiment and difficulty controlling the omnidirectional wheelchair can be addressed by proper application of intuitive control systems with corresponding haptic feedback. The goal of this research is to assist drivers of omnidirectional wheelchairs by producing an intuitive haptic controller for holonomic planar motion and developing a system enabling the user to sense and avoid obstacles surrounding the wheelchair.

The 3-DOF Haptic Joystick and feedback algorithm presented fulfill the initial goals of this research. The joystick provides an intuitive control system for the ball-wheeled vehicle and could easily be adapted to any holonomic omnidirectional wheelchair. Experimental evaluation verifies the feedback system's ability to alter the trajectory of the wheelchair in response to environmental obstacles.

The hardware design and manufacturing of the joystick produced a high-fidelity, high-resolution, haptic device reminiscent of the haptic paddles from which it was inspired. The pre-loaded capstan drive provides for very smooth, lash-free power transmission. The inverted mass of the joystick handle required the development of a

gravity compensation algorithm and the joystick must be constantly controlled to maintain the zero position. The primary shortfall of the joystick is the lack of power available from the motors. The lack of back-drivability in the gear heads forced their removal, robbing the haptic joystick of the designed torque and reducing its force capabilities.

The gravity compensated joystick control system was coupled to the wheelchair control system through the velocity gain K_v, and the dynamics of the combined systems were modeled as an inverted pendulum on a cart. Through root locus techniques, the combined system was proven to be stable for all values of K_v. However, as K_v increases the system becomes more oscillatory. The stability analysis was extended to include the mass of the rider and the mass, stiffness, and damping of the human hand. These additions may cause instability depending on how the user chooses to interact with the interface.

The potential field feedback law was designed around a virtual damping algorithm to discourage rapid velocities towards obstacles. However, the system also incorporates virtual stiffness to encourage the user to keep a minimum distance between the chair and any given obstacle. Experimentation revealed the need to limit the feedback to positive relative velocities in order to avoid a "sticky" feeling in the control system when pulling away from obstacles. Additionally, feedback was disabled in the absence of an active steering command.

Because the feedback causes a disturbance to the joystick, the stability analysis was extended to include the feedback law. The extended analysis showed that though stability can be affected by excessive feedback gains K_D, stability is maintained with

realistic values for K_D and within the same moderate gains of K_v which were used previously.

6.2 **Future Work**

Questions of how the system improves embodiment are better addressed by psychological researchers, but the optimization of the feedback law provides fertile ground for future research. In the near future, work on this system should focus on replacing the motors on the haptic joystick to provide additional torque for feedback.

Improvement of the feedback algorithm will require an improved sensor array. This could be accomplished by adding additional sensors in the dead zones near the corners. If additional funding were secured, laser range finders such as those used on the wheelchairs from the Toyohashi University of Technology would be useful. Alternatively, an intelligent vision system implemented with USB cameras similar to the work of Laura Marshal-Crespo at the University of California, Irvine would be worth pursuing.

With improved force feedback capability and an improved sensor array, significant work could be done to improve the understanding of human perception of obstacles in the environment. These obstacles need not be limited to physical objects in the path but could be defined as the limits of human comfort in holonomic planar motion. Further, employing the haptic concept of detents and haptic interface points, the system could also be adapted for use as a training system, or to encourage optimized path following. The availability of an omnidirectional vehicle with an integrated 3-DOF Haptic Joystick for control, provides a rich field for future research.

APPENDIX A

DERIVATIONS

A.1 Gravity Compensation

Table A.1: Numeric values of properties included in the gravity compensation algorithm.

m_h	.4	handle assembly mass [kg]
mm	.07	motor-encoder-capstan drive mass [kg]
m_y cap	.06	mass of Y capstan motor assembly [kg]
m_y mnt	.035	mass of Y motor mount [kg]
k_t	.193	torque constant mNm/Av
k_{Amp}	.2	joystick amplifier current gain A/volt input
L_h	.0613	distance from Y axis to cg of handle [m]
$L_{m3}y$	.036	distance from Y axis to cg of motor3 [m]
$L_{m3}x$	.009	distance from x axis to cg of motor3 [m]
L_y cap	.042	distance from x axis to y capstan [m]
L_y mnt	.029	distance from x axis to y motor mount [m]
$L_{m2}x$	.005	distance from x axis to cg of motor2 [m]

A.2 Second Order Approximations

The base equation for rotational motion in (A.1) is solved to obtain the generic transfer function given in (A.2). This transfer function along with the generic PD

controller from (A.3) is used in the unity feedback system shown in Figure A.1.

$$T(S) = J\theta(S)S^2 + b\theta(S)S \tag{A.1}$$

$$\frac{\theta(S)}{T(S)} = \frac{1}{(JS^2 + bS)} \tag{A.2}$$

$$PD_{JS} = (K_P + K_D S) \tag{A.3}$$

The resulting Closed Loop Transfer Function given (A.4) is reduced to the standard second order form in (A.5). Equation (A.6) gives the reduced standard form for a second order closed loop transfer function with a PD controller.

$$CLTF = \frac{\frac{K_D S + K_P}{JS^2 + bS}}{1 + \frac{K_D S + K_P}{JS^2 + bS}} \tag{A.4}$$

$$CLTF = \frac{\frac{K_P}{J} + \frac{K_D}{J} S}{S^2 + \frac{(b + K_D)}{J} S + \frac{K_P}{J}} \tag{A.5}$$

$$\frac{{\omega_n}^2 + \frac{K_D}{J} S}{S^2 + 2\zeta\omega_n S + {\omega_n}^2} \tag{A.6}$$

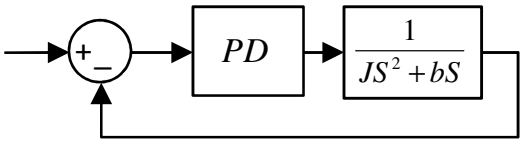

Figure A.1: Generic closed loop PD controller configuration used for the second order approximations of the joystick and wheelchair systems.

Setting (A.5) equal to (A.6) we can obtain numerical values for the transfer function by using the known values of K_P and K_D from the control system. The values of ξ and ω_n are determined from the system response to a step input using (A.7) and (A.8) respectively.

$$\zeta = \frac{-\ln\left(\%\,{}^{OS}/_{100}\right)}{\sqrt{\pi^2 + \ln^2\left(\%\,{}^{OS}/_{100}\right)}} \tag{A.7}$$

$$\omega_n = \frac{\pi}{T_p\sqrt{1-\zeta^2}} \tag{A.8}$$

The resulting numerical second order approximation for the joystick is then found using the relationship given in (A.9).

$$J = \frac{K_P}{{\omega_n}^2} \tag{A.9}$$

A.3 Derivation of K_{acc}

K_{acc} was determined with the free body diagrams for the wheelchair and joystick given in Figure A.2. Because there is no displacement in the Y direction, forces in the Y direction are ignored. The sum of the forces in the X direction on the wheelchair as shown in Figure A.2 (a) is given in

(A.10). Summing the forces in the X direction on the Joystick, the value of R_x is found and is given in

(A.11). This is the typical method for solving the inverted pendulum on a cart

problem, however in this case, it can be neglected because $m_{wc} >> m_h$.

$$F = R_x + b\dot{x} + m_{wc}\ddot{x} \tag{A.10}$$

$$R_x = m_h\ddot{x} + ml\ddot{\theta}\cos\theta - ml\dot{\theta}^2\sin\theta \tag{A.11}$$

Using the parallel axis theorem and the elements in Figure A.2 (b) the sum of the torques about the center of rotation is given in (A.12). The reaction forces R_x and R_y and the centripetal forces are neglected because they cause no moment on the axis of rotation.

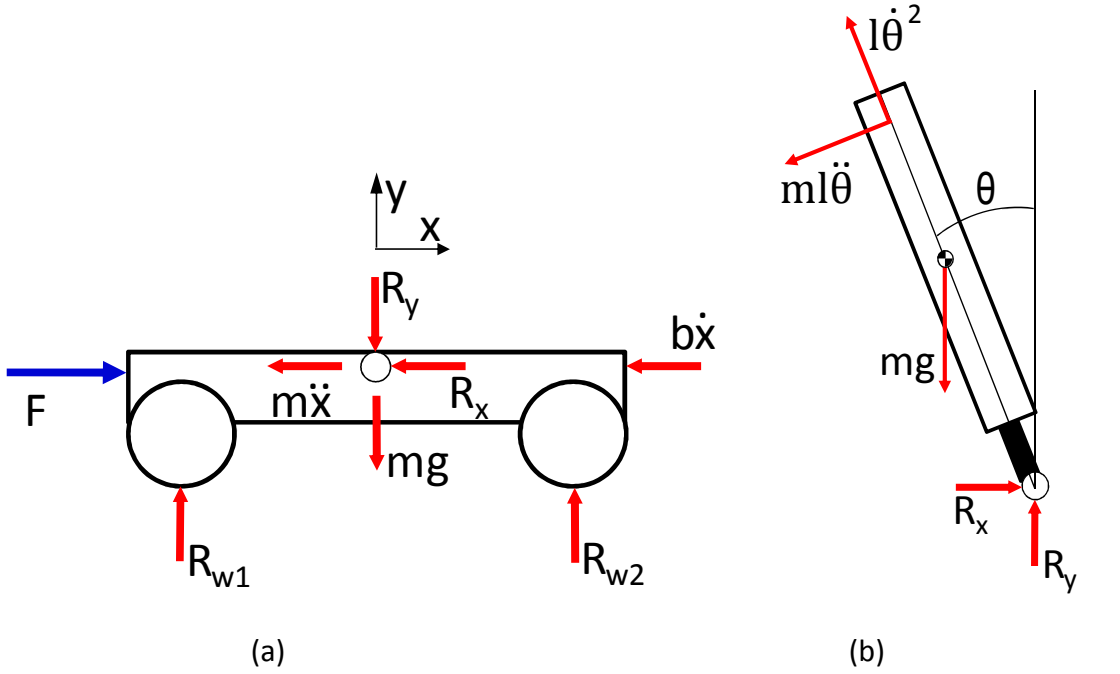

Figure A.2: These free body diagrams were used to determine the coupling between linear acceleration of the wheelchair and resulting torque in the handle. (a) shows the forces acting on the wheelchair and (b) the forces on the joystick. For the joystick the moments are summed about the axis of rotation.

$$(J + M_h l^2)\ddot{\theta} + M_h g l \sin\theta = -m_h l \ddot{X} \cos\theta \quad \textbf{(A.12)}$$

The gravity term can be safely neglected because it is eliminated by the gravity compensation algorithm in the controller. Linearization of the system is accomplished by the small angle approximation which results in equation (A.13).

$$(J + M_h l^2)\ddot{\theta} = -m_h l \ddot{X} \quad \textbf{(A.13)}$$

The left half of the equation is incorporated into the second order approximation of the joystick, leaving the gain and acceleration on the right, as shown in (A.19).

$$K_{acc} = -m_h l \quad \textbf{(A.14)}$$

A.4 Derivation of the Force Feedback Law:

Beginning with the sensor configuration shown in Figure 5.1 and keeping the positive acceleration toward the center of the wheelchair, the sum of the effective forces in the X direction for both virtual damping and virtual stiffness are given in (A.15). K is the virtual spring coefficient, B is the virtual damping coefficient, $c\theta$ is $\cos(\theta)$ and $s\theta$ is the $\sin(\theta)$.

$$\sum F_x = -Kc\theta x_2 - Bc\theta \dot{x}_2 - Kx_3 - B\dot{x}_3 - Kc\theta x_4 - Bc\theta \dot{x}_4 + Kc\theta x_6 + Bc\theta \dot{x}_6 + Kx_7 + B\dot{x}_7 + Kc\theta x_8 + Bc\theta \dot{x}_8 \quad \textbf{(A.15)}$$

Repeating the same for the Y direction the sum of the forces in the Y direction are given by (A.16).

$$\sum F_y = -Kx_1 - B\dot{x}_1 - Ks\theta x_2 - Bs\theta\dot{x}_2 + Ks\theta x_4 + Bs\theta\dot{x}_4 + Kx_5 + B\dot{x}_5 + Ks\theta x_6 + Bs\theta\dot{x}_6 - Ks\theta x_8 + Bs\theta\dot{x}_8 \quad \textbf{(A.16)}$$

The feedback torque about the Z axis given in (A.17) and is solved using the moment arms *a* and *b*, which are the respective distances from the center of rotation to the edge of the wheelchair. Positive torque is defined by the right hand rule about the Z axis.

$$\sum T_z = -bKs\theta x_2 + aKc\theta x_2 - bBs\theta\dot{x}_2 + aBc\theta\dot{x}_2 + bKs\theta x_4 - aKc\theta x_4 + bBs\theta\dot{x}_4 - aBc\theta\dot{x}_4 - bKs\theta x_6 + aKc\theta x_6 - bBs\theta\dot{x}_6 + aBc\theta\dot{x}_6 + bKs\theta x_8 - aKc\theta x_8 + bBs\theta\dot{x}_8 - aBc\theta\dot{x}_8 \quad \textbf{(A.17)}$$

Separating the stiffness and damping terms in each degree of freedom, these equations are reduced to equations (A.18)-(A.23).

$$F_{Kx} = -Kc\theta x_2 - Kx_3 - Kc\theta x_4 + Kc\theta x_6 + Kx_7 + Kc\theta x_8 \quad \textbf{(A.18)}$$

$$F_{Ky} = -Kx_1 - Ks\theta x_2 + Ks\theta x_4 + Kx_5 + Ks\theta x_6 - Ks\theta x_8 \quad \textbf{(A.19)}$$

$$T_{Kx} = -bKs\theta x_2 + aKc\theta x_2 + bKs\theta x_4 - aKc\theta x_4 - bKs\theta x_6 + aKc\theta x_6 + bKs\theta x_8 - aKc\theta x_8 \quad \textbf{(A.20)}$$

$$F_{Bx} = -B\dot{x}_1 - Bs\theta\dot{x}_2 + Bs\theta\dot{x}_4 + B\dot{x}_5 + Bs\theta\dot{x}_6 + Bs\theta\dot{x}_8 \quad \textbf{(A.21)}$$

$$F_{By} = -B\dot{x}_1 - Bs\theta\dot{x}_2 + Bs\theta\dot{x}_4 + B\dot{x}_5 + Bs\theta\dot{x}_6 + Bs\theta\dot{x}_8 \quad \textbf{(A.22)}$$

$$T_{Bz} = -bBs\theta\dot{x}_2 + aBc\theta\dot{x}_2 + bBs\theta\dot{x}_4 - aBc\theta\dot{x}_4 - bBs\theta\dot{x}_6 + aBc\theta\dot{x}_6 + bBs\theta\dot{x}_8 - aBc\theta\dot{x}_8 \quad \textbf{(A.23)}$$

Factoring out the B and K terms and solving both sets of equations for their respective position and velocities, these equations are put into matrix form in (A.24).

$$F_{fb} = [Q][\dot{X_s}] + [R][X_s] \tag{A.24}$$

where $[Q]$ and $[R]$ are given by equations (A.25) and (A.26).

$$[Q] = \begin{bmatrix} 0 & -Bc\theta & -B & -Bc\theta & 0 & Bc\theta & B & Bc\theta \\ -B & -Bs\theta & 0 & Bs\theta & B & Bs\theta & 0 & -Bs\theta \\ 0 & aBc\theta - bBs\theta & 0 & -aBc\theta + bBs\theta & 0 & aBc\theta - bBs\theta & 0 & -aBc\theta + bBs\theta \end{bmatrix} \tag{A.25}$$

$$[R] = \begin{bmatrix} 0 & -Kc\theta & -K & -Kc\theta & 0 & Kc\theta & K & Kc\theta \\ -K & -Ks\theta & 0 & Ks\theta & K & Ks\theta & 0 & -Ks\theta \\ 0 & aKc\theta - bKs\theta & 0 & -aKc\theta + bKs\theta & 0 & aKc\theta - bKs\theta & 0 & -aKc\theta + bKs\theta \end{bmatrix} \tag{A.26}$$

APPENDIX B

BLOCK DIAGRAM REDUCTION

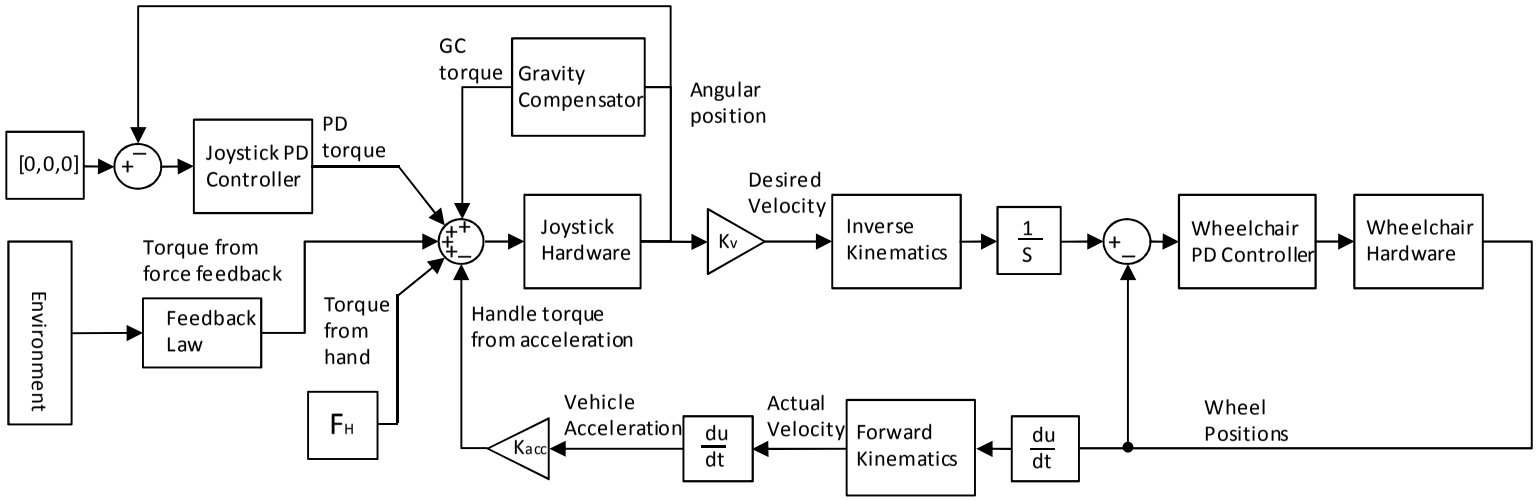

Figure B.1: Coupled Joystick-Wheelchair system with user input and envorinmetal input modeled as dsiturbances.

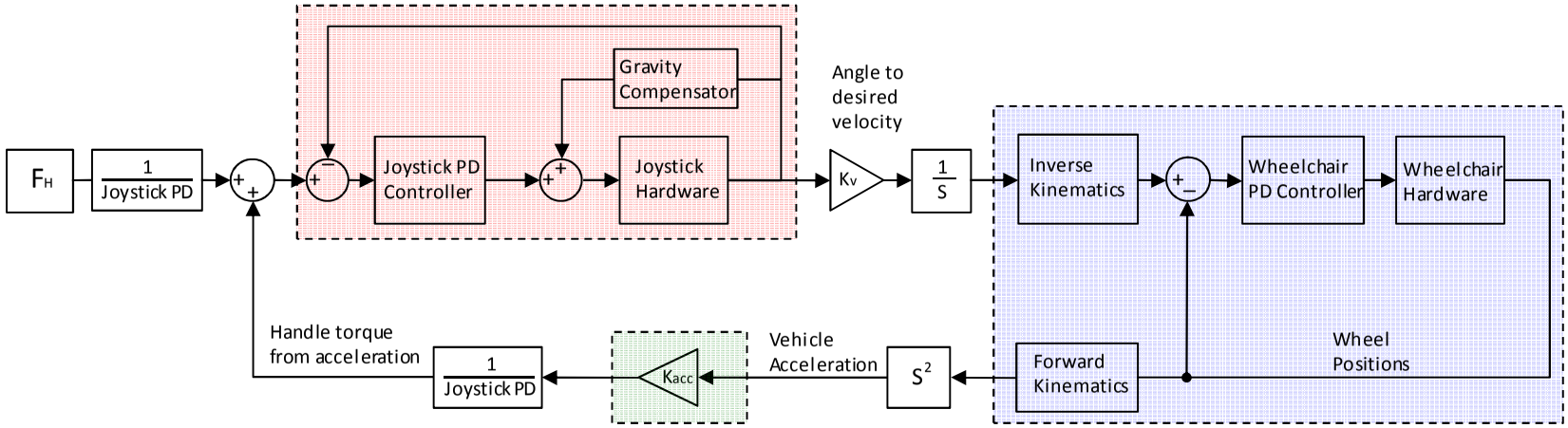

Figure B.2: First step in block diagram reduction environmental feedback removed. The two shaded boxes represent block segments which were replaced by the second order approximations.

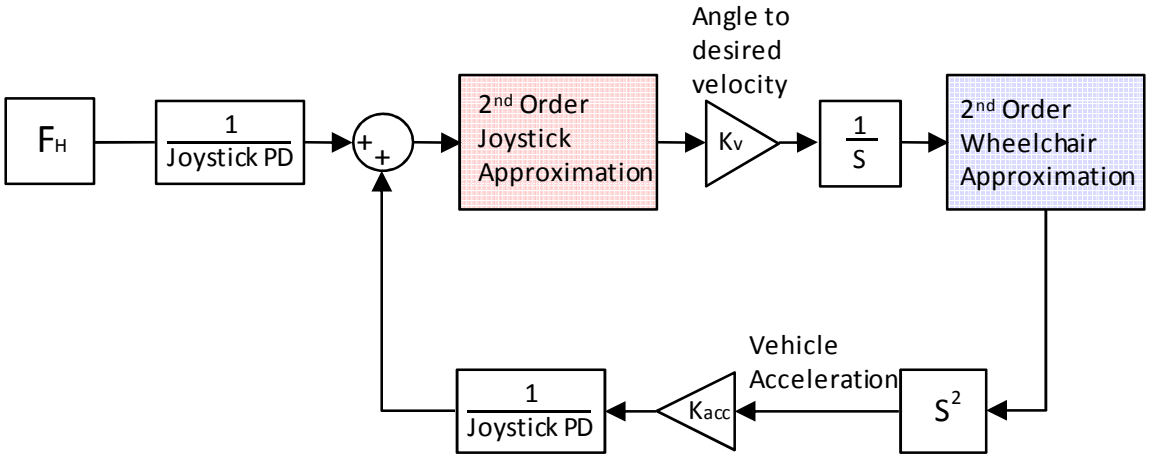

Figure B.3: Reduced control system, shaded areas indicate substituted second order approximations.

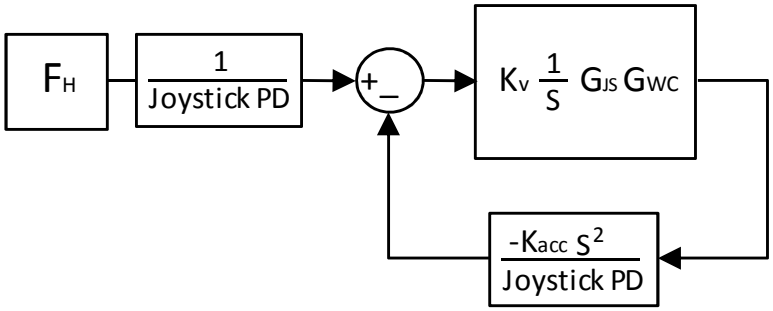

Figure B.4: Final block diagram used for analysis. Signs corrected to permit proper use of the Matlab feedback command, which is dependent on using negative feedback.

APPENDIX C

EMBEDDED MATLAB CODE

C.1 Gravity compensation code

```
function y = gravityComp(u)
% This block supports the Embedded MATLAB subset.
% See the help menu for details.

% Gravity compensation algorithm applies a counter torque to all
% eccentrically loaded elements.

g = 9.81;  %gravity
%mh = .332; %handle assembly mass [kg]
mh = .4;
mm = .07;  %motor-encoder-capstan drive mass [kg]
mycap = .06; % mass of Y capstan motor [kg]
mymnt = .035; % mass of y motor mount [kg]

k_t = .193; % torque constant mNm/A
k_Amp = .2; % joystick amplifier current gain A/volt input

% to simplify the CG of eccentric masses are treated as a
% point mass on the x and y axes

Lh = .06131;  % distance from Y axis to cg of handle [m]
Lm3y = .036;  % distance from Y axis to cg of motor3 [m]
Lm3x = .009;  % distance from x axis to cg of motor3 [m]
Lycap = .042; % distance from x axis to y capstan [m]
Lymnt = .029; % distance from x axis to y motor mnt [m]
Lm2x = .005;  % distance from x axis to cg of motor2 [m]

% convert encoder ticks to radians resoultuion
% 360 counts per rev of the motor, 15:1 ratio therfore
% 15 counts/degree, 0.0174533 radians/degree or 859.43 counts/radian
% rounded up to 860 counts per radian

radians = u./860; % convert counter inputs to radians;
thx = radians(1); % extract theta_X
thy = radians(2); % extract theta_Y

A = -mh*g*Lh*abs(cos(thy))*sin(thx);
B = -mm*g*Lm3x*abs(sin(thy))*cos(thx);
C = -mm*g*Lymnt*cos(thx);
D = -mycap*g*Lycap*cos(thx);
E = -mymnt*g*Lymnt*cos(thx);
F = -mh*g*Lh*sin(thy);
G = -mm*g*Lm3y*cos(thy);

y = [A+B+C+D+E, F+G , 0];
```

```
y = y./(k_t*k_Amp); % convert calculated torques to voltage outputs.
```

C.2 Dead Zone / Disable Feedback

```
function [cut,sig] = cutter(uncut,cutoff)
% This block supports the Embedded MATLAB subset.
% See the help menu for details.

%This block neglects any input of less than the specified cutoff range.
%When in the dead zone a signal is output to disable force feedback.

cut = zeros(length(uncut),1);
for i=1:length(uncut)
    if (abs(uncut(i))<cutoff)
        cut(i) = 0;
   elseif(uncut(i) > 0)
        cut(i) = uncut(i)-cutoff;
    else
        cut(i) = uncut(i) + cutoff;
    end
end
sig=sqrt(cut(1)^2+cut(2)^2+cut(3)^2);
```

C.3 Feedback Law

```
function F_fb = forcefb(X,X_dot,K,B,cut)
% This block supports an embeddable subset of the MATLAB language.
% See the help menu for details.

k_t = .193; % torque constant mNm/A
k_Amp = .2; % joystick amplifier current gain A/volt input

C = .707106781; % cos(45)
S = .707106781; % sin(45)
a = .29845; % distance from center of rotation to sensors along X
b = .75765; % distance from center of rotation to sensors along Y

for(i = 1:length(X_dot))
    if(X_dot(i) < 0)
        X_dot(i) = 0;
    end
end


Alpha = [0 -B*C -B -B*C 0 B*C B B*C;...
    -B -B*S 0 B*S B B*S 0 -B*S;...
    0 -a*B*C+b*B*S 0 a*B*C-b*B*S 0 -a*B*C+b*B*S 0 a*B*C-b*B*S];

Beta = [0 -K*C -K -K*C 0 K*C K K*C;...
    -K -K*S 0 K*S K K*S 0 -K*S;...
    0 -a*K*C+b*K*S 0 +a*K*C-b*K*S 0 -a*K*C+b*K*S 0 a*K*C-b*K*S];

if (cut == 0)
F_fb = [0;0;0];
else
F_fb = (Alpha*X_dot + Beta*X)./(k_t*k_Amp);
end

end
```

C.4 Inverse Kinematics

```
function w = I_kin(V_des)
% This block supports an embeddable subset of the MATLAB language.
% See the help menu for details.

% This is the Inverse Kinematics for the Omnidirectional wheelchair
% 3D desired velocity vector V_des is converted to required motor
% velociies W by the inverse Jacobian Jinv

% Note this code keeps the wheelchair in the local frame.

R =  .053975; %ball radius (meters)
phi = 30*pi/180;%Wheel Inclination (meters)
L1 = .1524; %Leg Length 1 (meters)
L2 = .291846; %Leg Length 2 (meters)
L3 = .349901; %Leg Length 3 (meters)
rz = 0;
sq = sqrt(2);
C = cos(rz+3*pi/2); % 3*pi/2 to rotate wheels to correct orientation.
S = sin(rz+3*pi/2);

alpha = (L2^2+L3^2-.25*L1^2)/(2*L2*L3);
Jinv = [-sq/2, sq/2, alpha*L3;
        -sq/2, -sq/2, alpha*L3;
        sq/2, -sq/2, alpha*L3;
        sq/2, sq/2, alpha*L3;];
Rz = [C, -S, 0;
      S, C, 0;
      0, 0, 1;];

w = 1 /(R*sin(phi))*Jinv*Rz'*V_des;
```

C.5 Forward Kinematics

```
function V_dot = F_kin(w)
% This block supports an embeddable subset of the MATLAB language.
% See the help menu for details.
% x_dot,y_dot,rz_dot

% This is the Forward Kinematics for the Omnidirectional wheelchair
% This converts the 4D motor velocity to a 3D velocity vector with
X_dot
% Y_dot and Theta_dot

% eta = 24/192;  %Gear Ratio
R =  .053975; %ball radius (meters)
phi = 30*pi/180;%Wheel Inclination (meters)
L1 = .1524; %Leg Length 1 (meters)
L2 = .291846; %Leg Length 2 (meters)
L3 = .349901; %Lenght 3 (meters)
rz = 0;

alpha = (L2^2+L3^2-.25*L1^2)/(2*L2*L3);
JLM = [-sqrt(2)/4, -sqrt(2)/4, sqrt(2)/4, sqrt(2)/4;
        sqrt(2)/4, -sqrt(2)/4, -sqrt(2)/4, sqrt(2)/4;
        1/(4*alpha*L3), 1/(4*alpha*L3), 1/(4*alpha*L3),
1/(4*alpha*L3)];
Rz = [cos(rz+3*pi/2), -sin(rz+3*pi/2), 0;
```

```
      sin(rz+3*pi/2), cos(rz+3*pi/2), 0;
      0, 0, 1;];

 V_dot = (R*sin(phi))*Rz*JLM*w;
```

C.6 Dead Reckoning Algorithm

```
function globalVel = deadreckon(x_dot,y_dot,th)
% This block supports an embeddable subset of the MATLAB language.
% See the help menu for details.

% This converts the local velocity vector to the global frame for to be
% integrated for dead reckoning. The input th is the integrated
% rotations from the actual wheelvelocities, x_dot and y_dot


rz = th;

Rz = [cos(rz+3*pi/2), -sin(rz+3*pi/2);
      sin(rz+3*pi/2), cos(rz+3*pi/2)];

globalVel = Rz*[x_dot,y_dot]';
      d
```

C.7 Matlab Code for Analysis of the Root Locus Plot as Mass, Damping, and Stiffness Are Varied

```
% secondOrderMod(mH,bH,kH,mRider)
% ctrl+scroll the mouse wheel to watch the root locus plot change

integrator_KV = tf(.25,[1 0]);
mH = 1+0*.1;
bH = 1+0*.1;
kH = 1+0*.1;
mRider = 1+0*.1;
rlocusMov = rlocusMov(1);
pzMov = pzMov(1);

for i = 1:4

    if i == 1
        scale = 1:.1:4;
    elseif i == 2
        scale = 1:.1:2.5;
    elseif i == 3
        scale = 1:.1:5;
    elseif i == 4
        scale = 1:.1:3;
    end

    for j = 1:length(scale)
        if i == 1
            mRider = scale(j);
            dispText =['Mass of Wheelchair + Rider =
',num2str(mRider*100),'% of Wheelchar'];
        elseif i == 2
            mH = scale(j);
            dispText =['Mass of Handle + Mass of Hand =
```

```
',num2str(mH*100),'% of Handle'];
        elseif i == 3
            bH = scale(j);
            dispText =['Joystick Damping + Hand Damping =
',num2str(bH*100),'% of Joystick Damping'];
        elseif i == 4
            kH = scale(j);
            dispText =['Joystick Stiffness + Hand Stiffness =
',num2str(kH*100),'% of Joystick Stiffness'];
        end

        [GJSMod, GWCMod, HMod, OLTFMod] = secondOrderMod(mH, bH, kH,
mRider);
        figure(1);
       rlocus(OLTFMod);



        set(gca,'fontSize',12,'fontName','Times');
        set(gcf, 'units', 'inches','outerPosition',[1 1 9 8 ]);
        axis([-100 5 -350 350]);
        text(-90,200,dispText);
        rlocusMov(end+1)=getframe;
        if j ==length(scale)
            rlocusMov(end+1:end+5) = rlocusMov(end);
        end

        figure(2);
        CLTFMod = feedback(integrator_Kv*GJSMod*GWCMod,HMod);
        pzmap(CLTFMod);
        set(gca,'fontSize',12,'fontName','Times');
        set(gcf, 'units', 'inches','outerPosition',[1 1 9 8 ]);
        axis([-100 5 -350 350]);
        text(-90,200,dispText);
        pzMov(end+1)=getframe;
        if j ==length(scale)
            figure(2)
            pzMov(end+1:end+5) = pzMov(end);
        end

    end
end

function [GJSMod, GWCMod, HMod, OLTFMod]= secondOrderMod(mHand, bHand,
kHand, mRider)
numJS=[9.768 488.4];
denJS=[1 11.47 488.4];

numWC = [96.38 8949];
denWC = [1 108.8 8949];


mHJS = .3320;
lHJS = .0613;
KpJS = .025;
KdJS = .0005;

KpWC = 65;
KdWC = .7;

jJS = KpJS/numJS(2);
J_hand = jJS*(mHand-1);

bJS = ((denJS(2)*jJS)-KdJS);
```

```
B_hand = (bJS+KdJS)*(bHand-1);

K_hand = KpJS*(kHand-1);

JeffJS = jJS+J_hand;
BeffJS = bJS+KdJS +B_hand;
KeffJS = KpJS+K_hand;

newNumJS = [(KdJS+B_hand)/JeffJS, KpJS/JeffJS];
newDenJS = [1 BeffJS/JeffJS KeffJS/JeffJS];

GJSMod = tf(newNumJS,newDenJS);

mWC = KpWC/numWC(2);
M_rider = mWC * (mRider-1);

newNumWC = [numWC(1)*mWC/(mWC+M_rider) numWC(2)*mWC/(mWC+M_rider)];
newDenWC = [1 denWC(2)*mWC/(mWC+M_rider) denWC(3)*mWC/(mWC+M_rider)];

GWCMod = tf(newNumWC,newDenWC);

HMod = tf([(mHJS+mHJS*(mHand-1))*lHJS 0 0 ],[KdJS,KpJS]);
%doubleDiff = tf([1 0 0],1);
integrator = tf(1,[1 0]);

OLTFMod = integrator*GJSMod*GWCMod*HMod;
```

APPENDIX D

MECHANICAL MODEL DRAWINGS

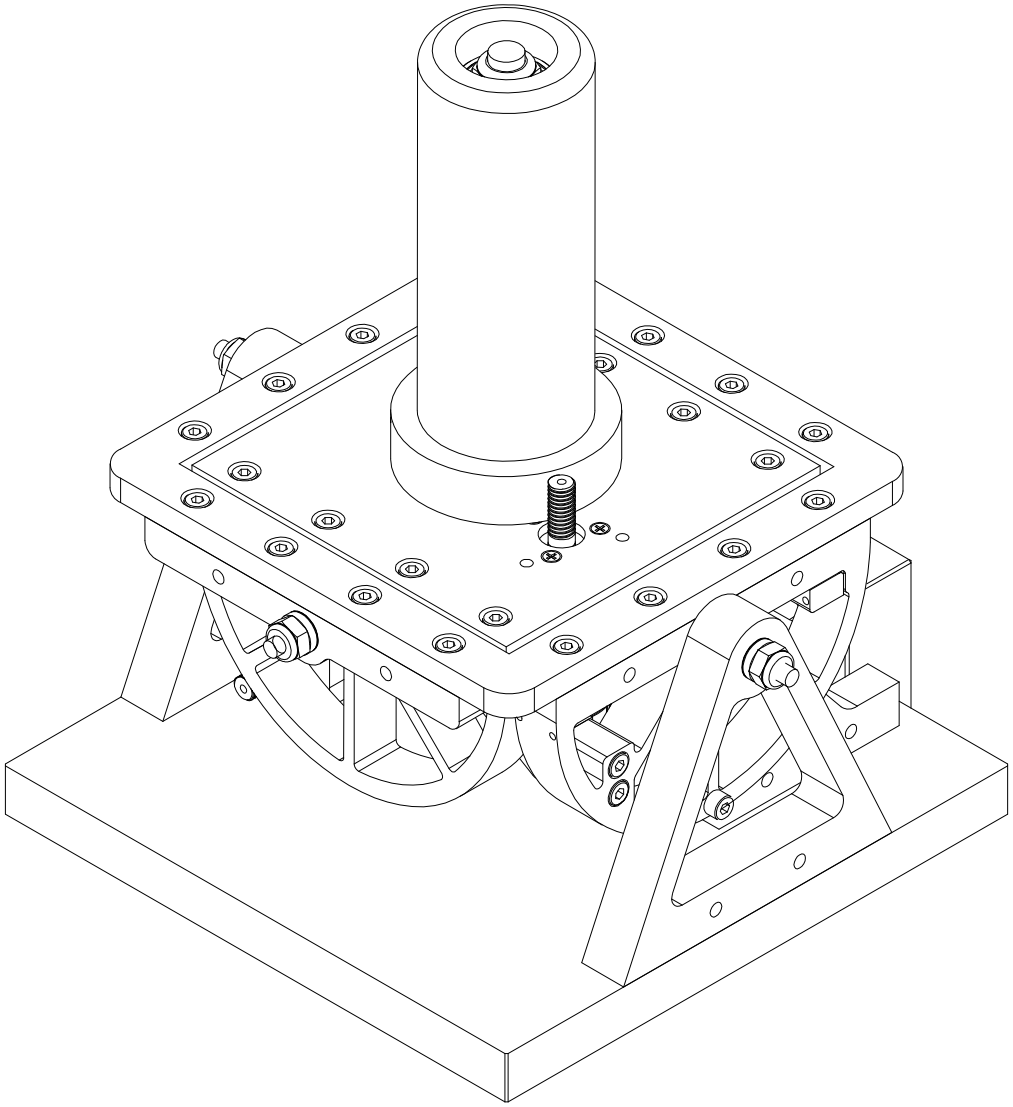

Figure D.1: Complete assembly of the Haptic Joystick

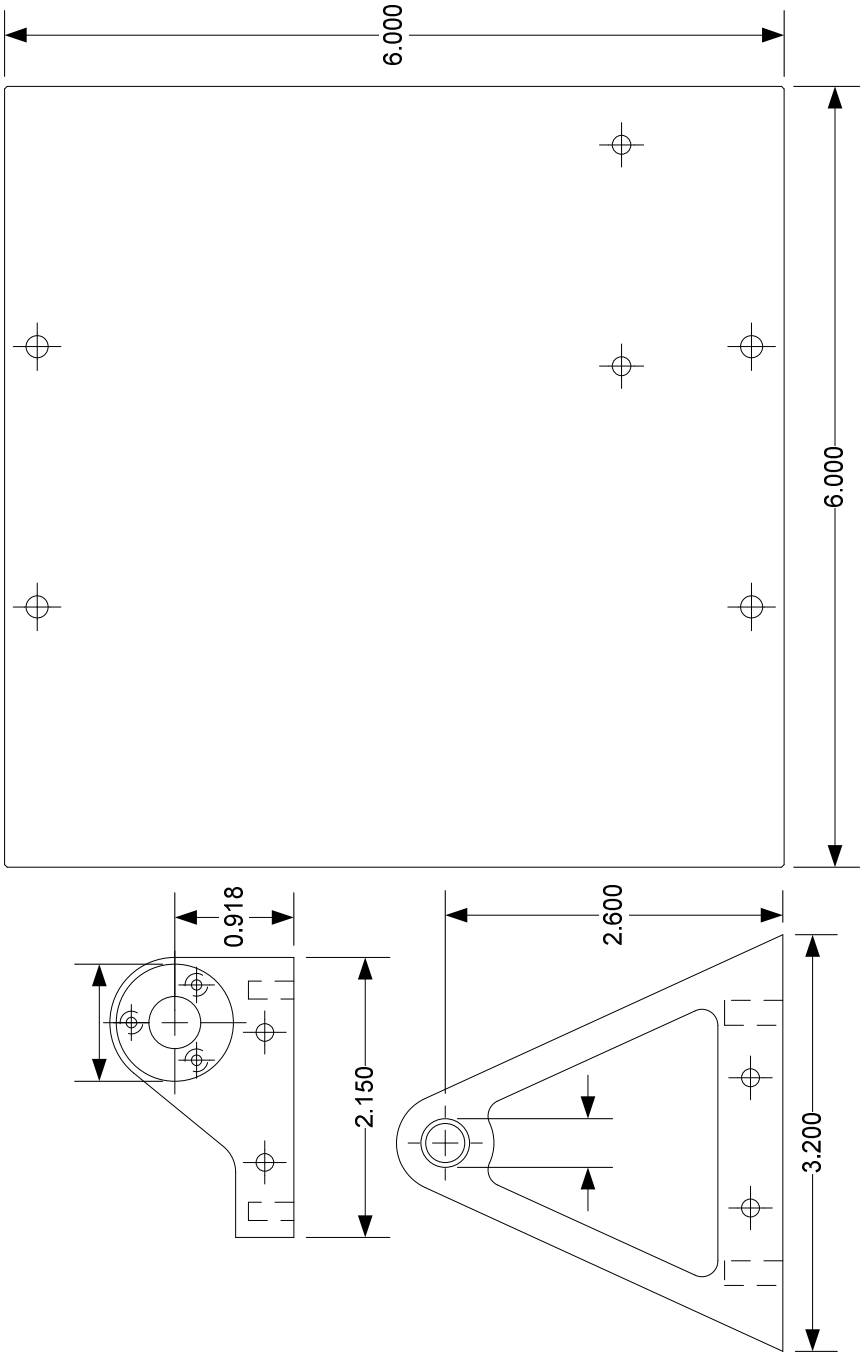

Figure D.2: Components of the joystick base assembly

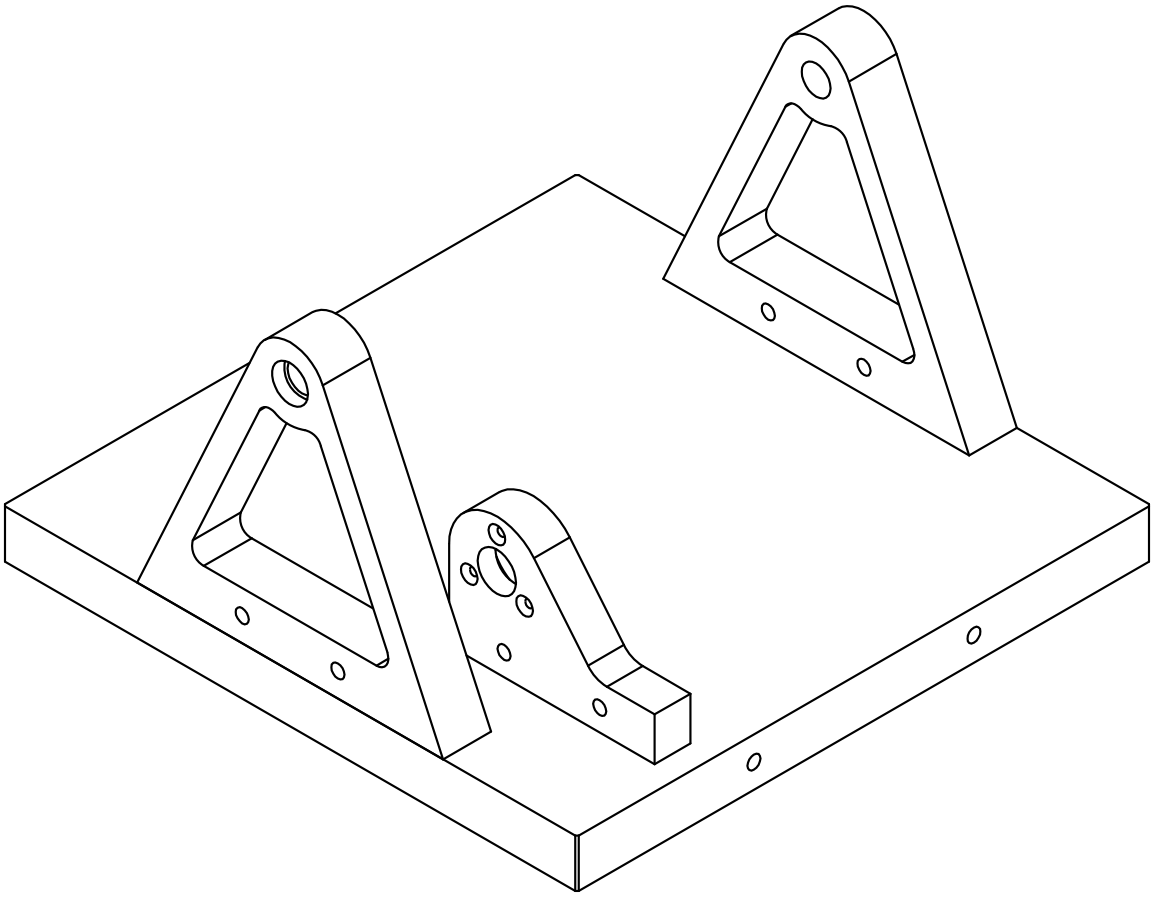

Figure D.3: Joystick base assembly including Base plate, X-stage motor mount, and two X-stage bearing risers.

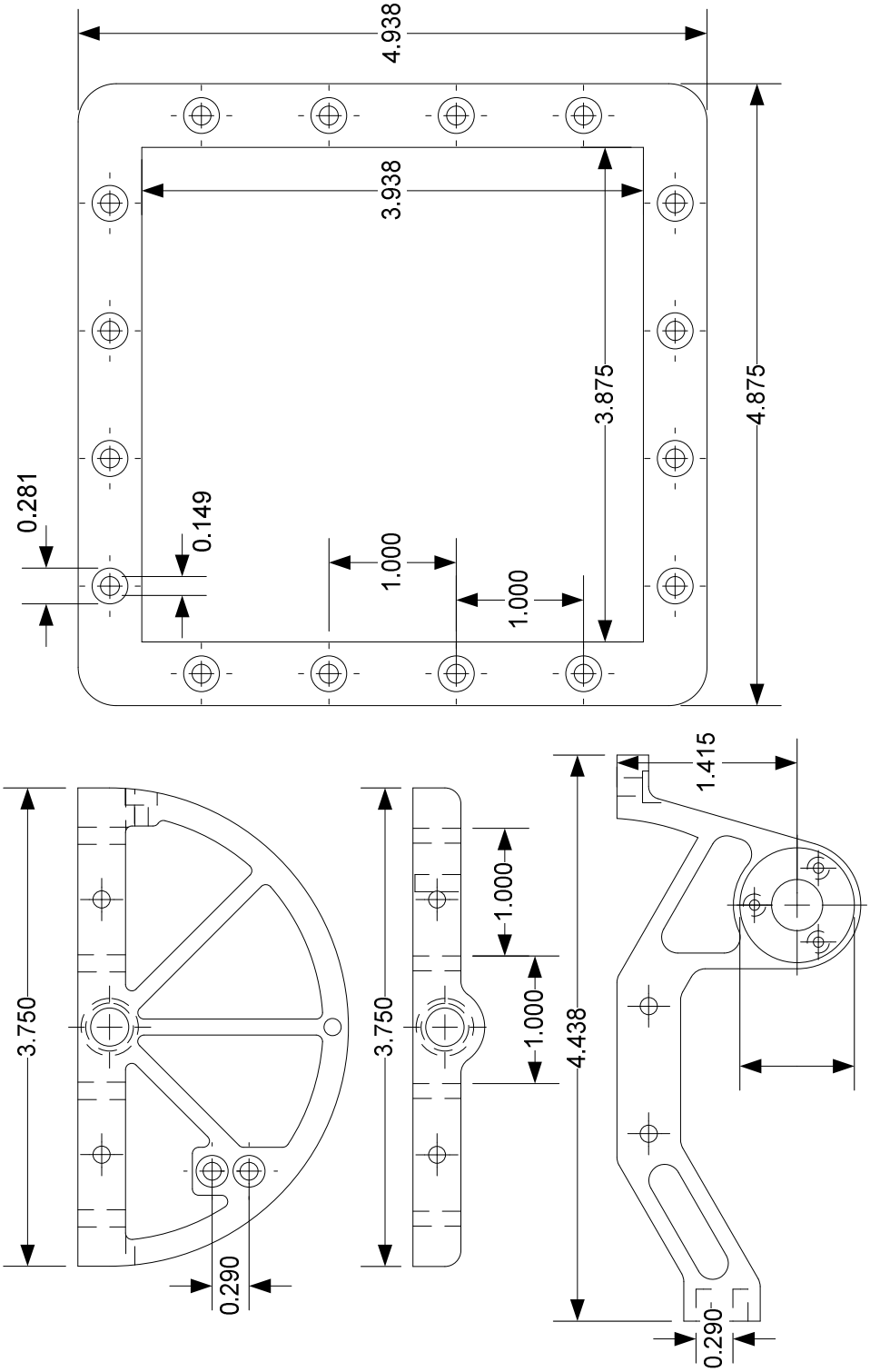

Figure D.4: Components of the X-stage assembly

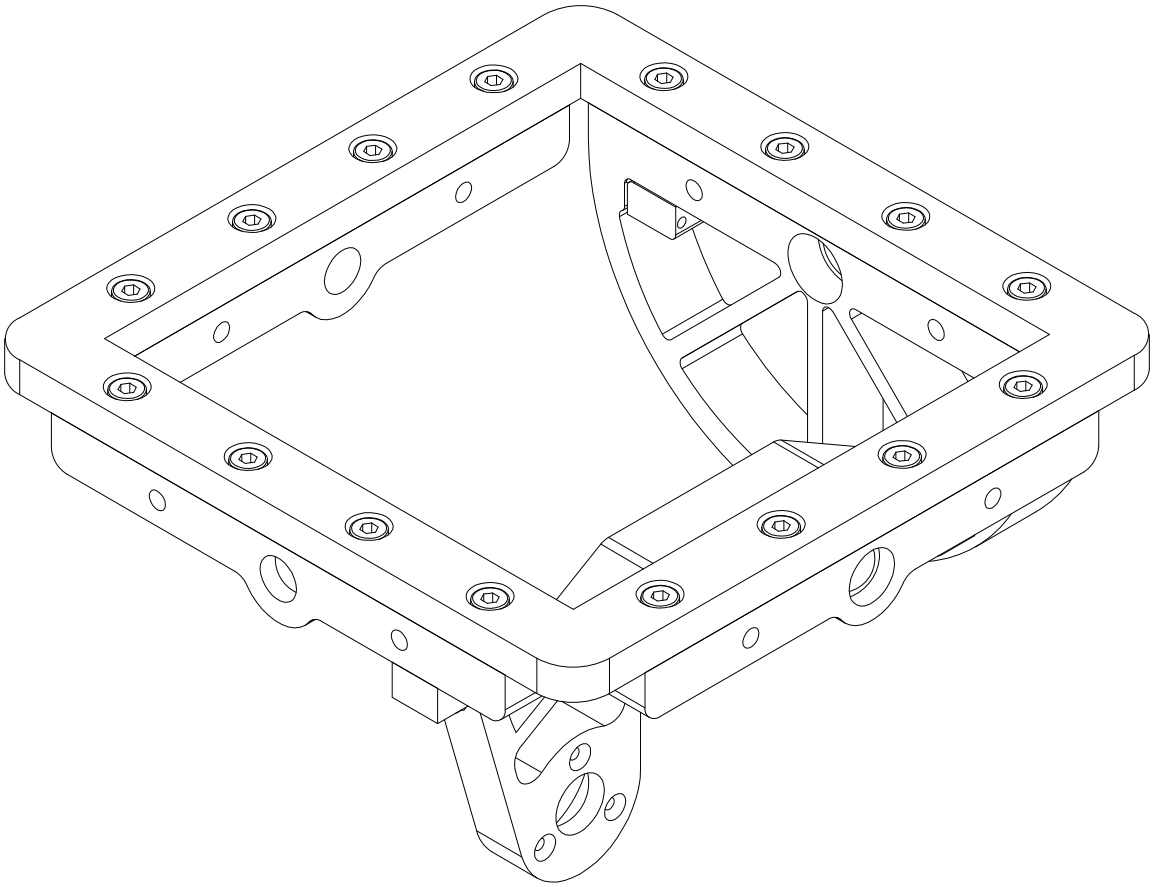

Figure D.5: X-stage assembly including the X-deck, X-stage capstan, X and Y stage bearing braces and Y-stage motor.

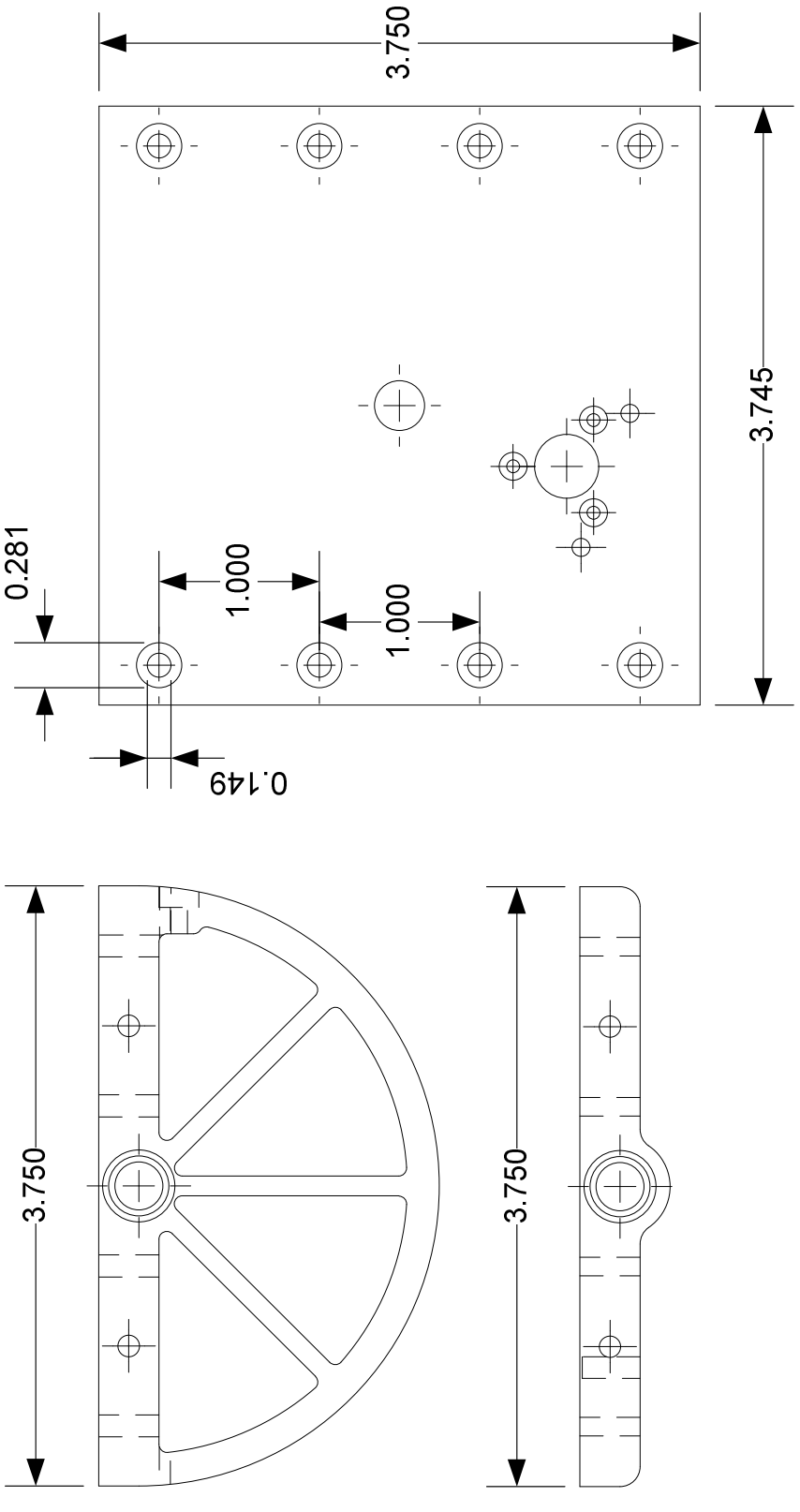

Figure D.6: Components Y-stage including center deck, Y-capstain, and Y-stage bearing brace.

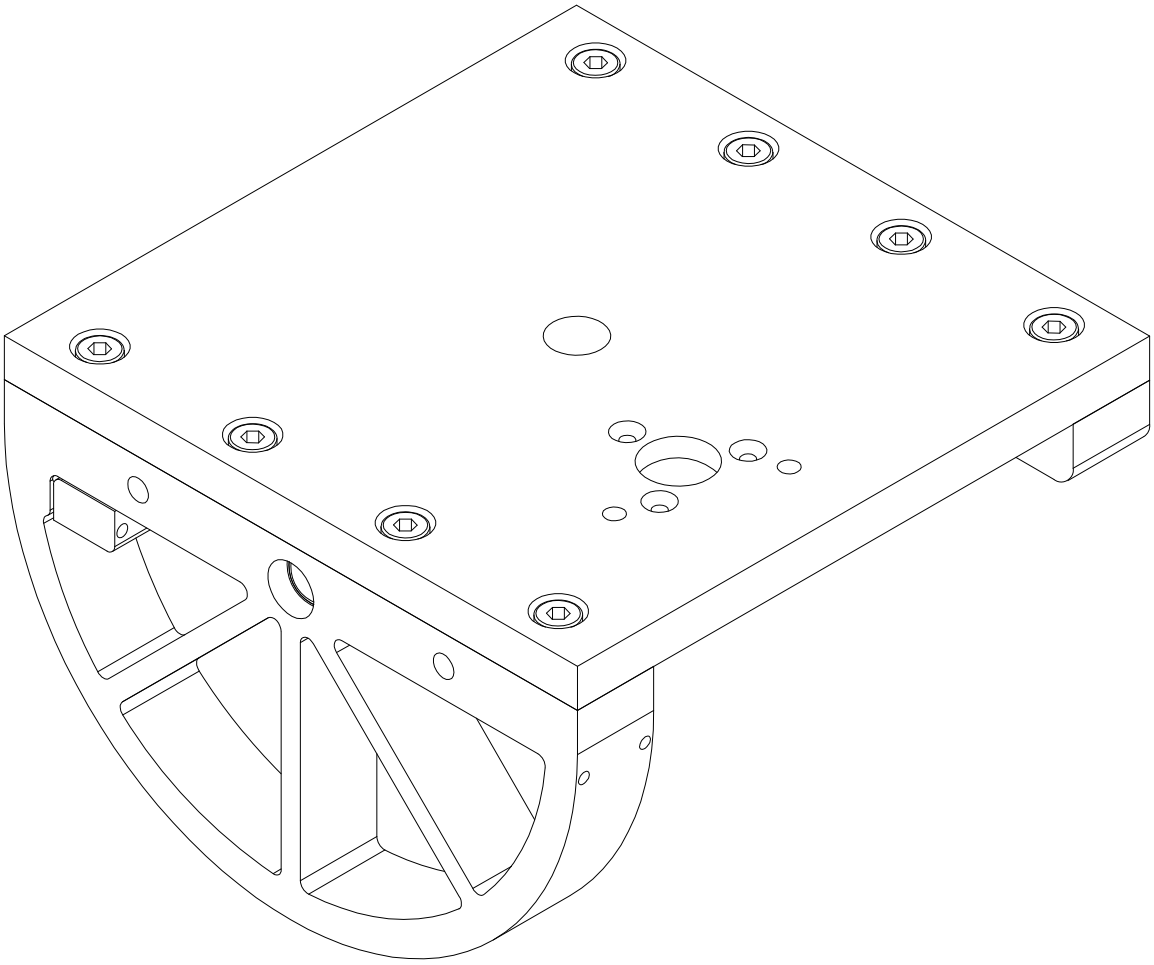

Figure D.7: Y-stage assembly

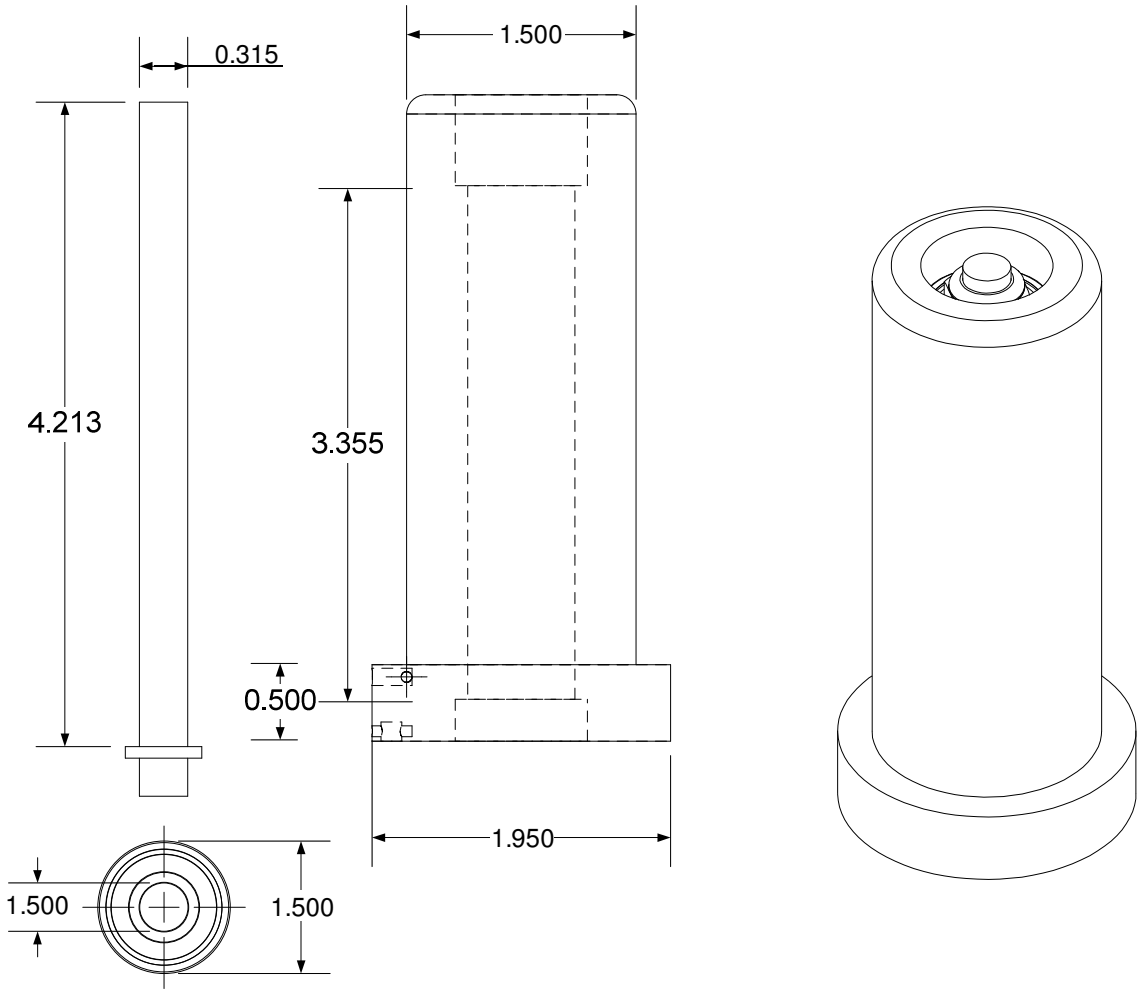

Figure D.8: Handle stage parts and assembly including handle, handle shaft, and bearings.

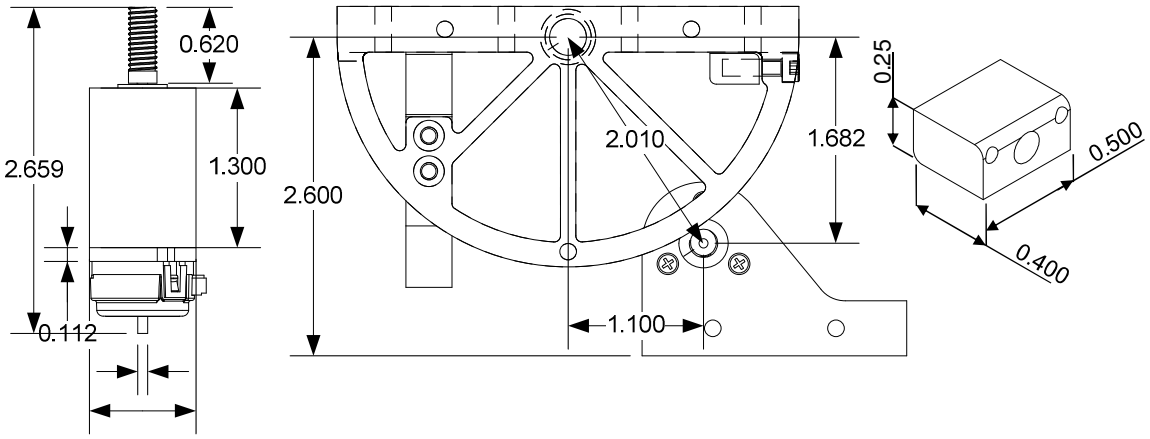

Figure D.9: Capstan drive details, including Maxon 2322 motor, US Digital E4P encoder, and capstan drive pulley. The positioning of the X-stage capstan and capstan drive pulley with respect to each other and a detail of the cable tensioning block.

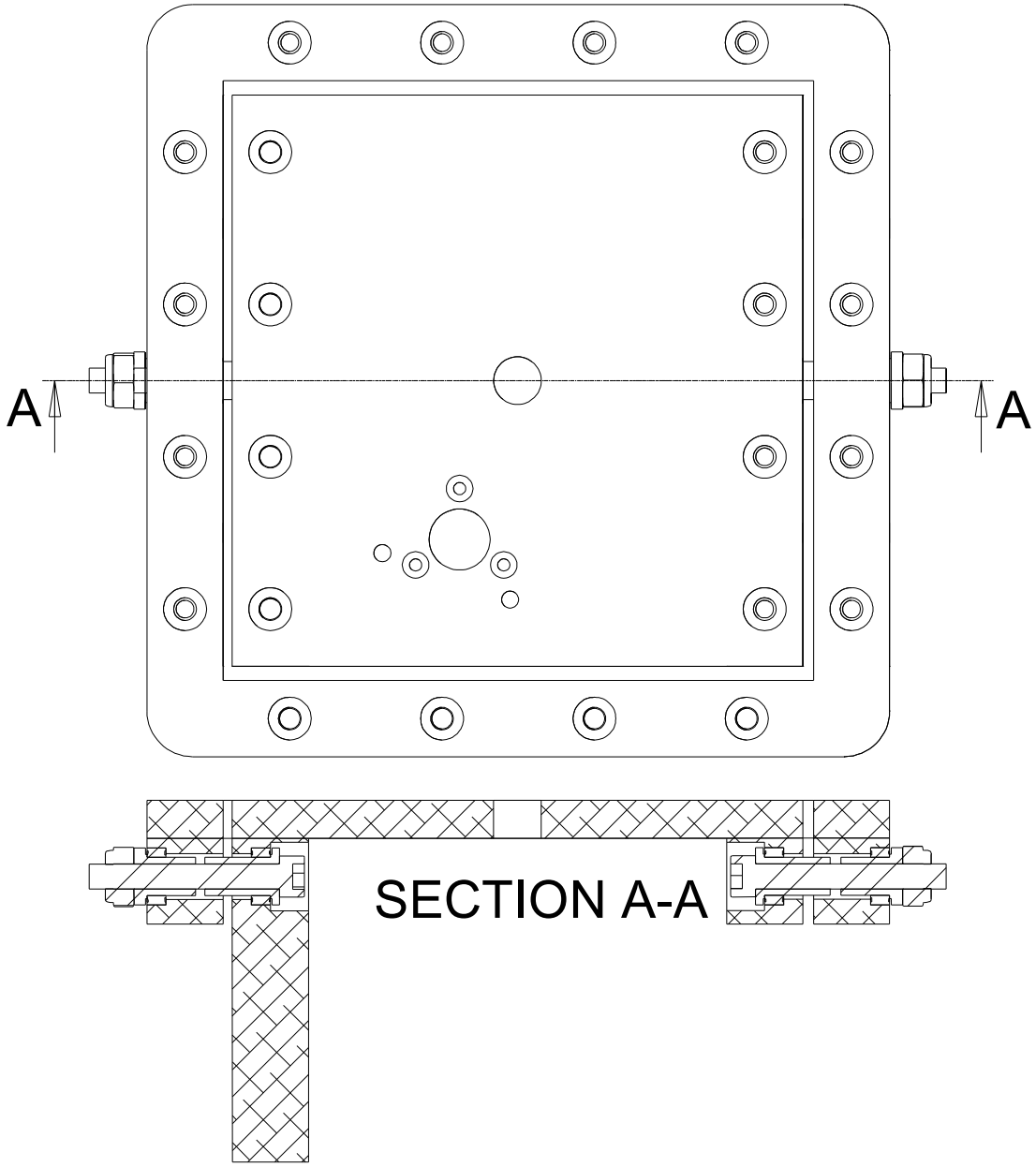

Figure D.10: Cross section of Y-stage bearings. This configuration is also repeated on the X-stage.

APPENDIX E

CONTROL SYSTEM SCHEMATIC

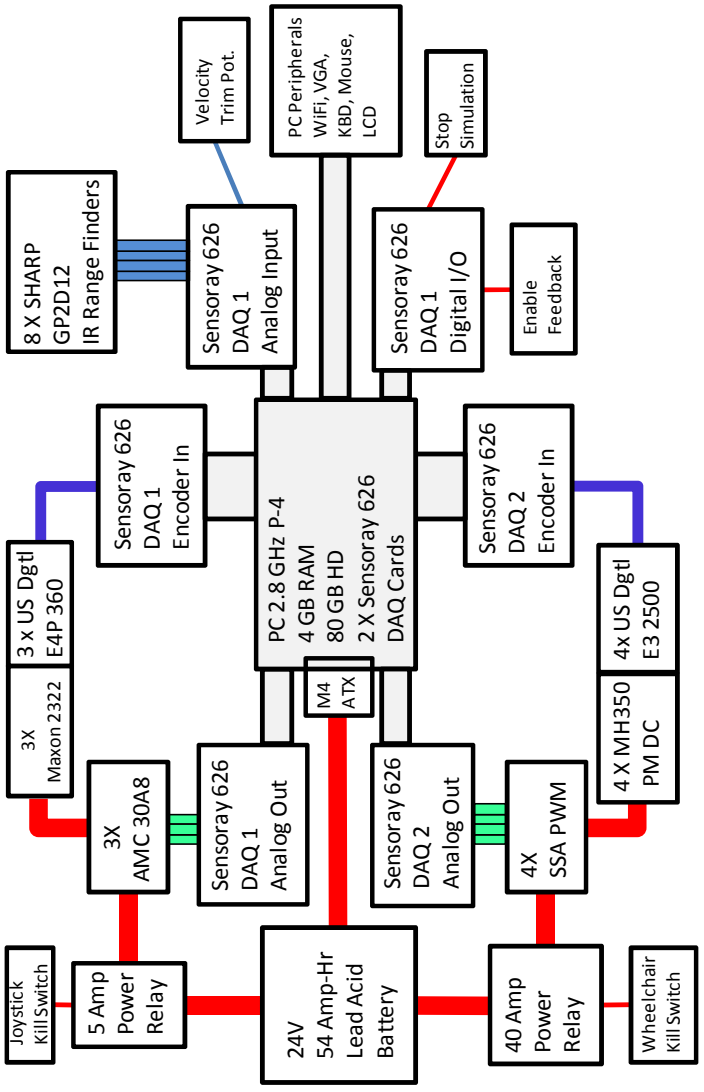

Figure E.1: Control system schematic

REFERENCES

[1] Administration on Aging, "Aging statistics" Jan 30, 2010, http://www.aoa.gov/aoaroot/aging_statistics/index.aspx

[2] W. Erickson and C. Lee, "2007 disability status report: United states," *Cornell University Rehabilitation Research and Training Center on Disability Demographics and Statistics.*, 2008.

[3] K. Berg, M. Hines, and S. Allen, "Wheelchair users at home: Few home modifications and many injurious falls," *Am J Public Health*, vol. 92, pp. 48, 2002.

[4] M. W. Brault, "Americans with disabilities:2005," *US Census Bureau*, 2008.

[5] C. Papadimitriou, "Becoming en-wheeled: The situated accomplishment of re-embodiment as a wheelchair user after spinal cord injury," *Disability & Society*, vol. 23, pp. 691-704, 2008.

[6] E. Thelen, G. Schöner, C. Scheier, and L. B. Smith, "The dynamics of embodiment: A field theory of infant perseverative reaching," *Behavioral and brain sciences*, vol. 24, pp. 1-34, 2001.

[7] S. Arzy, L. S. Overney, T. Landis, and O. Blanke, "Neural mechanisms of embodiment: Asomatognosia due to premotor cortex damage," *Archives of Neurology*, vol. 63, pp. 1022, 2006.

[8] S. W. D. O. Brose, D. J. P. Weber, B. A. B. S. Salatin, G. G. M. S. Grindle, H. M. S. Wang, J. J. M. S. Vazquez, and R. A. P. Cooper, *The role of assistive robotics in the lives of persons with disability. [review]*, vol. 89 (2) American Journal of Physical Medicine & Rehabilitation, 2010.

[9] U. Juan, T. Kazuhiko, M. Takanori, and K. Hideo, "Collision avoidance in an omni-directional wheelchair by using haptic feedback," in *Proceedings of the 4th WSEAS International Conference on Signal Processing, Robotics and Automation*. Salzburg, Austria: World Scientific and Engineering Academy and Society (WSEAS), 2005.

[10] L. Marchal-Crespo, "Haptic guidance for enhancing human motor learning: Application to a robot-assisted powered wheelchair trainer," *Mechanical and Aerospace Engineering*,University of California, Irvine, 2009.

[11] C. S. Harrison, M. Grant, and B. A. Conway, "Haptic interfaces for wheelchair navigation in the built environment," *Presence: Teleoperators and Virtual Environments*, vol. 13, pp. 534, 2004.

[12] B. Grychtol, H. Lakany, and B. A. Conway, "A virtual reality wheelchair driving simulator for use with a brain computer interface," presented at 5th UK & Republic of Ireland Postgraduate Conference in Biomedical Engineering and Medical Physics, Oxford England, 2009.

[13] A. M. Okamura, "Methods for haptic feedback in teleoperated robot-assisted surgery," *Industrial Robot: An International Journal*, vol. 31, pp. 499-508, 2004.

[14] X. Chen, C. Ragonesi, J. Galloway, and S. Agrawal, "Training toddlers seated on mobile robots to drive indoors amidst obstacles," *Neural Systems and Rehabilitation Engineering, IEEE Transactions on*, vol. PP, pp. 1-1, 2011.

[15] L. Marchal-Crespo, J. Furumasu, and D. J. Reinkensmeyer, "A robotic wheelchair trainer: Design overview and a feasibility study," *Journal of neuroengineering and rehabilitation*, vol. 7, pp. 40-40, 2010

[16] K. J. Kuchenbecker, W. R. Provancher, G. Niemeyer, and M. R. Cutkosky, "Haptic display of contact location," 2004.

[17] B. Siciliano and O. Khatib, "Springer handbook of robotics." New York: Springer-Verlag New York Inc, 2008, pp. 719-725.

[18] S. Technologies, "Specifications for the phantom omni® haptic device," Sensable Technologies, 1993.

[19] Sensable, "Phantom premium 1.5/6dof, 1.5 highforce/6dof and 3.0/6dof haptic devices," vol. 2011. Wilmington, MA, 2006, pp. Technical Specifications for the Sensable Phanton Premium.

[20] Quanser, "Quanser haptics and robotics, 5-dof haptic wand. Spec sheet for the quanser haptic wand.," vol. 2011. Markham, Ontario Canada, 2008, pp. Data sheet for Quanser 5-DOF Haptic Wand.

[21] F. Dimension, "Product brochure for the force dimension omega.6 haptic device," vol. 2009, F. Dimension, Ed. Nyon 2009.

[22] Novint, Technologies, and Inc., "Falcon technical specifications," vol. 2009. Albuquerque, NM 2009, pp. Technical Specifications for the Novint Falcon.

[23] R. B. Gillespie, M. B. Hoffman, and J. Freudenberg, "Haptic interface for hands-on instruction in system dynamics and embedded control," *Ann Arbor*, vol. 1001, pp. 48109.

[24] A. M. Okamura, C. Richard, and M. R. Cutkosky, "Feeling is believing: Using a

force-feedback joystick to teach dynamic systems," *JOURNAL OF ENGINEERING EDUCATION-WASHINGTON-*, vol. 91, pp. 345-350, 2002.

[25] C. Richard, A. M. Okamura, and M. R. Cutkosky, "Getting a feel for dynamics: Using haptic interface kits for teaching dynamics and controls," presented at ASME IMECE 6th Annual Symposium on Haptic Interfaces, Dallas, TX, 1997.

[26] K. Bowen and K. O. Marcia, "Adaptation of haptic interfaces for a labview-based system dynamics course," 2006.

[27] D. I. Grow, L. N. Verner, and A. M. Okamura, "Educational haptics," 2007.

[28] E. W. Christopher, "The snaptic paddle: A modular haptic device," presented at First Joint Eurohaptics Conference and Symposium on Haptic Interfaces for Virtual Environment and Teleoperator Systems, Pisa, Italy, 2005.

[29] B. Woods, "Omni-directional wheelchair," *School of Mechanical, Materials and Mechatronics Engineering*,University of Western Austrailia, 2006.

[30] A. Fattouh, M. Sahnoun, and G. Bourhis, "Force feedback joystick control of a powered wheelchair: Preliminary study," presented at Systems, Man and Cybernetics, 2004 IEEE International Conference on, 2004.

[31] G. Bourhis and M. Sahnoun, "Assisted control mode for a smart wheelchair," 2007.

[32] K. Park, B. Bae, and T. Koo, "A haptic device for pc video game application," *Mechatronics*, vol. 14, pp. 227-235, 2004.

[33] Y. Kondo, T. Miyoshi, K. Terashima, and H. Kitagawa, "Navigation guidance control using haptic feedback for obstacle avoidance of omni-directional wheelchair," presented at Haptic interfaces for virtual environment and teleoperator systems, 2008. haptics 2008. symposium on, 2008.

[34] Virtual-Realities, "Technical specifications for the impulse stick," 2007, Accessed April 14, 2011, http://www.vrealities.com/impulsestick.html

[35] O. Celik, M. K. O'Malley, C. Boake, H. Levin, S. Fischer, and T. Reistetter, "Comparison of robotic and clinical motor function improvement measures for sub-acute stroke patients," presented at Robotics and Automation, 2008. ICRA 2008. IEEE International Conference on, 2008.

[36] ADA, "Ada accessability guidelines for buldings and facilities (adaag)," 2002.

[37] M. West and H. Asada, "Design of a holonomic omnidirectional vehicle," Nice, Fr, 1992.

[38] H. Hoyer, "The omni wheelchair: An omnidirectional wheelchair with high

manoeuvrability and navigational intelligence," *Service Robot*, vol. 1, pp. 26-9, 1995.

[39] B. J. Yi and W. K. Kim, "The kinematics for redundantly actuated omnidirectional mobile robots," *Journal of Robotic Systems*, vol. 19, pp. 255-267, 2002.

[40] A. T. Bradley, S. A. Miller, G. A. Creary, N. A. Miller, M. D. Begley, and N. J. Misch, "Mobius, an omnidirectional robot utilizing mecanum wheels and fuzzy logic control," *Advances in the Astronautical Sciences*, vol. 121, pp. 251-266, 2005.

[41] A. Shimada, S. Yajima, P. Viboonchaicheep, and K. Samura, "Mecanum-wheel vehicle systems based on position corrective control," Piscataway, NJ, USA, 2005.

[42] M. Wada, "Omnidirectional control of a four-wheel drive mobile base for wheelchairs," Nagoya, Japan, 2005.

[43] K. Tadakuma and R. Tadakuma, "Mechanical design of "Omni-ball": Spherical wheel for holonomic omnidirectional motion," presented at Automation Science and Engineering, 2007. CASE 2007. IEEE International Conference on, 2007.

[44] K. Tadakuma, R. Tadakuma, and J. Berengeres, "Development of holonomic omnidirectional vehicle with "Omni-ball": Spherical wheels," presented at Intelligent Robots and Systems, 2007. IROS 2007. IEEE/RSJ International Conference on, 2007.

[45] K. Iida, H. Yoshikawa, T. Mori, and T. Hira, "Development of omnidirectional electric wheelchair with zabuton sensor," presented at Control, Automation and Systems, 2008. ICCAS 2008. International Conference on, 2008.

[46] M. Wada, "Step climbing capability of a 4wd omnidirectional wheelchair," presented at Intelligent Robots and Systems, 2008. IROS 2008. IEEE/RSJ International Conference on, 2008.

[47] M. Wada, "A 4wd omnidirectional wheelchair with a chair tilting system," presented at Mechatronics and Automation, 2008. ICMA 2008. IEEE International Conference on, 2008.

[48] Y. Kobayashi, Y. Kinpara, T. Shibusawa, and Y. Kuno, "Robotic wheelchair based on observations of people using integrated sensors," Piscataway, NJ, USA, 2009.

[49] S. Temizer and L. P. Kaelbling, "Holonomic planar motion from non-holonomic driving mechanisms: The front-point method," *Proceedings of Photonics Boston, Intelligent Systems and Advanced Manufacturing (Mobile Robots XVI)*, 2001.

[50] R. M. Murray and S. S. Sastry, "Nonholonomic motion planning: Steering using sinusoids," *Automatic Control, IEEE Transactions on*, vol. 38, pp. 700-716, 1993.

[51] S. Mascaro, "Force guided docking control of an omnidirectional holonomic vehicle and its application to wheelchairs," *Department of Mechanical Engineering*,Massachusetts Institute of Technology, 1997.

[52] O. Diegel, A. Badve, G. Bright, J. Potgieter, and S. Tlale, "Improved mecanum wheel design for omni-directional robots," 2002.

[53] A. Gfrerrer, "Geometry and kinematics of the mecanum wheel," *Computer Aided Geometric Design*, vol. 25, pp. 784-791, 2008.

[54] S. A. Miller, "Network interfaces and fuzzy-logic control for a mecanum-wheeled omni-directional robot," 2005.

[55] P. Viboonchaicheep, A. Shimada, and Y. Kosaka, "Position rectification control for mecanum wheeled omni-directional vehicles," Roanoke, VA, United states, 2003.

[56] H. Kitagawa, T. Miyoshi, and K. Terashima, "Skill-assist control of omnidirectional wheelchair using human-friendly interface," Bangkok, Thailand, 2008.

[57] H. Kitagawa, T. Nishigaki, T. Miyoshi, and K. Terashima, "Fuzzy power assist control system for omni-directional transport wheelchair," presented at Intelligent Robots and Systems, 2004. (IROS 2004). Proceedings. 2004 IEEE/RSJ International Conference on, 2004.

[58] H. Kitagawa, K. Terashima, T. Miyoshi, J. Urbano, and S. Nishisaka, "Power assist system for omni-directional transport wheelchair using fuzzy reasoning," presented at Control Applications, 2004. Proceedings of the 2004 IEEE International Conference on, 2004.

[59] L. Kitagawa, T. Kobayashi, T. Beppu, and K. Terashima, "Semi-autonomous obstacle avoidance of omnidirectional wheelchair by joystick impedance control," presented at Intelligent Robots and Systems, 2001. Proceedings. 2001 IEEE/RSJ International Conference on, 2001.

[60] K. Terashima, T. Miyoshi, J. Urbano, and H. Kitagawa, "Frequency shape control of omni-directional wheelchair to increase user's comfort," presented at Robotics and Automation, 2004. Proceedings. ICRA '04. 2004 IEEE International Conference on, 2004.

[61] I. Omnix Technology, "Omnix technology, inc. - directional componnents and integrated systems," 2008, Omnix Technology, Inc. , Accessed March 1st, 2010, http://www.omnixtechnology.com/direct_components.html

[62] S. Robotics, "Rmp 400 omni | segway robotic mobility platforms," 2010, Segway Robotics, Accessed March 2, 2010, http://rmp.segway.com/rmp-400-omni/

[63] S. P. Levine, D. A. Bell, L. A. Jaros, R. C. Simpson, Y. Koren, and J. Borenstein, "The navchair assistive wheelchair navigation system," *Rehabilitation Engineering, IEEE Transactions on*, vol. 7, pp. 443-451, 1999.

[64] B. Woods and N. Watson, "A short history of powered wheelchairs," *Assistive technology: the official journal of RESNA*, vol. 15, pp. 164, 2003.

[65] A. Fattouh, M. Sahnoun, and G. Bourhis, "Force feedback joystick control of a powered wheelchair: Preliminary study," 2004.

[66] R. C. Simpson, "Smart wheelchairs: A literature review," *J Rehabil Res Dev*, vol. 42, pp. 423-36, 2005.

[67] T. I. Hafid NINISS, "Electric wheelchair simulator for rehabilitation of persons with motor disability," presented at Symposium on Virtual Reality VIII, Belém,PA 2006.

[68] B. E. Dicianno, R. A. Cooper, and J. Coltellaro, "Joystick control for powered mobility: Current state of technology and future directions," *Phys Med Rehabil Clin N Am*, vol. 21, pp. 79-86, 2010.

[69] P. R. Giacobbi, Jr., C. E. Levy, F. D. Dietrich, S. H. Winkler, M. D. Tillman, and J. W. Chow, "Wheelchair users' perceptions of and experiences with power assist wheels," *Am J Phys Med Rehabil*, 2010.

[70] Y. Kondo, T. Miyoshi, K. Terashima, and H. Kitagawa, "Navigation guidance control using haptic feedback for obstacle avoidance of omni-directional wheelchair," in *Proceedings of the 2008 Symposium on Haptic Interfaces for Virtual Environment and Teleoperator Systems*: IEEE Computer Society, 2008.

[71] L. Marchal-Crespo, "A simulator and assist-as-needed control strategy for learning to drive a power wheelchair," *Mechanical and Aerospace Engineering*,University of California, Irvine, 2006.

[72] L. Marchal-Crespo and D. J. Reinkensmeyer, "Haptic guidance can enhance motor learning of a steering task," *Journal of motor behavior*, vol. 40, pp. 545-557, 2008.

[73] O. Khatib, "Real-time obstacle avoidance for manipulators and mobile robots," presented at Robotics and Automation. Proceedings. 1985 IEEE International Conference on, 1985.

[74] J. Borenstein and Y. Koren, "The vector field histogram-fast obstacle avoidance for mobile robots," *Robotics and Automation, IEEE Transactions on*, vol. 7, pp. 278-288, 1991.

[75] H. Seki, S. Shibayama, Y. Kamiya, and M. Hikizu, "Practical obstacle avoidance using potential field for a nonholonmic mobile robot with rectangular body," presented at Emerging Technologies and Factory Automation, 2008. ETFA 2008. IEEE International Conference on, 2008.

[76] M. R. Petry, A. P. Moreira, R. A. M. Braga, and L. P. Reis, "Shared control for obstacle avoidance in intelligent wheelchairs," presented at Robotics Automation and Mechatronics (RAM), 2010 IEEE Conference on, 2010.

[77] J. Urbano, K. Terashima, and H. Kitagawa, "Skill-assist control of an omni-directional wheelchair by neuro-fuzzy systems using attendants'force input," *International Journal of Innovative Computing, Information and Control*, vol. 2, pp. 1219-1248, 2006.

[78] Airtrax, "Sidewinder: Omni-directional lift truck " Accessed February 27, 2010, http://www.airtrax.com/vehicles/sidewinder.html

[79] K. R. Boff and J. E. Lincoln, "Engineering data compendium. Human perception and performance. Volume 3," HARRY G ARMSTRONG AEROSPACE MEDICAL RESEARCH LAB WRIGHT-PATTERSON AFB OH, 1988.

[80] F. J. Valero-Cuevas, F. E. Zajac, and C. G. Burgar, "Large index-fingertip forces are produced by subject-independent patterns of muscle excitation," *Journal of Biomechanics*, vol. 31, pp. 693-704, 1998.

[81] H. Z. Tan, M. A. Srinivasan, B. Eberman, and B. Cheng, "Human factors for the design of force-reflecting haptic interfaces," *Dynamic Systems and Control*, vol. 55, pp. 353-359, 1994.

[82] M. J. Massimino, "Improved force perception through sensory substitution," *Control Engineering Practice*, vol. 3, pp. 215-222, 1995.

[83] B. E. Dicianno, D. M. Spaeth, R. A. Cooper, S. G. Fitzgerald, M. L. Boninger, and K. W. Brown, "Force control strategies while driving electric powered wheelchairs with isometric and movement-sensing joysticks," *Neural Systems and Rehabilitation Engineering, IEEE Transactions on*, vol. 15, pp. 144-150, 2007.

[84] B. E. Dicianno, D. M. Spaeth, R. A. Cooper, S. G. Fitzgerald, and M. L. Boninger, "Advancements in power wheelchair joystick technology: Effects of isometric joysticks and signal conditioning on driving performance," *American journal of physical medicine & rehabilitation*, vol. 85, pp. 631, 2006.

[85] A. C. Castro, J. Postigo, and J. Manzano, "Integration of a force feedback joystick with a virtual reality system," *Latin American Applied Research Journal*, vol. 30, pp. 171–178, 2000.

[86] J. Werkmeister and A. Slocum, "Theoretical and experimental determination of capstan drive stiffness," *Precision Engineering*, vol. 31, pp. 55-67, 2007.

[87] J. E. Speich, L. Shao, and M. Goldfarb, "Modeling the human hand as it interacts with a telemanipulation system," *Mechatronics*, vol. 15, pp. 1127-1142, 2005.

[88] R. F. Chandler, C. E. Clauser, J. T. McConville, H. M. Reynolds, J. W. Young, and O. H. Air Force Aerospace Medical Research Lab Wright-Patterson Afb, *Investigation of inertial properties of the human body*: NTIS, National Technical Information Service, 1975.